Analysis of Storm Surge and Tidal Resonance

in the Bristol Channel

Chanshu Gao

Mansfield College

Department of Engineering Science

University of Oxford

A thesis submitted for the degree of

Master of Science by Research

Hilary 2017

Abstract

Analysis of Storm Surge and Tidal Resonance

in the Bristol Channel

A thesis submitted for the degree of Master of Science by Research
Chanshu Gao
Mansfield College, Oxford
Hilary Term 2017

The Bristol Channel is located in the south-west coast of Great Britain, which has the second largest tidal range in the world. Despite a number of previous studies which have been undertaken in the Bristol Channel, its complex tidal dynamics are not yet fully understood, in particular given its resonant nature and presence of large storm surges. This was the motivation for the development of a simplified two-dimensional model to simulate the tidal flows and storm surge in the Bristol Channel.

In the tidal resonance study, a small two-dimensional model has been developed using the discontinuous Galerkin (DG) version of ADCIRC programme. We first vary the frequency on the ocean boundary of the model and examine at which frequency the model is mostly excited. Secondly we apply a wind disturbance to the model and analyse the frequency at which it resonates. We also examine the sensitivity of these results to the bed friction and changes in the tidal amplitude on the boundary or the sea water level.

There are two main methods for estimating future changes in storm-surge heights: statistical analysis and dynamical modelling, and in this thesis we use both. Firstly the occurrence and severity of storm surge events in the Bristol Channel over the period 1961-2015 are examined by analysing field data derived from tide gauges at five key locations along the north and south coasts of the Channel. Then we explore the storm surges numerically on a large two-dimensional model using the continuous Galerkin (CG) version of ADCIRC. Different wind strengths and wind directions are considered, and the interactions between surge and tides are investigated. A reconstruction of the 30th January 1607 event in the Bristol Channel is also provided at the end of this study to further explore the physics of storm surges in the Channel.

Acknowledgement

First of all, I would like to express my gratitude to my supervisor Prof. Thomas Adcock for his insightful advice and scholarly guidance throughout this project. Tom has been really patient throughout the whole process of my research. Our meeting frequency is almost the highest compared to other students and their supervisors' in our research group, which helped me quickly work on track in my first year in Oxford. He also gave me advice on presentation and writing for both a conference and the PRS transfer. Sometimes I treated him more like a mentor than a supervisor.

Secondly, I am grateful to Dr. Sena Serhadlıoğlu who carried out a preliminary study of the tidal resonance topic in her DPhil project in the University of Oxford. She has also been a great support and help throughout the first year of this study. I am also grateful to Audrey Davies who did a preliminary study of the storm surge topic in her final year undergraduate project in the University of Oxford. She kindly sent me her wind forcing generating MATLAB code for ADCIRC and explained every question I asked via email.

I also wish to show my deepest appreciation to all my friends who have been so supportive and enlightened my life in Oxford.

Last but not least, I would like thank my family who is always there for me and supporting me with unconditional love.

Contents

Chapter 1

Introduction

1.1 Introduction

Storm surges caused by atmospheric forcing can be devastating with long-lasting and diverse consequences. Historically, the UK has suffered major storm surge events, including in the Bristol Channel, which has the second largest tidal range in the world. The Bristol Channel is an area of complex hydrodynamics and is situated in the southwest coast of Great Britain; even now its complex tidal dynamics are not yet fully understood. Therefore, this study aims at investigating the reason for its large tidal range and the potential conditions under which an extreme water level event might occur in the Bristol Channel.

Following a brief introduction to storm surges, the hydrodynamic environment of the Bristol Channel, especially its resonance system, is described in this chapter and followed by a summary of the historical severe storm surge events and their impact in this area. Consequently the need for further research into understanding the tides and surges in the Bristol Channel is stated, and the main results of the thesis are presented.

1.2 Storm surge and its impact

1.2.1 Introduction to storm surge

A storm surge is an abnormal rise of water generated by winds and low atmospheric pressure associated with a storm, over and above the predicted astronomical tides. Extreme positive storm surges are the major factor in coastal flooding along the shoreline with shallow water and low-lying coastal environment, particularly when storm surge coincides with normal high tide (Lee, 2014). In the statistical analysis of this study, a storm surge is defined as the difference between the observed and predicted tidal levels. In the modelling study, the storm surge is investigated using two different terms: 'surge' and 'residual'. 'Residual' is the result affected by both winds and tides; otherwise, we refer to "surge" which is a genuine meteorological without tidal contribution to sea level. In reality, storm surge only makes up a part of what causes water levels to rise along the coast. There are also tides, waves and freshwater input which together with the storm surge make up the total water level.

Storm surges are long waves, with a characteristic time-scale of several hours to one day and a wavelength approximately equal to the width of the centre of the meteorological storm depression typically between 150 and 800km (CIRIA *et al.*, 2007). Therefore these long waves can be adequately modelled by shallow water equations, which will be discussed in the following chapter.

1.2.2 Factors that influence storm surge and its impact

Storm surges are scientifically complex, because meteorological, oceanographic and geographic factors influence the height, extent and duration for storm surge flooding. Such

factors include depth of depression, wind speeds, storm size, storm forward speed, the angle of approach to coast, shape of the coast line, width and slope of the ocean bottom and local features (Needham and Keim, 2011).

Storm surges are extremely dangerous because they are capable of flooding large coastal areas, causing severe devastation. Inundation events are among the most frequent, costly, and deadly coastal hazards that can affect coastal communities. In addition to the great threat to life, storm surge creates flooding that destroys buildings and carries debris out to sea, lifts ships onto land, contaminates food and water supplies, brings down communication and power lines, disrupts transportation, and takes out critical facilities and services for extended periods of time. Poor drainage means that waters that flow into low-lying areas can remain for weeks. When the storm has passed and the winds finally settle, massive damage may be left in its wake. The most serious flooding often results when an extreme storm surge event occurs concomitantly with a tidal maximum (Lowe *et al*., 2001).

Fig 1.1 shows wave overtopped during a storm surge event occurred in the East coast of UK on 19 October 2016. Eleven flood alerts had been issued for various sections of the Norfolk, Suffolk and Essex coast for high tide on that day. The forecast surge heights in Essex and Suffolk were 0.15m and 0.38m. Examples of more devastating historical storm surge events will be introduced in the next section.

Fig 1.1 High tides and storm surge put East coast of UK on flood alert on 19 October 2016 (www.itv.com).

1.2.3 Storms around the UK

Basically, there are two types of storms—tropical and extratropical; and their effects have very different characteristics.

Tropical storms are known variously as hurricanes (USA), cyclones (India), typhoons (Japan), cyclones (Australia) and baguios (Phlippines), and are usually small (100-1000km) and very intense. They are generated at sea, then they move in a relatively unpredictable way until they meet the coast. Here they produce exceptionally high flood levels within a confined region of width around tens of kilometres.

Storm surges occurring around Britain are usually due to extratropical storms, and their responses to the weather forcing are not very uniform. The more extensive spatial scales (>1000km) and longer periods of extratropical storms mean the effects of the earth's rotation (Coriolis forces) are more important in determining the seas' dynamical response; so too are the natural resonant period of the seas and basins themselves (Pugh, 1996).

1.3 Complex hydrodynamics in the Bristol Channel

The Bristol Channel and Severn Estuary constitute one of the largest semi-enclosed water basins in the UK. The Bristol Channel is located in the south-west coast of Great Britain (Fig 1.2 and Fig 1.3). The Severn Estuary is situated at the upper reaches of the Bristol Channel, which has the second largest semi-diurnal tidal range worldwide. The

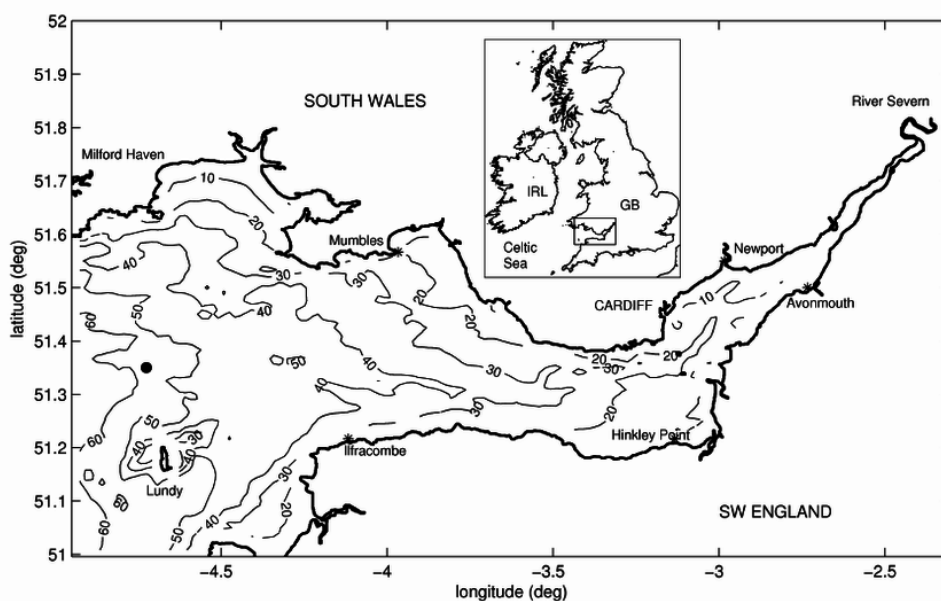Fig 1.2 Map of the Bristol Channel (accessed from worldatlas.com).

Fig 1.3 Bathymetric contour map of the Bristol Channel (Neil and Couch, 2011).

Bristol Channel is an area of complex hydrodynamics, which includes a very large tidal range, strong currents, extensive intertidal areas and river inputs, all of which contribute to frequent storm surges and flooding (Williams *et al*., 2012).

1.3.1 Tidal resonance in the Bristol Channel

The typical mean spring tidal range and fast currents observed in the Bristol Channel and the Severn Estuary are driven by two mechanisms: one is the funneling effect at the upper reaches of the Channel due to its wedge-shaped geometry and shallow bathymetry (Fig 1.3); the other mechanism is the quarter wavelength resonance of the Channel with the incident North Atlantic tidal wave (Fong and Heaps, 1978).

Systems that are forced by oscillations close to their natural period have large amplitude responses, this phenomenon is called resonance (Pugh, 1996). In oceanography, a tidal resonance occurs when the tide excites one of the resonant modes of a local region of the ocean. This occurs when a continental shelf is about a quarter wavelength wide. The whole global ocean system seems to be near to resonance at semidiurnal tidal frequencies and the observed tides are substantially larger than the Equilibrium Tide (Baker, 1991; Pugh and Woodworth, 2014).

In some studies, the phenomenon of quarter wavelength resonance was explained by analogy to a standing wave (Pugh, 1996; Pugh and Woodworth, 2014). Consider the simplest case of a wave travelling in a long channel being reflected without loss of amplitude at a closed end. The superposition of incident and reflected waves can resemble
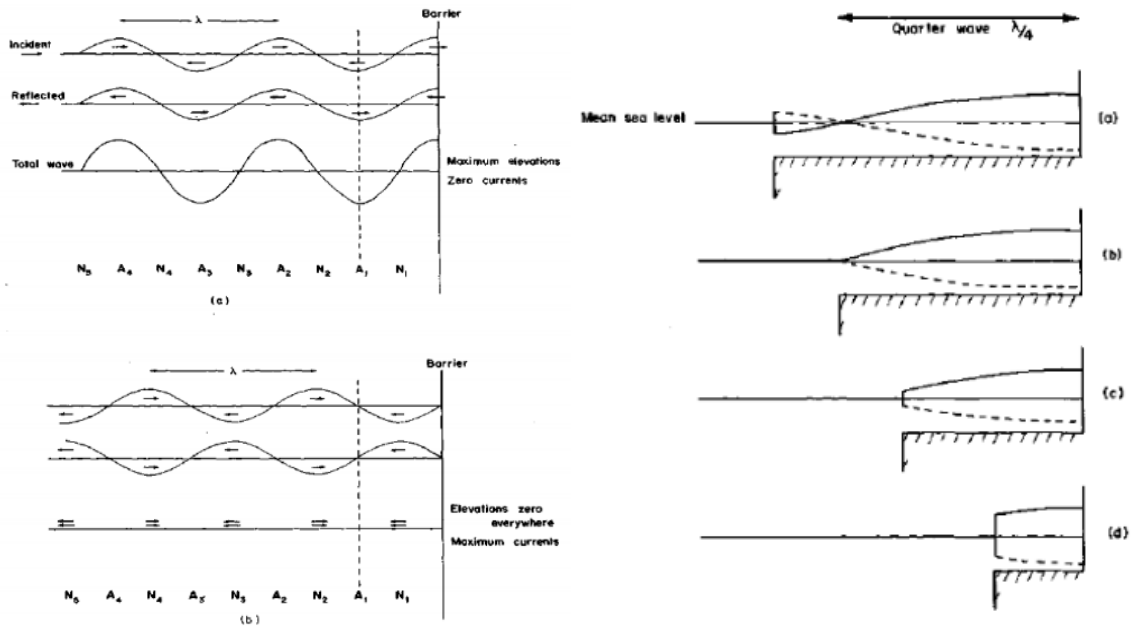
Fig 1.4 Standing waves (left-handed) and an open box model explaining the standing wave theory (right-handed) (Pugh, 1996).

a standing wave which have alternate nodes (positions where the amplitude is zero) and antinodes (positions where the amplitude is a maximum), each separated by a distance $\lambda/4$ where λ is the wavelength of the original progressive wave (Pugh, 1996). A model of an open box approximates to the tidal behaviour of many shelf sea basins (Pugh, 1996). Consider the movement of water in a box whose length is a quarter wavelength with one closed end and one open end, and the water is driven by oscillatory in and out currents at the open end. In the case where the open end is at the first node and currents at the entrance could produce large changes of level at the head. Although a geometry of the exact quarter-wave dimensioning would be very unlikely, the possibility of tidal amplification still exists.

The resonances in the Bristol Channel have practical significance as well as theoretical interests. Proposed tidal power barrages in the Severn Estuary, Bristol Channel were studied intensively in 1980s, by a UK government committee chaired by Bondi (see Bondi

et al., 1981). The suitability of tidal stream turbine deployment sites in Wales along the Bristol Channel has also been studied by Willis *et al.* (2010). The plan for a tidal lagoon project in the vicinity of the Port of Swansea, South Wales, was developed in 2011, and was presented to the global audiences at COP21, the 2015 Paris Climate Conference. It is aimed to start on site in 2018. Construction of the entire project will take four years, with first power generated in year three (http://www.tidallagoonpower.com/).

1.3.2 Historical storm surge events in the Bristol Channel

In the United Kingdom, particularly in the Bristol Channel, storm surges have occurred throughout history and have been the cause of substantial damage and flooding from the sea both in the past and more recently.

Possibly the worst coastal flooding on record was at approximately 0900 on 30th January 1607 (GMT). The lowlands surrounding the Bristol Channel suffered extensive flooding — covering 200 square miles of land with water and killing 2,000 people, and the estimated economic damage would be equivalent to between £7 billion to £13 billion in today's money (Horsburgh and Horritt, 2006; RMS, 2007). Although the sea defenses that line the Bristol Channel have been raised since 1607, if the excess sea levels experienced in the event occurred today, the consequences would be catastrophic. The storm surge of 31st January – 1st February 1953 was one of the most devastating natural disasters in Western Europe in the last century, claiming over 300 lives in southeast England and a further 1,900 in the Netherlands (Wolf and Flather, 2005; Horsburgh and Horritt, 2006). The highest water levels experienced in the Bristol Channel in a century occurred during the storm of 13th December 1981 when severe flooding was experienced along the north

Somerset coast (Williams *et al.*, 2012). According to the *SurgeWatch* database produced by Haigh *et al.* (2015), this event produced a significantly high water level with an estimated return period as high as 102 years at Avonmouth. This has been the highest return period event on record on that site.

More recently, over the winter of 2013/14, a large storm surge hit the east coast of the UK which was considered more extreme than expected, causing the loss of a number of lives in addition to significant economic damage; current estimates predict the final costs will surpass the £600 million in damage caused by the floods of 2012 (Ward, 2014).

Although not all of the damage mentioned above is attributable directly to storm surge, much of the fluvial flooding is related to the increased sea water levels as this reduces the ability of water to drain away from the river system.

1.4 Aims and thesis outline

A number of previous studies have been undertaken for the tides and surges in the Bristol Channel, but despite this the complex hydrodynamic system of the Channel is not yet fully understood, particularly given its resonant nature and frequent storm surge events. Therefore, a good knowledge and understanding of the tidal dynamics and storm surge characteristics of the Bristol Channel is very helpful in understanding its hydrodynamics and also in assessing the associated severe flood risks that might occur, both now and in the future.

In this study two numerical 2D models were used to investigate the tidal resonance phenomenon and storm surge characteristics of the Bristol Channel. First, a literature review is given within Chapter 2, discussing previous tide and surge modelling studies,

particularly in the area of the Bristol Channel. Chapter 3 describes the two models developed from Serhadlıoğlu *et al*. (2013) for tidal resonance and storm surge studies respectively, their validations are also presented in this chapter. Following this, Chapter 4 investigates the tidal resonances and their sensitivities in the Bristol Channel; Chapter 5 examines the influence of wind conditions on the storm surge events in the Bristol Channel. Some preliminary work by means of extreme values statistics using *in situ* data to better understand the characteristics of the storm surge in the Channel is also described in this chapter. The 30th January 1607 storm surge event in the Bristol Channel is reconstructed in Chapter 6 to explore the wind and tidal conditions of this event. Lastly, in Chapter 7 the main conclusions of this thesis are presented and suggestions for further work are made.

Chapter 2

Literature review

2.1 Introduction

Both two-dimensional and three-dimensional models have been widely used to study the tides and surges, and many comparisons between two- and three-dimensional model simulation results have come out recently (see Zheng *et al.*, 2013; Herry and Girard, 2011; Shim *et al*., 2013; Sheng *et al*., 2013). The intrinsic difference between 2-D and 3-D models is that by vertically integration, a 2-D model simplifies the vertical structure by neglecting the vertical velocities, while a 3-D model is capable of representing the complex vertical velocity patterns in a more realistic manner. However, considering the scale of the model area we are interested, the vertical scale of flow in the Bristol Channel is much smaller than all the hozizontal scales. Therefore, a 2-D model is the most straight-forward and efficient approach to tide and surge simulation.

Sometimes it is possible that the 2-D model can be approximated as a 1-D problem by integrating across the cross-channel width. It is still essentially a shallow water problem but with one dimension removed. This is used as an approximate model by some studies, and it has been used in the Bristol Channel (e.g. Fong and Heaps, 1978). In this study, the Bristol Channel resonance length problem is produced as a 1-D problem and detailed discussions can be found in Chapter 4.

In this chapter, we are going to look at the Shallow Water Equations (SWEs), which are widely used in 2-D modelling and are efficient for our study objectives. This chapter

first presents the SWEs with discussions of their limitations. A brief comparison is then made between the continuous Galerkin (CG) method and the discontinuous Galerkin (DG) method, which can be used to numerically solve the SWEs. Chapter 2 also reviews and discusses previous studies on storm surge and tidal resonance in the UK coasts.

2.2 Shallow water modelling

2.2.1   Shallow Water Equations (SWEs) and their limitations

2.2.1.1 Shallow Water Equations

Depth-integrated hydrodynamic models have wide application in modelling sea level heights and currents on continental shelves due to astronomical forcing and storm surges. Applications of these models include sea state and tidal forecasting, disaster planning and management, for coastal engineering and storm impact studies (Hubbert and Mclnnes, 1999).

One of the most widely used numerical methods in depth-integrated hydrodynamic models is based on the Shallow Water Equations (SWEs). The SWEs are a system of hyperbolic/parabolic Potential Differential Equations (PDEs) which can be used to model the fluid flow in the oceans, coastal regions, estuaries, rivers and channels. The SWEs can be obtained through several different approaches, the one which is adopted in this study involves the depth integrations of the continuity equation and the Navier-Stokes equations with free surface under the modelling hypothesis that the pressure is hydrostatic, gradually varying and the horizontal length scale is much greater than the vertical length scale of the ocean flow (Bresch and Nobel, 2007; Falconer, 1993).

Although actual shallow water flows are three-dimensional by nature, the assumptions

above allow a simplification to be made by integrating the horizontal velocity over the vertical direction to obtain a representative depth-averaged velocity flow field. The two-dimensional SWEs consist of the depth-averaged continuity equation and the *x*- and *y*-momentum equations written here in conservative form with all the terms will be used in this thesis included:

$$\frac{\partial \zeta}{\partial x} + \frac{\partial}{\partial x}(Hu) + \frac{\partial}{\partial y}(Hv) = 0, \tag{2.1}$$

$$\frac{\partial}{\partial t}(uH) + \frac{\partial}{\partial x}\left[Hu^2 + \frac{1}{2}g(H^2 - h^2)\right] + \frac{\partial}{\partial y}(Huv) = g\zeta\frac{\partial h}{\partial x} + F_x, \tag{2.2}$$

$$\frac{\partial}{\partial t}(vH) + \frac{\partial}{\partial x}(Huv) + \frac{\partial}{\partial y}\left[Hu^2 + \frac{1}{2}g(H^2 - h^2)\right] = g\zeta\frac{\partial h}{\partial y} + F_y, \tag{2.3}$$

where *H* is the total depth of the water column (*H=h+ζ*), which is equivalent to the sum of the free surface elevation (*ζ*) and the bathymetric depth (*h*). The variables *u* and *v* represent the depth-averaged velocity components in *x*- and *y*- directions. *g* is the gravitational acceleration (Serhadlıoğlu, 2014; Kubatko *et al*., 2009). F_x and F_y represent some additional terms; in this study they represent Coriolis term, bed friction and wind shear stress which will be further discussed in the following subsection.

2.2.1.2 Additional source terms in the Shallow Water Equations (SWEs)

Three additional source terms are used in this study: Coriolis term, bed friction and wind shear stress.

The Coriolis term is represented as a Coriolis parameter *f, f=2Ωsinφ* where *Ω* is the rotation rate of the Earth and *φ* the latitude. In this study the Coriolis Effect is always included as a spatially varied term. Since we are investigating large scale problems, it will make small difference in a large model with or without Coriolis term. If it is a small model that only includes the Bristol Channel, Coriolis term does not have much influence.

There are various methods used to represent bed friction. For instance, engineers

usually use a quadratic friction law for bed shear stress:

$$F_s = \frac{1}{2}\rho C_d \boldsymbol{u}|\boldsymbol{u}|,\qquad(2.4)$$

where $\mathbf{u}=(u,v)^{\mathrm{T}}$ and c_d is a drag coefficient. c_d can be related to a Darcy-Weisbach

resistance coefficient f_{DW}, or equivalently a Chézy coefficient c or Manning's coefficient n,

through the relationships (Soulsby, 1997):

$$c_d = \frac{f_{DW}}{8} = \frac{g}{c^2} = \frac{gn^2}{h^{1/3}}.\qquad(2.5)$$

Alternatively, if the turbulent tidal flow is assumed to have a logarithmic velocity

profile of the form:

$$u_*(z) = \frac{u_f}{\kappa}\ln\left(\frac{z}{z_0}\right), \quad \text{with } u_f = \left(\frac{|\tau_b|}{\rho}\right)^2,\qquad(2.6)$$

where $\kappa=0.4$ is the von Karman constant and z_0 describes a roughness length, the drag

coefficient according to Equation (2.6) can be defined as (Soulsby, 1997):

$$c_d = \left(\frac{\kappa}{1 + \ln\left(\frac{z_0}{h}\right)}\right)^2.\qquad(2.7)$$

ADCIRC inputs wind in units of stress rather than velocity. The relationship between

wind stress and wind velocity can be described by the following equations:

$$F_s = \rho_{air}C_D v^2,\qquad(2.8)$$

where C_D represents the drag coefficient between the water surface and the air, and v

represents the wind velocity, which is assumed to be 10m 10-minute averaged value in

ADCIRC .

Earlier as well as recent measurements have confirmed the logarithmic nature of the

wind profile near, but not overly close, to the water surface (Roll, 1965); and equation (2.6)

also became the usual law for wind profiles, suggesting that wind speed increase

logarithmically with height (Wu, 1980). In 1955, Charnock used this equation by

conducting a laboratory experiment and comparing with wind profiles with other

researchers. He characterised the relationship between roughness depth and friction

velocity of wind using the following equation (Charnock, 1955):

$$\frac{Z_0}{U_*^2/g} = constant = \alpha, \tag{2.9}$$

in which g is the gravitational acceleration, Z_0 is the roughness length of the sea surface,

U_* is the friction velocity of wind and α is the so-called Charnock constant. The Charnock

constant has long been used as a basis for many subsequently studies. However, the

proportionally constant does not account for the sea state, which is affected by both the

wind fields and pre-existing swell systems, limiting its accuracy and usability.

In 1977, Garratt addressed the following four major methods used to measure wind

stress: surface water tilting, geostrophic flow departure, wind profile, and eddy correlation

(Reynolds flux) (Bryant and Akbar, 2016). He complied data from 1967 to 1975, and

proposed two options for calculating the neutral drag coefficient. They consisted of a

power law relation (Garratt, 1977):

$$C_D \times 10^3 = 0.51U_{10}^{0.46}, \ 4\text{m/s} < U_{10} < 21m/s, \tag{2.10}$$

and a linear relation

$$C_D \times 10^3 = 0.75 + 0.067U_{10}, \ 4\text{m/s} < U_{10} < 21m/s. \tag{2.11}$$

Garratt's results have been published in a multitude of textbooks, and his review

analysis influenced numerous other investigators. Garratt's linear law for the drag

coefficient, Equation (2.11), is used in the ADCIRC model (ADCIRC user's manual v51,

2015). It is also widely used in other models (Johnson *et al.*, 1991; Joseph *et al.*, 2000;

Dietrich *et al.*, 2010). Garratt's formula is a widely-used formulation and it has been found to work well for storm surge applications.

Although the wind velocities used in simulations in this thesis are likely to slightly exceed the 21ms^{-1} limit for v suggested, the ADCIRC value for C_D will be taken as acceptable for the purposes of this thesis.

2.2.1.3 Limitations of the Shallow Water Equations (SWEs)

The SWEs can be used to predict tides, storm surge levels and coastline changes from hurricanes, ocean currents, and to study dredging feasibility; they also arise in atmospheric flows and debris flows. However, in certain situations the ability of 2-D SWEs models to simulate tidal flows is limited.

Firstly, if there are strong vertical components to the flow, or if the tidal wavelength is not long enough compared to the depth, i.e. the flow is 3-D, the shallow water equations would have broken down locally. There are clearly areas in which we are not modelling the local flows correctly at times, but all of these are essentially localised problems. It is certainly a much bigger problem for tidal energy extraction than for tidal resonance and storm surges. Tidal energy development requires investigation of the local tidal flows and the local interactions between tidal barrages/turbines and tidal flows. There are locations where we do not get the local flow field right when applying a 2-D model, however many 2-D models have been applied to the Bristol Channel and have shown good agreement with measurements (e.g. Serhadlıoğlu, 2014; Liang *et al*., 2014).

Secondly, we apply the bed friction under the assumption that the vertical profile is a log profile in ADCIRC, however in practice the real vertical velocity profile differs

significantly from the fixed profile. Although the fixed vertical velocity profile assumption is valid given the boundary layer of the water column is fully developed, it is not possible to specify the bed friction coefficient accurately without further modelling the boundary layer (Stansby and Lloyd, 2001).

Moreover, two-dimensional shallow water models also perform poorly in areas where abrupt variations in density occur. This is generally observed in regions where fresh water sources flow into estuaries (Serhadlıoğlu, 2014).

However, since the focus of this study is to understand the hydrodynamic systems, particularly the tidal and surge heights variations rather than tidal energy extraction or vertical velocity variation in the Channel, a more computationally efficient 2-D numerical model is highly desirable and captures the leading order physics required for these simulations. Additionally, due to the large tidal range (12.2m in average), fast current speed (up to 4m/s in the Severn crossing) and relatively small river discharge (61.7m^3/s in average), the flow in the Severn Estuary and the Bristol Channel does not display any significant stratification, which also justifies the use of the SWEs in the hydrodynamic analyses (Li, 2006).

2.2.2   Comparisons between the continuous Galerkin (CG) and discontinuous Galerkin (DG) finite element methods

Finite different, finite volume and finite element techniques are commonly used to solve the SWEs, the finite element method is selected here to solve SWEs This method was originally implemented by structural engineers in 1960s and first used to solve linear plane elasticity problems (Karniadakis and Sherwin, 2013). The finite element method is

preferred primarily due to its combination of higher-order accuracy and ability to handle complex geometries, and also its faculty to deal with unstructured girds. The spatial discretization of the computational domain is established by using unstructured elements which are connected to each other at nodal points (Serhadlıoğlu, 2014).

The traditional continuous Galerkin (CG) and discontinuous Galerkin (DG) finite element methods are both applied in this study. The main difference between CG and DG method is that CG discretisation requires integrals to be evaluated only over the element interiors, while DG discretisation requires the evaluation of integrals over the element interiors and the element boundaries. Fig 2.1 shows the difference between CG and DG method. In a CG method (top figure), the variable $u(x)$ is appropriated globally in a continuous manner. In contrast, in a DG method (bottom figure), the variable is approximated globally in a discontinuous manner and locally in each element in a continuous way (Bokhove and van der Vegt, 2005).
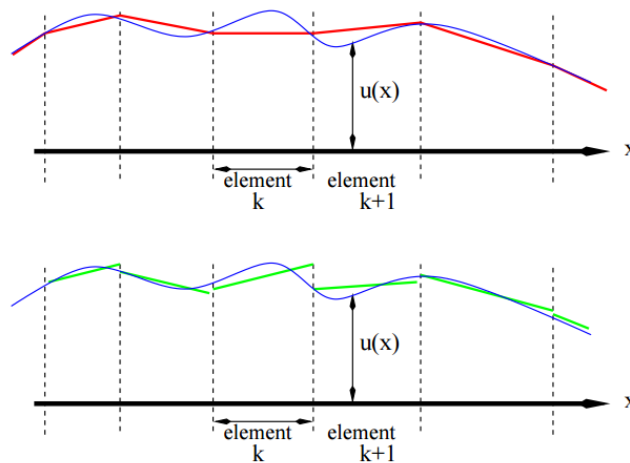
Fig 2.1 Comparison between CG and DG method.

Compared to CG, the DG model has several appealing features: its ability to capture smooth physically damped solutions to the wave propagation problem; its ability to handle

advection dominated flows including problems with hydraulic jumps or bores (discontinuities) and its inherent elemental mass and momentum conservation properties, which are highly valued in fluid dynamics modelling. However, one of the downsides of the DG model is that it requires memory and runs about four times slower than the CG model on a single core. This is because the DG errors are generally an order of magnitude lower than that in the CG solution on meshes of the same resolution (Kubatko *et al.*, 2006). Therefore, CG is usually used to trade off the modelling accuracy for speed.

Simulations on a single core for both CG and DG methods have been run with harmonic forcing of M_2 tide interpolated from Serhadlıoğlu's model (2014) but no current specified at the ocean boundary, and all other parameters are same between these two models. The model results are shown in Fig 2.3. It took 4 hours using CG method while 15.5 hours for DG method. Fig 2.2 shows the model map for the Bristol Channel. 16 model stations were taken along the Channel to compare the M_2 response amplitudes
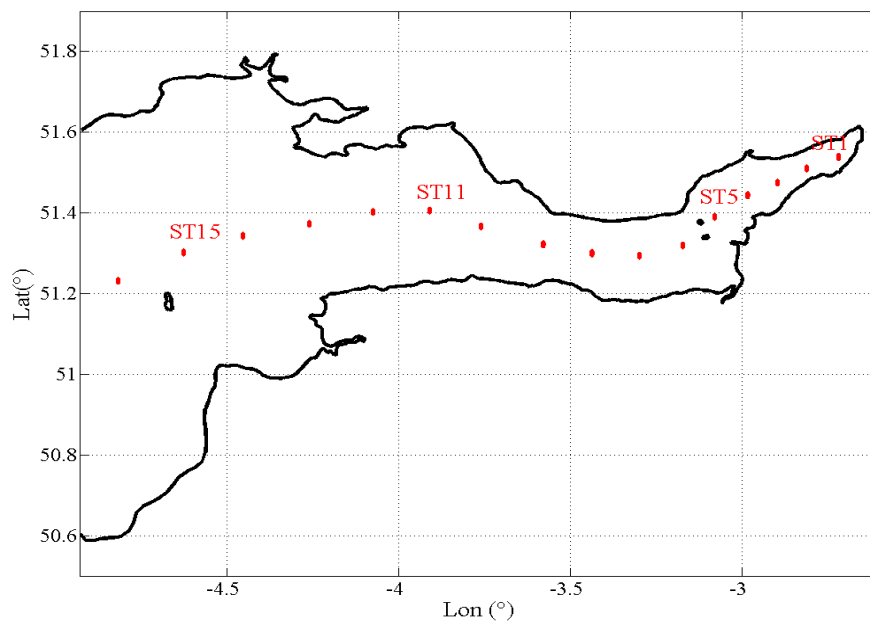
Fig 2.2 Model map and 16 model stations.
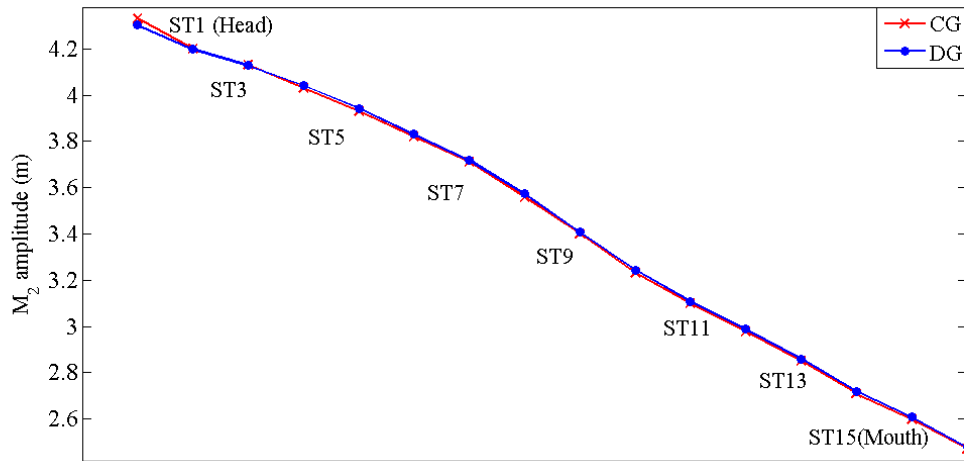
Fig 2.3 Comparison between the results from CG and DG methods, ST1-ST16 are
stations numbers along the Channel.

between CG method and DG method. It is seen that model results between CG and DG are almost same despite some difference occurs at the Channel head. It is presumably due to the way boundaries are handled rather than an artifact of the solver. Considering the longer simulation time of a DG model than a CG model, the CG method was adopted in the large (storm surge) model including the Bristol Channel, the English Channel, the Irish Sea and Celtic Sea; while the DG method was adopted in the small (tidal resonance) model including the Bristol Channel only.

2.2.3   Grid convergence analysis and model improvements from previous studies

A grid convergence study was conducted by Serhadlıoğlu (2014) to obtain the necessary level of resolution required in this Bristol Channel configuration, and the model refinement was undertaken by choosing from five unstructured triangular finite element meshes with different resolutions of the coastline boundary.

The model includes the inter-tidal zones around the Bristol Channel using a wetting

and drying treatment in the computation. The coastline is interpolated with 6m above the

mean sea level, which means a wall effect but only for extreme events (Fig 2.4). In

validating the model with wetting and drying treatment, the model results have been

compared against field observations by Serhadlıoğlu (2014).
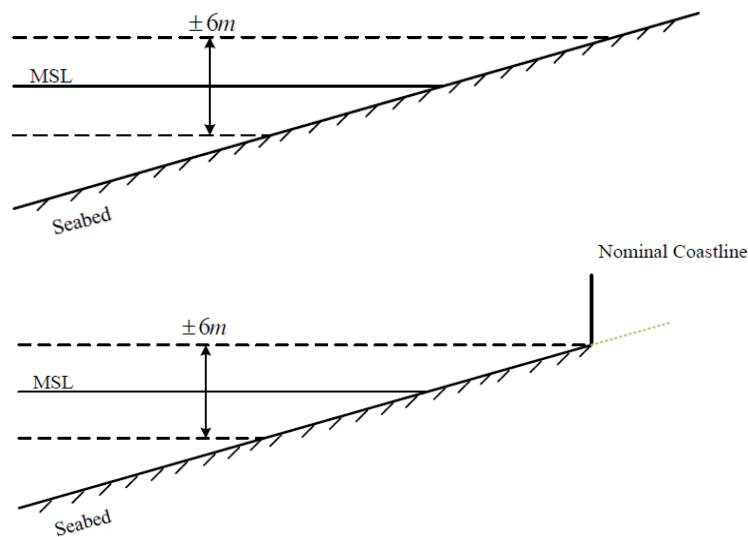
Fig 2.4 The representation of coastline in a natural case (top) and our ADCIRC model (bottom).

2.3 Previous studies on tide and surge in the UK coasts.

2.3.1 Statistical analysis

The foundation for extreme value modelling as a statistical discipline appropriate for

extreme risk measurement were laid in 1950s (Coles and Tawn, 2005). Early analysis of

extreme 'storm' water level return periods for design typically proceeded via analysis of

observed water levels consisting of astronomical tides combined with meteorologically

driven (surge) levels (Walton, 2000). In 1963, Lennon (1963b) published the results of six

different techniques of analysing annual observed sea level maxima on the west coast of

England. In the same year, Suthons (1963) used the Jenkinson method (1955) to analyse

the occurrence of observed annual maxima for ports on south east coasts of England. In addition to previous well-established extreme value methods of extrapolating observed annual maxima or the *n* highest levels in *n* years to predict rarer events, the format of Suthons' original approach was adopted in the detailed analysis of ten south coast ports by Blackman and Graff (1978), while alternative schemes of extreme value analysis were adopted by Davies and Webber (1976). In 1979, Graff and Blackman (1979) presented a summary of Lennon (1963b) and Suthons' (1963) work and revised their earlier study. They found that, although annual observed sea level maxima provide an attractive basis for analysis procedures, it is less likely that such treatment of single annual tidal observations will provide a satisfactory standard level of reliable information for practical design purposes. By restricting the analysis to annual maxima, useful information is ignored compared to a peaks-over-threshold analysis over the period of data. Thus the statistical predictions are inevitably less robust.

More recent literature on analysis of extreme water level return periods have recognised the need for separating the astronomical component of tide which is effectively deterministic from that of the meteorological surge component which is stochastic (Walton, 2000). Pugh and Vassie's proposal (1979) comprised a separate analysis of the deterministic tide and stochastic surge components, followed by a convolution to obtain the probability distribution of the sum. This study was revolutionary and later refined by Tawn and Vassie (1989, 1990) and Tawn (1992), resulting in an approach that combined the idea of process decomposition with the latest techniques for efficient modelling of extremes of stationary processes. Before Pugh and Vassie's proposal (1979), Ackers and

Ruxton (1974) studied surge levels on the Essex coast of Britain with a similar technique, but only for surges that occurred at high water, in which they added surge residuals at the time of predicted high waters to predicted high water levels.

Two contrasting models were developed enabling an inference on extremes that exploited more of the relevant available information than the annual maxima: Pickands (1971, 1975) employed a threshold-based analysis; Tawn (1988a, b) limited joint distribution of the several largest observations in a sequence. A development of considerable importance has been the study of multivariate extreme value models (Tawn, 1988b; Coles and Tawn, 1990). Many of the further recent improvements for the specific modelling of sea-level extremes tended to combine the statistical analysis with dynamical model studies (e.g. Coles and Tawn, 2005).

2.3.2 Extreme value analysis

Extreme value analysis is a widely-used statistical methodology for drawing inferences about the extremes of a stochastic process using only data on relatively extreme values of that process (Coles *et al*., 2001). Using this statistical approach allows us to describe temporal trends in storm surge characteristics, whilst properly accounting for the effects of natural variability (Butler *et al*., 2007). The likelihood of recurrence of a storm surge can be assessed by examining the return period of the surge component by fitting a generalized extreme value (GEV) distribution to the extreme surge levels using Maximum Likelihood. Bootstrapping can then be used to test the accuracy of the prediction. In statistics, bootstrapping can refer to any test that relies on random sampling with replacement (Diaconis and Efron, 1983). It offers a simple approach for estimating statistical

uncertainty when only a random sample is available.

If we assume *n* years of hourly surge data, t_1, ..., t_n, and let x_j denote the annual maximum surge for t_j. A standard procedure would be to assume that the annual maxima x_1, ..., x_n follow a GEV distribution with distribution function:

$$F(x; \mu, \sigma, \xi) = \exp\left\{-\left[1 + \xi\left(\frac{x - \mu}{\sigma}\right)\right]^{-\frac{1}{\xi}}\right\},$$ (2.12)

where the parameters μ, σ, ξ are location, scale and shape parameters respectively. The value of shape parameter ξ differentiates between the three types of extreme value distribution: $\xi < 0$ corresponds to the Weibull (type III); $\xi = 0$ and $\xi > 0$ correspond to the Gumbel distribution (type I) and Fréchet (type II) distribution respectively (Fig 2.5). However, interest usually lies not in estimates of the GEV parameters themselves, but in how we can use the fitted model to estimate other quantities, for example, the height of a
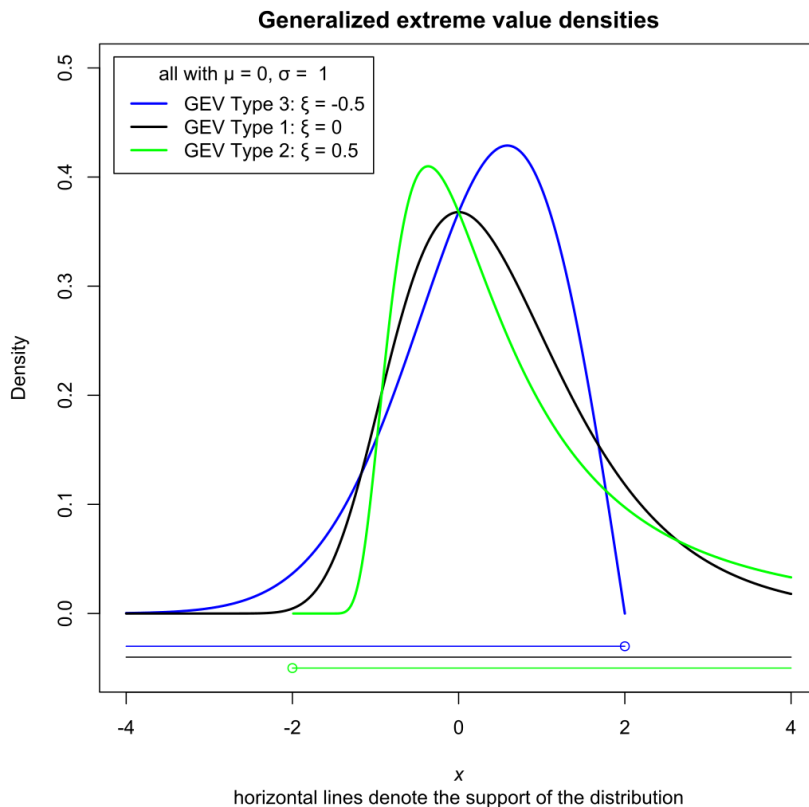
Fig 2.5 An example of Weibull (type III), Gumble (type I) and Fréchet (type II) distributions.

sea wall to protect against the once in a hundred year sea surge. Such quantity, in extreme value terminology, is usually referred to as return levels. Provided we have faith in our fitted model being suitable beyond the range of our observed data, we can estimate the n year return level z_n for any period by setting the GEV distribution function (Equation 2.12) equal to 1-1/n and solving for z_n.

2.3.3 Dynamical model studies

Following the east-coast floods of 1953 in the UK, research has been conducted at the direction of the Advisory Committee on Oceanographic and Meteorological Research into the mechanics of storm surge generation as applicable to the west coasts of the UK (Sutcliffe and Lennon, 1963). Following the famous 1953 storm surge, Brewer (1962) used a physical model to investigate the interactions between tides and storm surge in his DPhil under the supervision of Alexander Thom in the University of Oxford.

In 1963, Sutcliffe and Lennon (1963) identified the developing meteorological patterns which could be responsible for a major storm surge on the west coast of the British Isles. Since then, the prediction of storm surges in the Bristol Channel has mainly been performed by reference to Lennon's criteria (Proctor and Flahther 1989). In 1976, a new surge prediction scheme, based on numerical finite difference models of the atmosphere and of the sea, was established at Proudman Oceanographic Laboratory (POL) then and used in a routine manner at the UK Meteorological Office to predict storm surges (Flather, 1976). Although the model was primarily intended for surge prediction on the east coast of Britain, since it covered the whole of the northwest European continental shelf, it also provided predictions for ports on the west coast, including the Bristol Channel (Proctor

and Flather, 1989). Later in 1979, Flather forecasted the surges based on a numerical sea model, Continental Shelf Sea Model (CSM). However it had been felt for some time that the CSM could not be expected to provide forecasts of the required accuracy on the West Coast (Flather, 1979). Then a higher resolution sea model, West Coast Sea Model (WCM) was developed intending to provide improved results (Flather, 1981). Flather *et al.* (1982) tried to examine the forecasts produced by these models for the period of the 1981 Bristol Channel floods, but the results gave no indication of a danger of flooding, probably due to poor meteorological forecasts and poor accuracy and reliability of some tide gauge measurements. In 1989, the introduction by the Meteorological Office of the new 15-level higher resolution numerical atmospheric model led to an overall improvement of storm surge forecasts, especially in area with large tidal range such as the Bristol Channel; however, the new model was unable to adequately predict a secondary depression, similar to that which occurred on 13th December 1981 (Proctor and Flather, 1989). Flather *et al*. (1998) used a two-dimensional tidal-surge model for the northwest European continental shelf. This model was demonstrated to provide a good representation of tides and surges on the shelf and was formerly the model used for operational flood forecasting and warning in the UK, but it could not represent surges accurately where the model resolution was too coarse (e.g. in the Bristol Channel and eastern Irish Sea) (Woodworth *et al*. 2007; Flather and Williams, 2000).

In 2005, Wolf and Flather (2005) examined the severity of waves and storm surge in the 1953 event by means of extreme value statistics and model studies; Lowe and Gregory (2005) made some new estimates of future changes in extreme water levels around the UK

coastline. One of the largest surge events that occurred at Liverpool in the last 10 years, in January 2007, has been simulated using both POLCOMS-WAM and the Operational Surge model at POL (CS3X) to demonstrate their robust application in the Liverpool Bay area (Brown and Wolf, 2009). Later in 2012, Williams *et al*. (2012) re-visited the storm surge event of December 1981 by running the operational BCM/SRM models with meteorological forcing from the ERA-Interim reanalysis data. ERA-Interim is a global atmospheric reanalysis from 1979, continuously updated in real time (Dee *et al*., 2011). Williams and Horsburgh (2013) have identified and analysed the five largest storm surge events which occurred from 2008 to 2012 in the Bristol Channel by comparing the results from three Bristol Channel operational models (CS3X, BCM and SRM) with various measurements. Davies (2014) investigated the likely qualitative conditions of the significant storm surges in the Bristol Channel and the event of January 1607 by using the program ADCIRC. In 2016, a 2-D depth averaged tidal NEMO-surge configuration (Nucleus for European Modelling of the Ocean) has been developed as part of a joint project between the Met Office and the National Oceanographic Centre (NOC). The new configuration gives good results in terms of harmonic tidal constituents derived at UK Class A tide gauges when compared to observations. The results are comparable to, if not better than, tide only runs of the operational surge model CS3X (O'Neil *et al.,* 2016).

2.3.4   Previous studies on resonant period of the Bristol Channel

In recent forty years, the resonance phenomenon in the Bristol Channel and Severn Estuary have been of particular interest to engineers and scientists since cross-channel tidal barrages have been and are being considered for the Bristol Channel. Fong and Heaps

(1978) presented a summary of the significant numerical studies of estimating the resonant period of the Bristol Channel/Celtic Sea system. Table 2.1 is an extended version of this. To investigate the possible resonance in the system, Fong and Heaps (1978) first considered the amplification of the magnitudes of the main tidal constituents, K_2 (period of 11.97 hours), S_2 (period of 12 hours), M_2 (period of 12.42 hours), N_2 (period of 12.66 hours), K_1 (period of 23.93 hours), from the Atlantic continental shelf to the Celtic Sea into the Bristol Channel. Their results showed that the magnitudes of the semi-diurnal constituents were increased approximately four times from the outer continental shelf to the Severn Estuary (Avonmouth). In their study, Fong and Heaps (1978) found that the resonant period of the Bristol Channel is close to that of the semi-diurnal tidal band (Serhadlıoğlu, 2014).

Heath (1981) applied a simple linear resonant response model with four dominant tidal constituents (M_2-12.42hours, S_2-12hours, K_2-23.93hours, N_2-12.66hours) taken into consideration. His estimates of the resonant periods of the Celtic Sea are 10.8-11.1 hours, and he believed the more meaningful estimates in terms of a resonant response are those for observations near the entrance to the Bristol Channel, giving between 7.3 and 9 hours for the resonant period.

A 2-D hydrodynamic model was generated by Liang *et al.* (2014) covering the Bristol Channel, Severn Estuary and downstream reach of the River Severn. In their study, the resonance mode was tested by varying the tidal period at the seaward boundary and monitoring the water levels at some virtual tidal gauge stations. It was found that the resonant mode of oscillation in the Severn Estuary occurred at the tidal period of around 8

hours.

    Serhadlıoğlu (2014) has worked on the resonance in the Bristol Channel using a two-dimensional unstructured triangular model mesh, which was the one that the present study built on. The model domain includes the Irish Sea, the Celtic Sea, the English Channel and the Bristol Channel. In Serhadlıoğlu's study the model was excited with a single tidal component with the amplitude of the M_2 tide but with the frequency varied, and a resonant period of 10.3-11.2 hours was found.

References	Comment	Areas included	Friction coefficient	Fundamental period (hours)	ω/ω_{M_2}
Fong and Heaps (1978)	1-D numerical model to investigate the quarter-wave tidal resonance in the Bristol Channel-Celtic Sea shelf area	Celtic Sea and Bristol Channel	Not included	Celtic Sea: 12.2 – 12.6	0.98 – 1.02
Heaths (1981)	A linear resonant model fitted to the semi-diurnal tidal constituents	Celtic Sea, Bristol Channel and the southern Irish Sea	N/A	Celtic Sea: 10.8 – 11.1 Bristol Channel: 7.3-9.0	1.12-1.15
Liang *et al.* (2013)	1-D computational model to predict the response tidal characteristics	Severn Estuary and Bristol Channel	Roughness height: 35mm (same as in Falconer, 2009)	Bristol Channel: 8-9	1.38-1.55
Serhadlıoğlu (2014)	2-D unstructured computational model to investigate the resonance of the system	European continental shelf, Irish Sea, Celtic Sea and Bristol Channel	0.0025	Bristol Channel: 10.3-11.3	1.1-1.2

Table 2.1 Estimates of the fundamental resonant period of the Bristol Channel and the Celtic Sea derived from various theoretical models (extended table taken from Fong and Heaps (1978). ω/ω_{M_2} is the ratio between the tidal forcing frequency of dominant resonant mode and the frequency of M_2 tide.

Chapter 3

Model

3.1 Introduction

We use two different models in this study for investigating tidal resonance and storm surge simulations respectively. Model calibrations and validations have been done for both models. This involved finding the optimal bed friction and showing the simulations results are in close agreement with various measurements.

3.2 Small model

3.2.1 Model set up

As seen in Fig 3.1, the model domain covers the Severn Estuary and the Bristol Channel, with the seaward boundary set from Bosherston to Polzeath on the west and the riverine boundary at Severn Bridge towards the east. The domain is approximately 160km long, narrowing down dramatically towards the head of the Estuary, from around the width of 112km at the seaward boundary to about 1.4km at the landward boundary. The coastline, including the river boundary, is permitted to inundate more than 6m above the sea level. The depth is from 65m to -9m from ocean boundary to the river boundary. The model domain is divided into 14606 unstructured triangular cells varying in size 500m-5km.

From harmonic tidal analysis, the dominant constituent in the Bristol Channel is the M_2 tide, followed by the S_2, N_2 and μ_2 (Hashemi *et al*., 2008) tides, However in our study of tidal resonance, attention is restricted to the dominant harmonic constituent, the M_2 tide. The open seaward boundary is forced with a single sinusoidal constituent with an
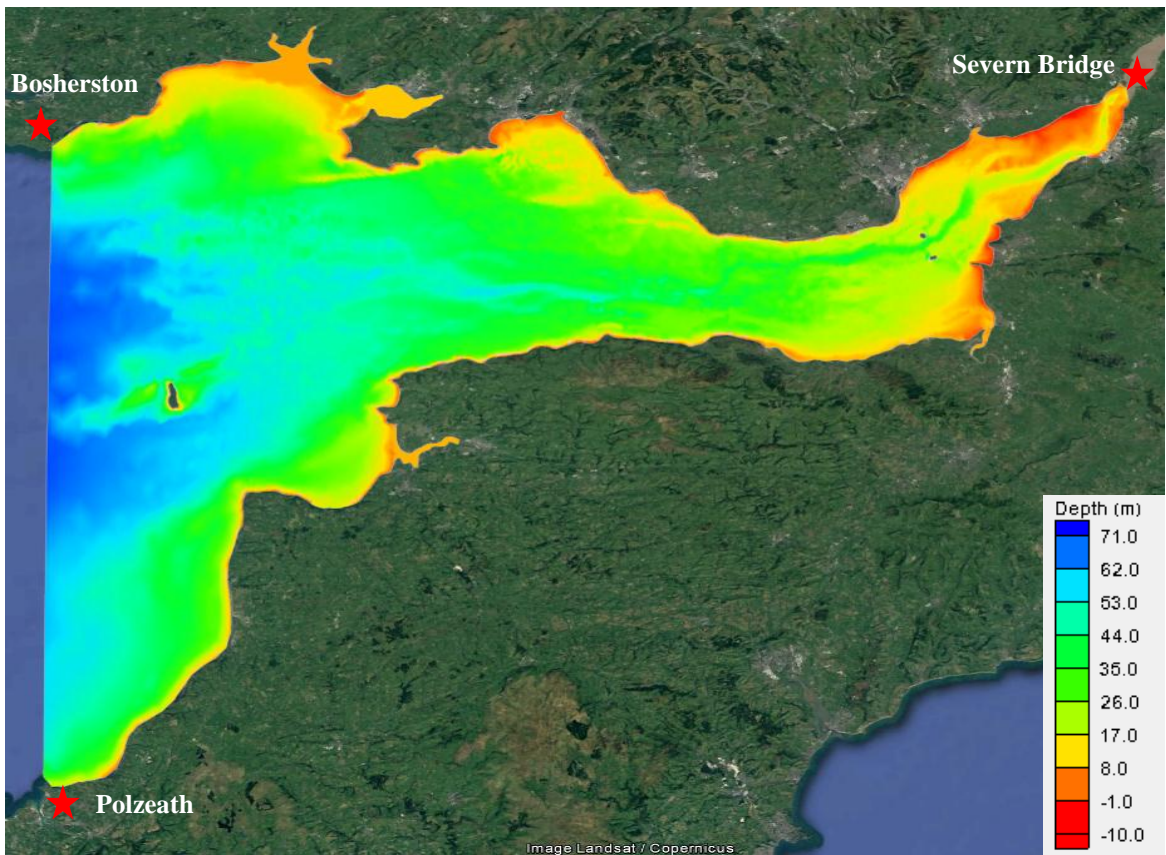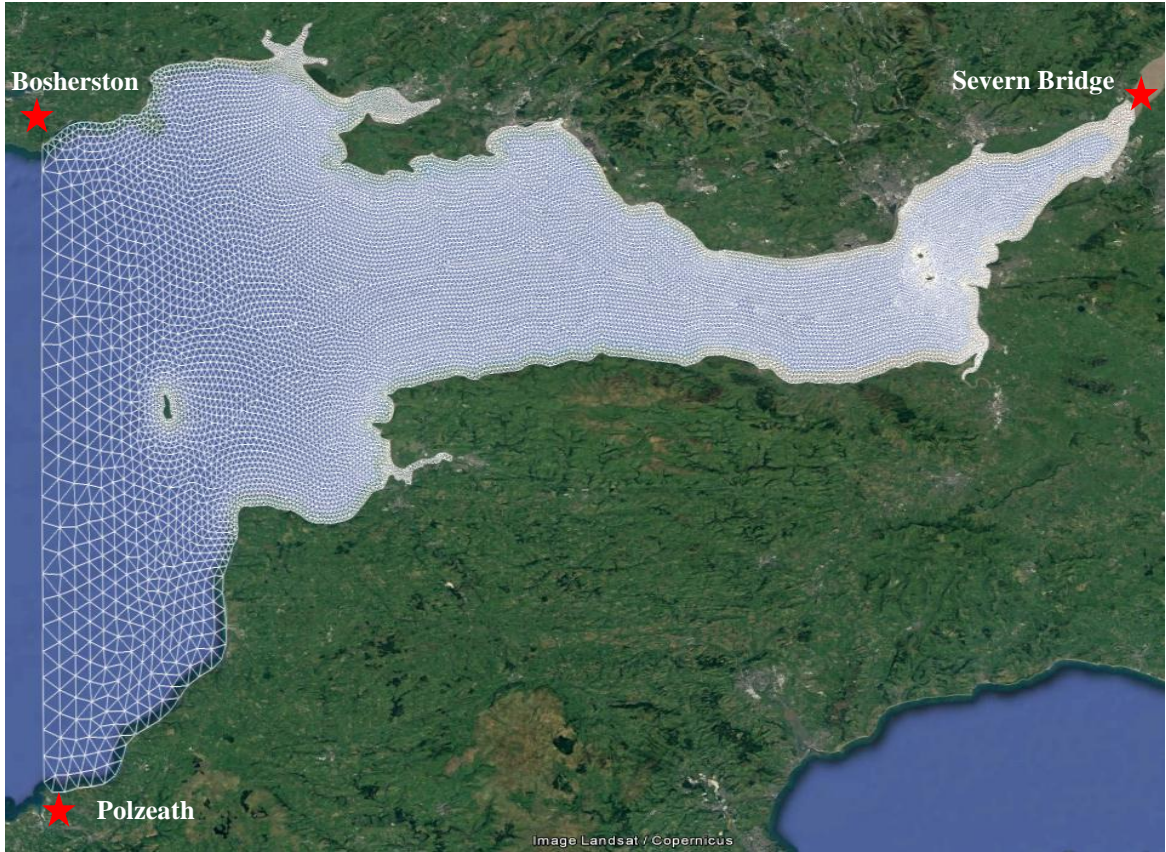
Fig 3.1 Model mesh (top) and colour-filled bathymetric contour map (bottom) shown in Google Earth.

amplitude distribution across the boundary given by that of the M_2 constituent interpolated from the same model (Serhadlıoğlu's, 2014). The DG-ADCIRC modelling parameters were set as constant throughout the study: All parameters, except for time step and bed friction coefficient, were taken as the default values recommended by the ADCIRC model developers and Serhadlıoğlu's study (2014) (Table 3.1). Initially, the simulations were run without any meteorological input, in order to observe the general flow of tides though the region. On the open boundary, the water depths were interpolated from the model of Serhadlıoğlu *et al.* (2013) relevant to their positions. The appropriate harmonic M_2 tide level was forced in time at the open boundary but with no current specified. There are free-slip boundary conditions at the coastline. In the real fluid the slip boundary condition cannot happen, but the boundary layer thickness here in the model is much smaller than mesh size therefore a slip boundary condition is appropriate.

Parameter name	Values	Descriptions
NOLIFA	2	Finite amplitude terms are included in the model run and wetting and drying function is enabled
NTIP	1	Tidal potential forcing is used
G	9.80665	Gravitational acceleration (m/s^2)
TAU0	-1	Weighting factor that weights the relative contribution of the primitive and wave portions of the GWCE
DT	1	ADCIRC time step (in seconds)
H0	0.25	Minimum water depth (units of length)
ESLM	8	Spatially constant horizontal eddy viscosity for the momentum equations (units of $length^2/time$)

Table 3.1 Basic DG-ADCIRC parameters and their descriptions.

3.2.2 Model calibration

In order to achieve the most accurate results, the model was tuned by adjusting the quadratic bottom friction coefficient (c_d) until the model predicted and observed M_2 tidal elevations and phases were in closest agreement. The observational data were from the

Station	M_2 Amplitude (m)					M_2 Phase (°)				
	Obs.	$c_d(1)$	$c_d(2)$	$c_d(3)$	$c_d(4)$	Obs.	$c_d(1)$	$c_d(2)$	$c_d(3)$	$c_d(4)$
Stackpole Quay (51.63,4.85)	2.51	2.52	2.52	2.51	2.51	168	172	172	172	172
Mumbles (51.57,4)	3.18	3.10	3.05	3.04	3.01	171	173	176	176	178
Swansea (51.62,3.93)	3.19	3.15	3.12	3.10	3.03	173	174	176	177	179
Port Talbot (51.58,3.78)	3.13	3.17	3.15	3.12	3.07	173	174	176	177	179
Barry (51.4,3.28)	3.92	3.90	3.80	3.74	3.62	185	182	188	190	193
Steep Holm island (51.33,3.1)	3.87	4.04	3.94	3.88	3.75	186	183	189	191	196
Cardiff (51.48,3.17)	4.01	4.07	3.95	3.89	3.79	191	186	190	193	199
Weston-super-Mare (51.35,2.97)	3.95	4.17	4.01	4.00	3.87	181	184	189	193	199
Hinkley Point (51.2,3.13)	3.8	4.00	3.89	3.83	3.71	195	181	186	188	193
Minehead (51.2,3.47)	3.59	3.70	3.64	3.59	3.49	183	176	180	182	186
Porlock Bay (51.22,3.6)	3.42	3.54	3.47	3.43	3.36	179	173	176	178	181
Ilfracombe (51.2,4.12)	3.04	3.00	2.99	2.97	2.94	162	165	166	167	168
Appledore (51.05,4.18)	2.57	2.62	2.59	2.57	2.52	165	170	172	173	174
Port Isaac (50.58,4.82)	2.47	2.42	2.42	2.42	2.41	144	151	151	151	151

Table 3.2 Comparison of the observed M_2 tidal elevations and phases against model results using various bed friction coefficients: $c_d(1)$=0.0025; $c_d(2)$=0.0035; $c_d(3)$=0.004; $c_d(4)$=0.005.

United Kingdom and Ireland Admiralty tide tables. The final results for fourteen calibration sites are summarised in Table 3.2. The computed M_2 phases at the both ends of the ocean boundary (Stackpole Quay and Port Issac) show a 4°-7° shift from the observed values. Therefore the computed phases that are around 5° larger than the observed values should be the best fit for model calibration. For each location in Table 3.2, the best results are in the grey shaded boxes. Over all, it is seen from the table that the model results show a best agreement with the observed data when using a bed friction coefficient c_d =0.004. This estimation is used on the entire area and does not reflect real spatial variability in frictional forces.

3.3 Large model

3.3.1 Model set up

The basic mesh used is that in Serhadlıoğlu's model of the Irish Sea, the Celtic Sea and the Bristol Channel (Serhadlıoğlu *et al*., 2013). The English Channel part of the model came from Adcock and Draper (2014). As seen in Fig 3.2, the domain includes three ocean boundaries: the northern boundary which extends towards the Scottish Isles of Tiree and Coll, the western boundary in the Celtic Sea and the eastern boundary in the English Channel. We chose this model domain because it covers the area of the Bristol Channel and seas around the UK that may influence the water levels and tidal wave propagation in the Bristol Channel (e.g. Irish Sea and Celtic Sea). Serhadlıoğlu (2014) found that instabilities occurred when the English Channel was not included. Therefore the English Channel is also included in this study. The model domain is divided into 31341
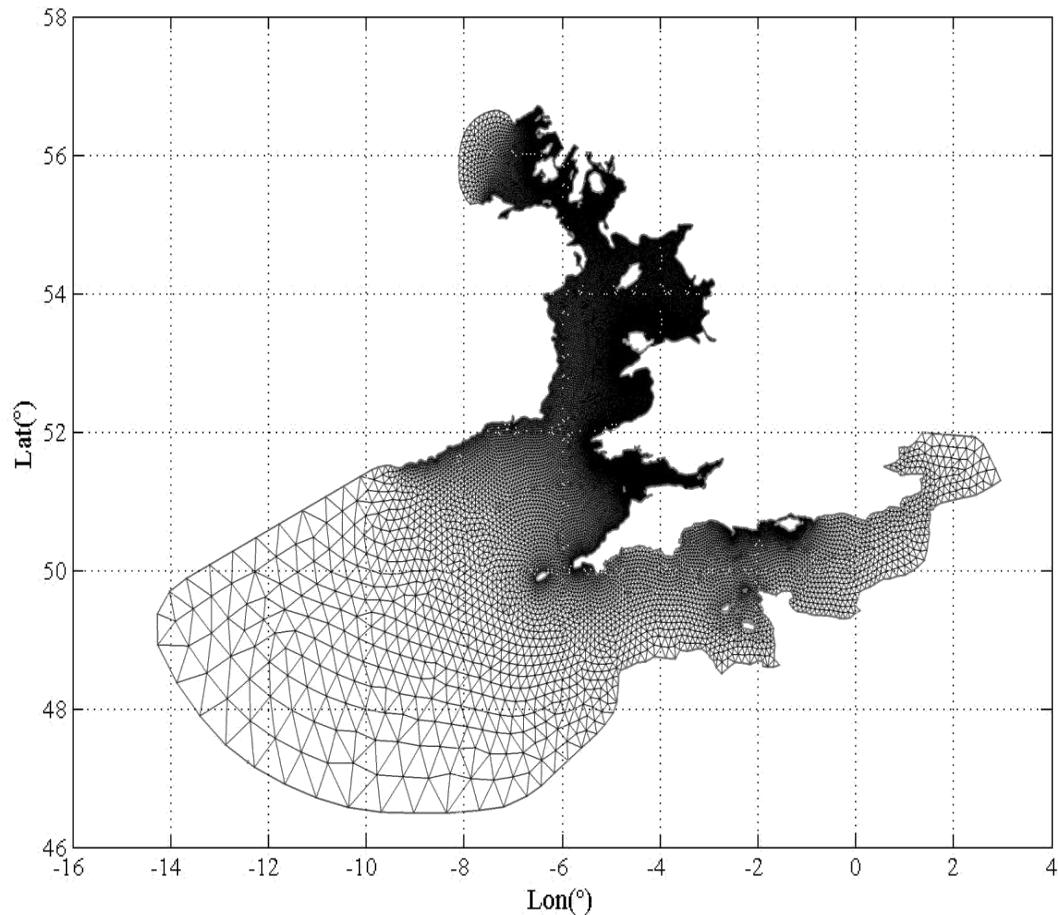
Fig 3.2 Model mesh, including the Irish Sea, the Celtic Sea, the English Channel and the Bristol Channel.

unstructured triangular cells and allows a large variation in the scales of regions of interest, which in this study is 0.5-54km.

The CG-ADCIRC modelling parameters were set as constant and are the same with that of the tidal resonance DG-ADCIRC model (see Table 3.1). On the open boundary, the water depths were prescribed from the model of Serhadlıoğlu *et al*. (2013) with no current specified, there the bathymetry data was obtained from SeaZone Ltd in shapefile format and was input to SMS (Serhadlıoğlu *et al*., 2014). The model was forced by harmonic M_2 and S_2 tidal constituents, which are the dominant semi-diurnal and diurnal tidal components and comprise approximately 95% of the total tidal amplitude in the Bristol Channel (Serhadlıoğlu *et al*., 2013). Although not precisely reflective of water levels, this

provides an excellent approximation to the tidal variations at this site. Initially, the simulations were run for a spring-neap cycle (14 days) without any meteorological input, in order to observe the general flow of tides though the region.

3.3.2 Model calibration

For the large model, the calibration was done by adjusting the quadratic bottom friction coefficient (c_d) until the model predicted and observed M_2 and S_2 tidal amplitudes and phases were in closest agreement, and is shown in Table 3.3, and for each location the best results are in the grey shaded boxes. The observational data are from the United Kingdom and Ireland Admiralty tide tables of the year 1997. Since we are mainly interested in the hydrodynamic system of the Bristol Channel, the calibration stations are all located in the Channel rather than over the whole model domain.

By comparing the predicted M_2 and S_2 tidal amplitudes and phases with the observed values, the best bed friction coefficient should be c_d =0.003 (Table 3.3 and 3.4). However, it seems that in the upper Channel (from Mumbles to Minehead) the calibration results agree well with c_d =0.003, but for deeper areas the results agree well when c_d =0.0025. This indicates that the numerical modelling of the Bristol Channel requires a very careful decision on the bed friction value, particularly the shallow areas where the water depth is no more than 20m. Therefore, to improve the model it would be better to apply a spatially varied bed friction coefficient. Here we tried two improved methods in order to have a higher accuracy of the calibration results.

Station	M$_2$ Amplitude (m)					M$_2$ Phase (°)				
	Obs.	c_d (1)	c_d (2)	c_d (3)	c_d (4)	Obs.	c_d (1)	c_d (2)	c_d (3)	c_d (4)
Milford Haven (51.716,5.04)	2.22	2.23	2.19	2.16	2.12	173	171	174	176	178
Stackpole Quay (51.63,4.85)	2.51	2.58	2.52	2.48	2.44	168	169	172	175	178
Tenby (51.67,4.7)	2.62	2.7	2.65	2.61	2.55	170	170	173	175	178
Burry Port (51.67,4.23)	2.74	2.7	2.62	2.55	2.47	176	180	185	189	194
Mumbles (51.57,4)	3.18	3.24	3.20	3.16	2.98	171	170	174	178	182
Swansea (51.62,3.93)	3.19	3.29	3.24	3.19	2.9	173	170	171	173	181
Port Talbot (51.58,3.78)	3.13	3.26	3.18	3.09	2.99	173	170	171	173	182
Barry (51.4,3.28)	3.82	3.95	3.82	3.69	3.55	185	178	181	185	193
Flat Holm (51.37,3.12)	3.9	4.12	3.97	3.84	3.72	190	179	186	192	198
Steep Holm (51.33,3.1)	3.87	4.11	3.96	3.83	3.72	186	178	182	189	193
Cardiff (51.48,3.17)	4.01	4.22	4.07	3.96	3.79	191	182	188	191	198
Hinkley Point (51.2,3.13)	3.8	4.06	3.92	3.79	3.65	185	176	182	187	192
Minehead (51.2,3.47)	3.59	3.78	3.66	3.55	3.45	183	172	177	181	185
Ilfracombe (51.2,4.12)	3.04	3.06	2.98	2.92	2.86	162	162	165	168	171
Lundy (51.17,4.65)	2.67	2.59	2.54	2.5	2.45	160	157	159	160	166
Boscastle (50.68,4.68)	2.36	2.47	2.42	2.38	2.34	143	150	152	155	158
Newquay (50.43, 5.07)	2.24	2.31	2.26	2.23	2.2	142	143	140	142	150

Table 3.3 Comparison of the observed M$_2$ tidal elevations and phases against model results using various bed friction coefficients: c_d (1)=0.002; c_d (2)=0.0025; c_d (3)=0.003; c_d (4)=0.004. Shaded boxes are the ones that match the measurements best.

Station	S$_2$ Amplitude (m)					S$_2$ Phase (°)				
	Obs.	c_d (1)	c_d (2)	c_d (3)	c_d (4)	Obs.	c_d (1)	c_d (2)	c_d (3)	c_d (4)
Milford Haven (51.716,5.04)	0.81	0.85	0.83	0.81	0.79	217	215	218	221	224
Stackpole Quay (51.63,4.85)	0.9	0.99	0.95	0.92	0.88	214	214	217	220	223
Tenby (51.67,4.7)	1.01	1.03	1	0.96	0.92	215	214	218	221	224
Burry Port (51.67,4.23)	0.95	0.96	0.92	0.88	0.84	219	231	236	241	246
Mumbles (51.57,4)	1.12	1.21	1.16	1.13	1.1	221	216	218	222	232
Swansea (51.62,3.93)	1.14	1.25	1.19	1.12	1.05	221	217	218	222	232
Port Talbot (51.58,3.78)	1.14	1.26	1.21	1.16	1.11	220	217	218	222	233
Barry (51.4,3.28)	1.37	1.56	1.48	1.4	1.32	240	228	235	241	247
Flat Holm (51.37,3.12)	1.35	1.63	1.54	1.46	1.38	246	230	238	245	252
Steep Holm (51.33,3.1)	1.37	1.63	1.55	1.46	1.37	240	229	236	243	250
Cardiff (51.48,3.17)	1.45	1.68	1.58	1.5	1.42	246	233	241	248	255
Hinkley Point (51.2,3.13)	1.42	1.61	1.52	1.44	1.36	237	226	233	240	247
Minehead (51.2,3.47)	1.24	1.49	1.41	1.35	1.29	235	220	227	233	239
Ilfracombe (51.2,4.12)	1.1	1.19	1.14	1.1	1.05	209	206	211	215	219
Lundy (51.17,4.65)	0.94	1	0.96	0.94	0.91	207	210	206	209	212
Boscastle (50.68,4.68)	0.89	0.95	0.92	0.89	0.87	201	192	196	199	200
Newquay (50.43, 5.07)	0.79	0.88	0.85	0.83	0.8	182	185	188	191	193

Table 3.4 Comparison of the observed S$_2$ tidal elevations and phases against model results using various bed friction coefficients: c_d(1)=0.002; c_d (2)=0.0025; c_d (3)=0.003; c_d (4)=0.004. Shaded boxes are the ones that match the measurements best.

For Approach A, we ran the simulations using combinations of different bed friction coefficients on different model areas. A combination of two different bed frictions and three bed frictions were applied to the model, and the decision of choosing bed frictions for different sections were based on the M_2 and S_2 measurements for different stations (see Table 3.3 and Table 3.4). We first applied c_d =0.003 in the Channel head and applied c_d =0.0025 for the rest of the model areas; then further divided the upper Channel into three sections, and applied c_d =0.0035 in the shallower areas in the Channel head and c_d =0.003, c_d =0.0025 in the rest of the Channel and the rest of the model areas respectively (Fig 3.3a and 3.3b). However it can be seen from Table 3.5 and Table 3.6 that with multiple c_d the M_2 amplitude and phase calibration results have not improved the model's accuracy compared to applying a constant c_d=0.003 over the whole model areas.

Alternatively, in Approach B a hybrid nonlinear bottom friction law is applied. Using this approach, in the deep water the bed friction coefficient is constant and a quadratic bottom friction law results; while in shallow water the friction coefficient increases as the depth decreases. An equation describing the hybrid nonlinear bottom friction law coded in the ADCIRC model is given below:

$$c_d = c_{dmin} \left[\left(1 + \frac{H_{break}}{H} \right) \theta \right] \left(\frac{\gamma}{\theta} \right), \tag{3.1}$$

where H_{break} is the break depth (units of length) in the hybrid bottom friction relationship.

(a)

(b)

Fig 3.3 Coloured model map with different sets of bed friction: Approach A: c_d=0.003 (green area), c_d=0.0025 (red area); Approach B: c_d=0.0035 (blue area), c_d=0.003 (green area), c_d=0.0025 (red area).

Station	M$_2$ Amplitude (m)					M$_2$ Phase (°)				
	Obs.	A	B	c_d (2)	c_d (3)	Obs.	A	B	c_d (2)	c_d (3)
Milford Haven (51.716,5.04)	2.22	2.27	2.26	2.19	2.16	173	172	173	174	176
Stackpole Quay (51.63,4.85)	2.51	2.53	2.52	2.52	2.48	168	171	173	172	175
Tenby (51.67,4.7)	2.62	2.68	2.66	2.65	2.61	170	172	173	173	175
Burry Port (51.67,4.23)	2.74	2.59	2.55	2.62	2.55	176	187	189	185	189
Mumbles (51.57,4)	3.18	3.1	3.07	3.20	3.16	171	173	174	174	178
Swansea (51.62,3.93)	3.19	3.12	3.15	3.24	3.19	173	174	175	171	173
Port Talbot (51.58,3.78)	3.13	3.2	3.18	3.18	3.09	173	174	176	171	173
Barry (51.4,3.28)	3.82	3.83	3.79	3.82	3.69	185	184	187	181	185
Flat Holm (51.37,3.12)	3.9	4	3.97	3.97	3.84	190	188	190	186	192
Steep Holm (51.33,3.1)	3.87	4	3.96	3.96	3.83	186	182	189	182	189
Cardiff (51.48,3.17)	4.01	4.01	3.98	4.07	3.96	191	190	192	188	191
Hinkley Point (51.2,3.13)	3.8	3.95	3.92	3.92	3.79	185	183	186	182	187
Minehead (51.2,3.47)	3.59	3.69	3.65	3.66	3.55	183	178	179	177	181
Ilfracombe (51.2,4.12)	3.04	3.01	2.98	2.98	2.92	162	164	165	165	168
Lundy (51.17,4.65)	2.67	2.51	2.51	2.54	2.5	160	159	161	159	160
Boscastle (50.68,4.68)	2.36	2.42	2.42	2.42	2.38	143	152	153	152	155
Newquay (50.43, 5.07)	2.24	2.25	2.29	2.26	2.23	142	146	148	140	142

Table 3.5 Comparison of the observed M$_2$ tidal elevations and phases with a constant bed friction coefficient and with multiple bed friction coefficients. c_d (2)=0.0025; c_d (3)=0.003. Shaded boxes are the ones that match the measurements best.

Station	S₂ Amplitude (m)					S₂ Phase (°)				
	Obs.	A	B	c_d (2)	c_d (3)	Obs.	A	B	c_d (2)	c_d (3)
Milford Haven (51.716,5.04)	0.81	0.87	0.86	0.83	0.81	217	222	223	218	221
Stackpole Quay (51.63,4.85)	0.9	0.97	0.96	0.95	0.92	214	222	223	217	220
Tenby (51.67,4.7)	1.01	1.03	1.02	1	0.96	215	223	224	218	221
Burry Port (51.67,4.23)	0.95	0.93	0.9	0.92	0.88	219	243	246	236	241
Mumbles (51.57,4)	1.12	1.2	1.18	1.16	1.13	221	226	227	218	222
Swansea (51.62,3.93)	1.14	1.18	1.22	1.19	1.12	221	227	229	218	222
Port Talbot (51.58,3.78)	1.14	1.25	1.23	1.21	1.16	220	227	229	218	222
Barry (51.4,3.28)	1.37	1.5	1.47	1.48	1.4	240	243	245	235	241
Flat Holm (51.37,3.12)	1.35	1.59	1.56	1.54	1.46	246	247	250	238	245
Steep Holm (51.33,3.1)	1.37	1.59	1.56	1.55	1.46	240	245	248	236	243
Cardiff (51.48,3.17)	1.45	1.55	1.52	1.58	1.5	246	250	253	241	248
Hinkley Point (51.2,3.13)	1.42	1.56	1.53	1.52	1.44	237	242	245	233	240
Minehead (51.2,3.47)	1.24	1.45	1.42	1.41	1.35	235	234	236	227	233
Ilfracombe (51.2,4.12)	1.1	1.16	1.15	1.14	1.1	209	216	218	211	215
Lundy (51.17,4.65)	0.94	0.96	0.95	0.96	0.94	207	210	211	206	209
Boscastle (50.68,4.68)	0.89	0.93	0.92	0.92	0.89	201	201	202	196	199
Newquay (50.43, 5.07)	0.79	0.85	0.87	0.85	0.83	182	194	195	188	191

Table 3.6 Comparison of the observed S₂ tidal elevations and phases with a constant bed friction coefficient and with multiple bed friction coefficients. c_d (2)=0.0025; c_d (3)=0.003. Shaded boxes are the ones that match the measurements best.

If the water depth (H) is greater than H_{break}, bottom friction approaches a quadratic function of depth-averaged velocity with $c_d = c_{dmin}$. If the water depth is less than H_{break}, c_d will increase as the depth decreases. θ is a dimensionless parameter that determines how rapidly the hybrid bottom friction relationship approaches its deep water and shallow water limits when the water depth is greater than or less than H_{break}. γ is a dimensionless parameter that determines how the friction factor increases as the water depth decreases. For example, setting this to 1/3 gives a Manning friction law type of behaviour.

Here we set $H_{break} = 1m$ and 10m and compare the M_2 and S_2 amplitudes and phases with that of constant bed friction. However the calibration results with applying a hybrid nonlinear bottom friction law do not show significant improvements compared to that with a constant bed friction coefficient (Table 3.7 and Table 3.8).

Therefore for simplicity, a constant quadratic bed friction coefficient is used in the study and $c_d = 0.003$ is chosen here to be the best fit for the storm surge modelling.

Station	M$_2$ Amplitude (m)					M$_2$ Phase (°)				
	Obs.	1m	10m	c_d (2)	c_d (3)	Obs.	1m	10m	c_d (2)	c_d (3)
Milford Haven (51.716,5.04)	2.22	2.27	2.26	2.19	2.16	173	173	173	174	176
Stackpole Quay (51.63,4.85)	2.51	2.64	2.63	2.52	2.48	168	173	173	172	175
Tenby (51.67,4.7)	2.62	2.77	2.76	2.65	2.61	170	172	172	173	175
Burry Port (51.67,4.23)	2.74	3.04	2.97	2.62	2.55	176	186	189	185	189
Mumbles (51.57,4)	3.18	3.29	3.28	3.20	3.16	171	173	172	174	178
Swansea (51.62,3.93)	3.19	3.36	3.35	3.24	3.19	173	174	174	171	173
Port Talbot (51.58,3.78)	3.13	3.4	3.41	3.18	3.09	173	174	174	171	173
Barry (51.4,3.28)	3.82	4.28	4.27	3.82	3.69	185	181	181	181	185
Flat Holm (51.37,3.12)	3.9	4.51	4.5	3.97	3.84	190	183	183	186	192
Steep Holm (51.33,3.1)	3.87	4.5	4.49	3.96	3.83	186	182	182	182	189
Cardiff (51.48,3.17)	4.01	4.62	4.63	4.07	3.96	191	186	185	188	191
Hinkley Point (51.2,3.13)	3.8	4.42	4.41	3.92	3.79	185	179	179	182	187
Minehead (51.2,3.47)	3.59	4.06	4.05	3.66	3.55	183	175	175	177	181
Ilfracombe (51.2,4.12)	3.04	3.18	3.17	2.98	2.92	162	164	164	165	168
Lundy (51.17,4.65)	2.67	2.67	2.66	2.54	2.5	160	158	158	159	160
Boscastle (50.68,4.68)	2.36	2.53	2.52	2.42	2.38	143	152	152	152	155
Newquay (50.43, 5.07)	2.24	2.36	2.35	2.26	2.23	142	146	146	140	142

Table 3.7 Comparison between the M$_2$ tidal elevations and phases with a constant bed friction coefficient and with hybrid nonlinear bed friction law. c_d (2)=0.0025; c_d (3)=0.003. Shaded boxes are the ones that match the measurements best.

Station	S₂ Amplitude (m)					S₂ Phase (°)				
	Obs.	1m	10m	c_d (2)	c_d (3)	Obs.	1m	10m	c_d (2)	c_d (3)
Milford Haven (51.716,5.04)	0.81	0.82	0.82	0.83	0.81	217	222	222	218	221
Stackpole Quay (51.63,4.85)	0.9	0.95	0.94	0.95	0.92	214	222	222	217	220
Tenby (51.67,4.7)	1.01	0.99	0.99	1	0.96	215	222	222	218	221
Burry Port (51.67,4.23)	0.95	0.97	0.91	0.92	0.88	219	250	253	236	241
Mumbles (51.57,4)	1.12	1.18	1.17	1.16	1.13	221	226	225	218	222
Swansea (51.62,3.93)	1.14	1.2	1.2	1.19	1.12	221	228	227	218	222
Port Talbot (51.58,3.78)	1.14	1.21	1.22	1.21	1.16	220	228	228	218	222
Barry (51.4,3.28)	1.37	1.55	1.55	1.48	1.4	240	241	241	235	241
Flat Holm (51.37,3.12)	1.35	1.65	1.64	1.54	1.46	246	244	244	238	245
Steep Holm (51.33,3.1)	1.37	1.64	1.64	1.55	1.46	240	244	243	236	243
Cardiff (51.48,3.17)	1.45	1.66	1.69	1.58	1.5	246	248	247	241	248
Hinkley Point (51.2,3.13)	1.42	1.61	1.61	1.52	1.44	237	240	240	233	240
Minehead (51.2,3.47)	1.24	1.47	1.47	1.41	1.35	235	232	233	227	233
Ilfracombe (51.2,4.12)	1.1	1.15	1.15	1.14	1.1	209	216	216	211	215
Lundy (51.17,4.65)	0.94	0.97	0.97	0.96	0.94	207	210	210	206	209
Boscastle (50.68,4.68)	0.89	0.91	0.91	0.92	0.89	201	201	201	196	198
Newquay (50.43, 5.07)	0.79	0.84	0.84	0.85	0.83	182	194	194	188	191

Table 3.8 Comparison between the S₂ tidal elevations and phases with a constant bed friction coefficient and with hybrid nonlinear bed friction law. c_d (2)=0.0025; c_d (3)=0.003. Shaded boxes are the ones that match the measurements best.

3.4 Model validation

Model validation was undertaken against alternative predictions by some numerical models and Admiralty's TotalTide software (www.admiralty.co.uk). TotalTide is a comprehensive tidal prediction programme providing tidal height and tidal stream predictions for more than 7,000 ports and 3,000 tidal streams worldwide. The data is based on Admiralty data derived from field measurements.

First we compared the tidal harmonic analysis results against predictions by other numerical models (Davies and Jones, 1992) for the whole model domain as a
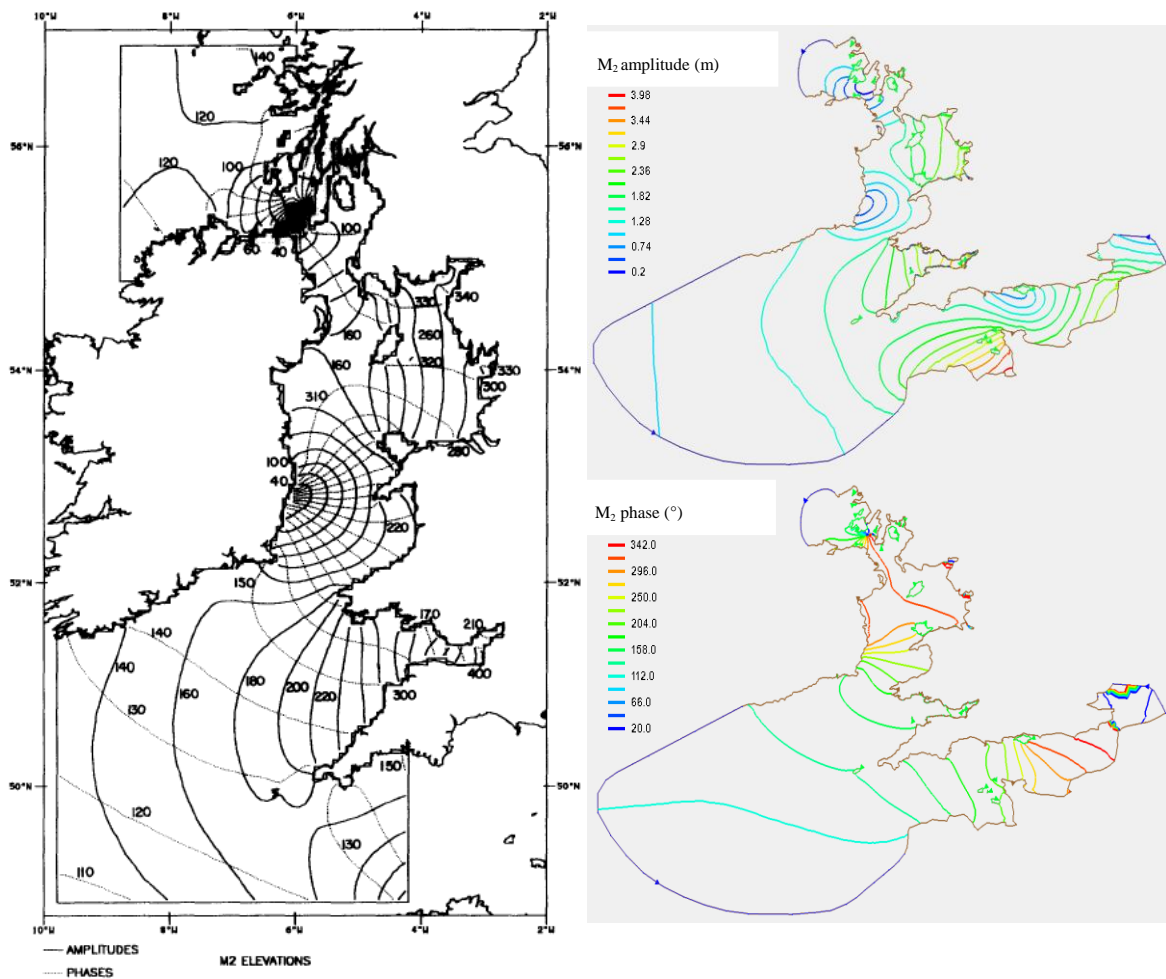
Fig 3.4 Comparison between the cotidal charts of phase (dashed line) and amplitude (solid line) from Davies and Jones' study (1992) and ADCIRC generated harmonic analysis for M_2 tidal component.

supplementary method to model calibration in the small and large models. The contours of the computed M_2 and S_2 tidal amplitudes and phases were compared with the cotidal charts in Fig 3.4 and Fig 3.5, and they were found to be in close agreement.
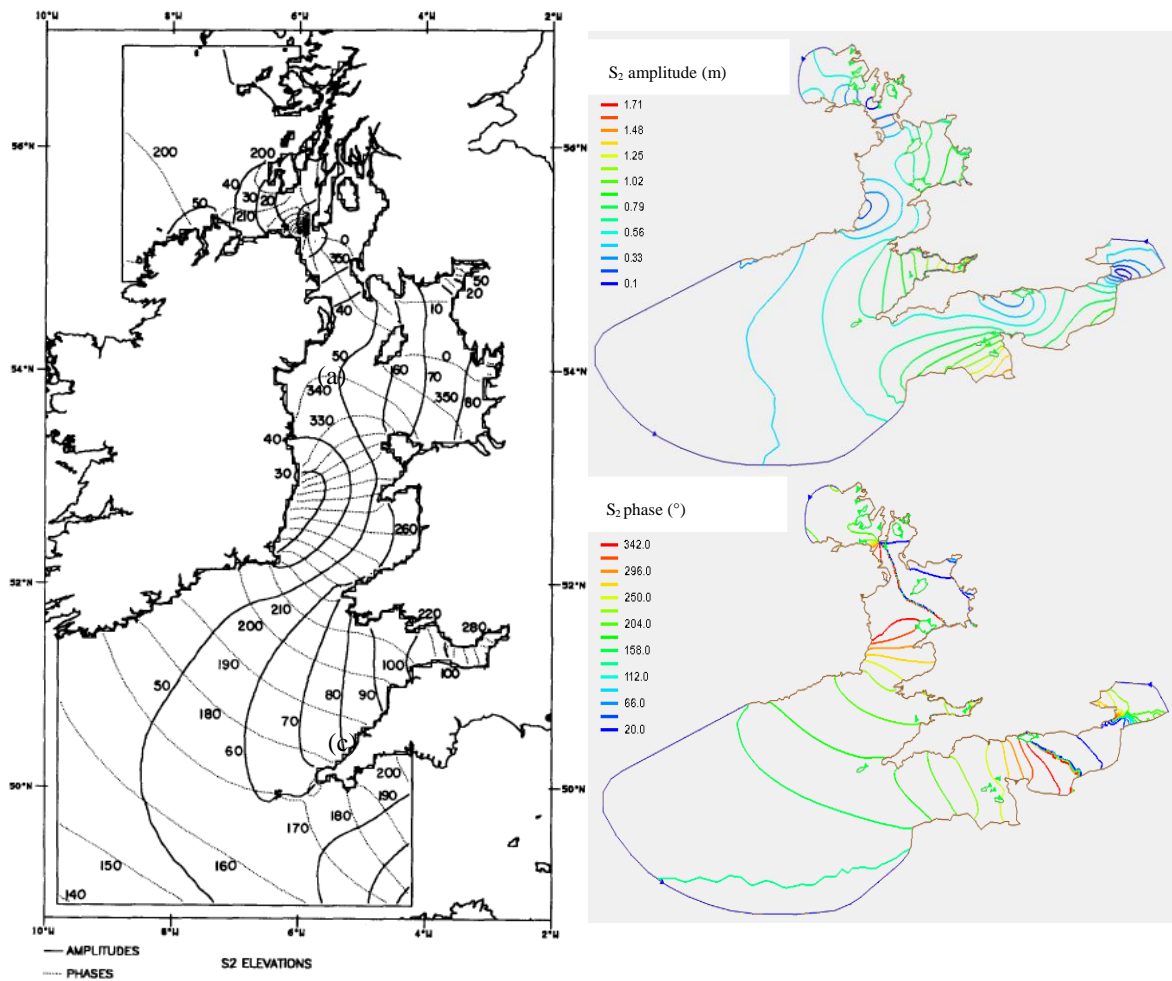
Fig 3.5 Comparison between the cotidal charts of phase (dashed line) and amplitude (solid line) from Davies and Jones' study (1992) and ADCIRC generated harmonic analysis for S_2 tidal component.

Since our focus is the Bristol Channel and we did not made any validation on the current data in this region, a comparison of tidal current data between the simulation results and the TotalTide software results was also made. The current magnitude between ADCIRC and TotalTide database has been made and the results are shown below. Three

stations are taken along the Bristol Channel, ST1 (51°23.23'N 3°05.07'W), ST2 (51°19.33'N 3°32.38'W) and ST3 (51°22.03'N 4°15.07'W) which are shown in Fig 3.6.
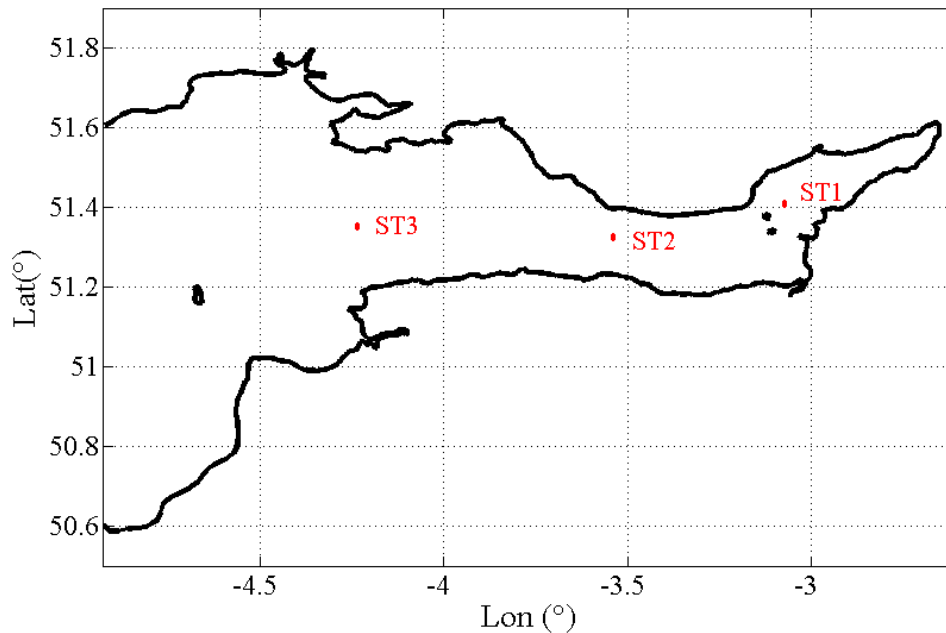
Fig 3.6 Bristol Channel model area and three observation stations.

It is seen from Fig 3.7 that the ADCIRC simulation results from ST2 and ST3 are very consistent with that from TotalTide, while for ST1 there is small discrepancy. The ADCIRC current magnitude is always 0.3ms^{-1} lower than that from TotalTide. This indicates that there is too much friction in the Channel head. ST1 is located in the Channel head where the water is very shallow and sensitive to many factors, such as wetting/drying and bed friction. Considering the difficulty of capturing all the physics in a shallow area using ADCIRC and the importance of model stability, it is acceptable that there is some difference between the two curves at ST1, and the overall results seem to give us confidence to further investigate the storm surge events in the Bristol Channel.
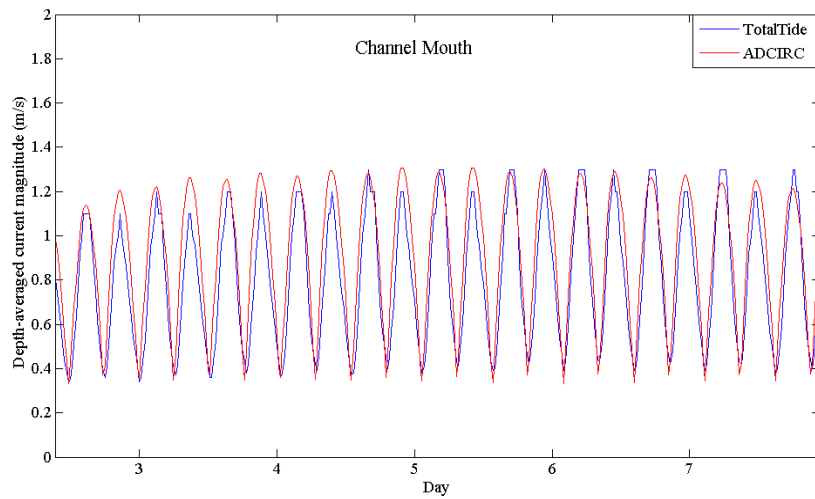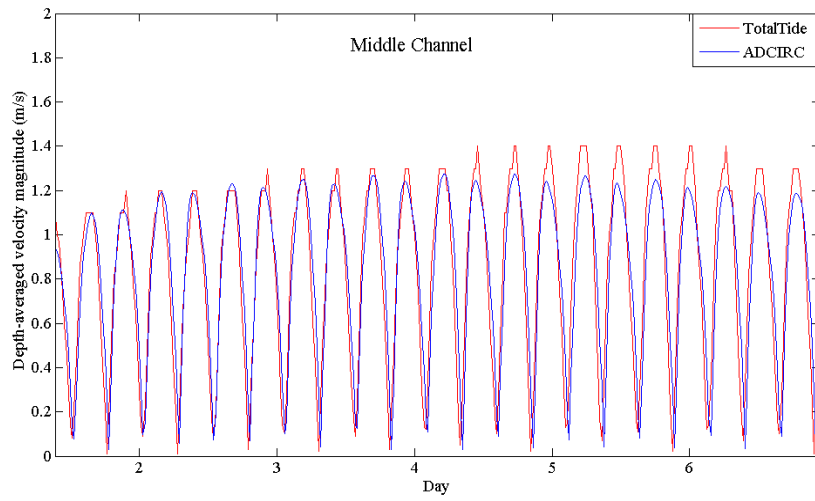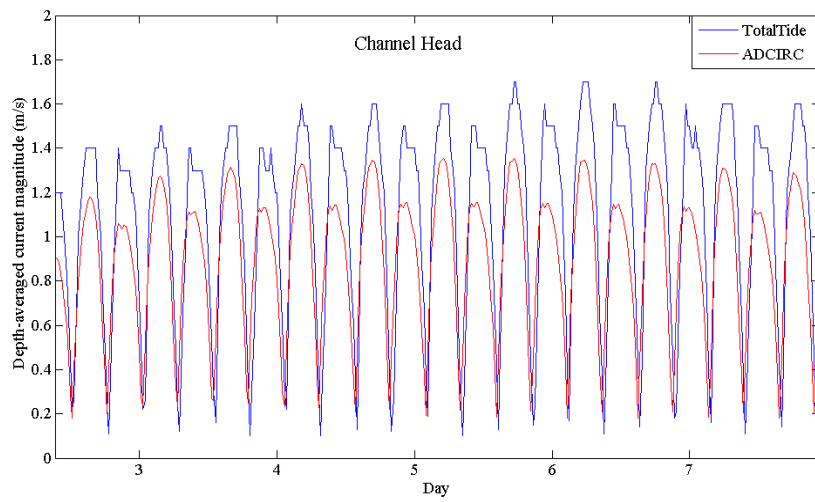
Fig 3.7 Comparison of depth-averaged current magnitude between ADCIRC against TotalTide database (ST1-Head, ST2-Middle, ST3-Mouth are from the top, middle and bottom figure respectively).

Chapter 4

Tidal resonance

4.1 Introduction

The Bristol Channel has one of the largest tidal ranges in the world. A key cause for this is the resonance with the dominant semi-diurnal tides. In this chapter we use numerical simulations to investigate this resonance. We first vary the frequency on the boundary of the model and examine at which frequency in the model is excited. Secondly, we apply a disturbance to the model and analyse the frequency at which it resonates. We examine the sensitivity of these results finding them sensitive to the bed friction used (with possible implications for energy extraction) but insensitive to small changes in the tidal amplitude on the boundary or the mean-water level. A modified version of this chapter was accepted for publication in the International Journal of Offshore and Polar Engineering (IJOPE) in January, 2017.

4.2 Quarter-wave tidal resonance?

Looking ahead the response of the system using the natural forcing frequency (ω/ω_{M_2}=1.0), it is found that the dominant frequency of the Bristol Channel response is larger than the natural frequency (Fig 4.2, Fig 4.3, Fig 4.6 and Fig 4.7). This indicates that the basin length of the Bristol Channel is shorter than the quarter wavelength required for resonance. This is consistent with the result when we compare the M_2 quarter wavelength with the length of the Channel. Tidal waves in the Bristol Channel behave as 'long waves' since their wavelength is much greater than the water depth implying vertical motion may be neglected. The wavelength of a shallow wave is given by the formula below:

$$L = \frac{2\pi\sqrt{gH}}{\omega},\qquad\qquad\qquad\qquad\qquad\qquad\qquad\qquad\qquad\qquad (4.1)$$

where g is the gravitational acceleration (ms^{-2}), H is the water depth (m) and ω is the angular frequency of the tidal component (radians s^{-1}) (Godin, 1993). If we take $H \approx 40m$ for the Bristol Channel, since $\omega = 1.405 \times 10^{-4} s^{-1}$ for the constituent M$_2$, we find $\frac{1}{4}L = 221km$ for the Bristol Channel. This model shows that the length of the Channel is around 160km, therefore somewhat shorter than an M$_2$ quarter wavelength. The tidal resonance theory indicates that the ocean basin must satisfy the well-known quarter wavelength requirement. Godin (1993) found that the restricted concept was a necessary but not sufficient condition for the phenomenon to occur, especially for deeper embayments. Serhadlıoğlu (2014) found the Bristol Channel is shorter than the quarter wavelength for the M$_2$ tidal period. The results presented in this paragraph agree with previous findings and suggest the quarter wavelength requirement may become more relaxed for shallow basins.

4.3 Resonant period

The M$_2$ response curves of the Bristol Channel have been investigated by exciting the model using artificially altered M$_2$ forcing frequencies (ω), and applying a ratio (ω/ω_{M_2}) varying between 0.5175 and 5.175 but with the same driving amplitude at the outer boundary. The simulated results of M$_2$ elevations were sampled at 16 model stations along the Bristol Channel and at 5 stations across the mid-Channel (Fig 4.1). Station C is overlapped with ST11.
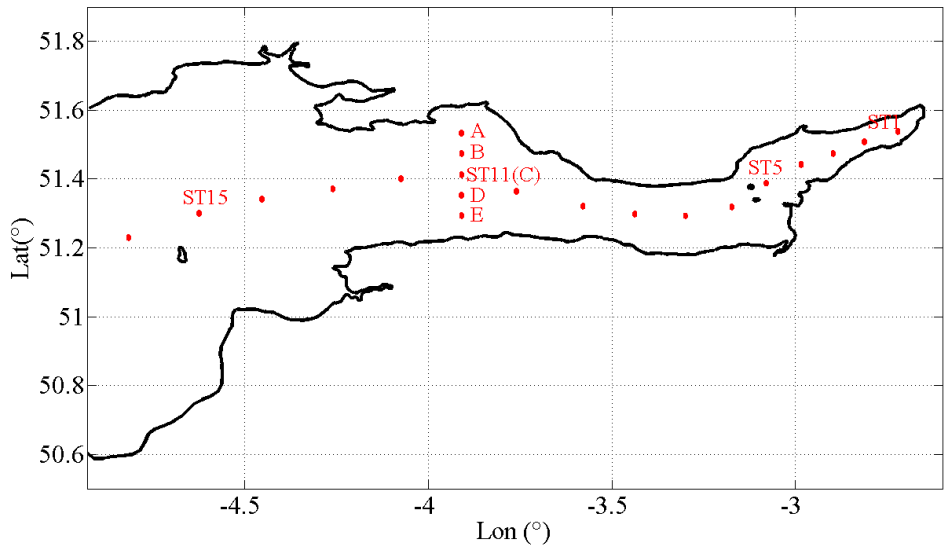
Fig 4.1 Sixteen stations along the Channel and 5 stations across the mid-Channel.

The response curves of several stations taken along the Bristol Channel are plotted in Fig 4.2, in which four stations (ST3/5/7/9) represent the inner section of the Channel while three stations (ST11/13/15) represent the outer Channel. In Fig 4.2, the response curves follow a similar pattern at all the stations considered, but differ in magnitude due to the location of the observation station. It is shown that all the stations
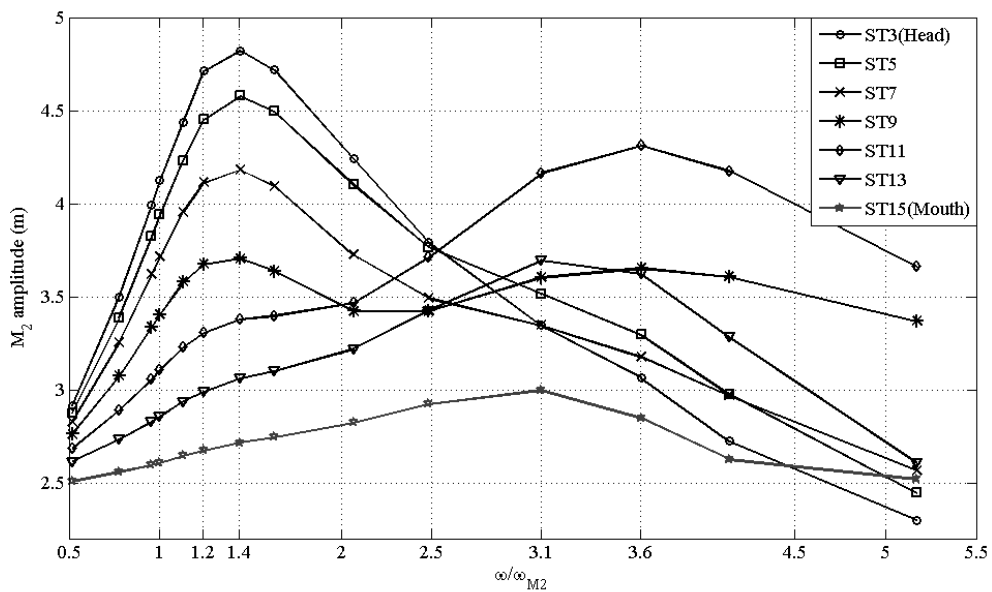
Fig 4.2 Response curves of several stations along the Bristol Channel: ST3, ST5, ST7 and ST9 represent the inner Channel response; ST11, ST13 and ST15 represent the outer Channel response.

show a peak in response at around a ratio of 1.2-1.4 which indicates the quarter wavelength resonance of the system with a period of approximately 8.6-10 hours. A second peak is observed at ω/ω_{M_2}=3.1-3.6 in the outer Channel, and the peak variation is seen to be very site-dependent. Equation (4.1) suggests, this may be a resonance occurring at the Channel entrance.

Fig 4.3 shows the response curves of all the five stations across the mid-Channel. It is seen that at around the forcing frequency of ω/ω_{M_2}=3-4 there is a significant increase in the M$_2$ amplitude response. When approaching the coasts, the response slightly increases which is probably due to the decrease in water depth. Increase of response amplitudes in Station A and B are more obvious, this may be attributed to the topography of the coast near them compared to the other side (see Fig 3.1).

The resonant period calculated from the model results is within range suggested by previous studies, which suggested a resonant period between 7.3-11.3 hours (see Chapter 2 Table 2.1). It should be noticed that the resonant period is consistently estimated to be longer when the Celtic Sea is included. The method used in this study was same with
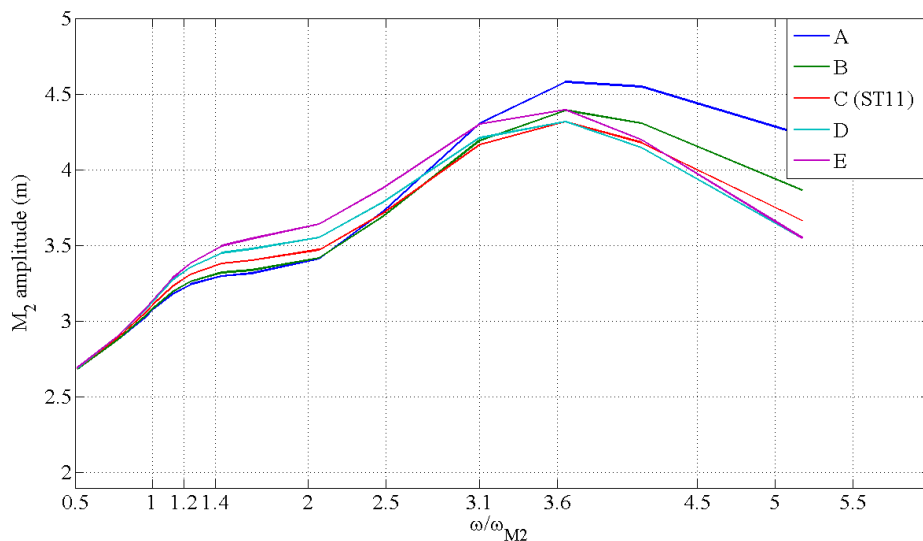
Fig 4.3 Response curves of stations across the mid-Channel near Swansea Bay.

Serhadlıoğlu (2014) but the dominant tidal period obtained here is slightly lower than that in her study. This subtle difference might be due to the coupled nature of two different modelling systems and this reason was also suggested by Serhadlıoğlu (2014). In the present study the model domain only includes the Bristol Channel while in Serhadlıoğlu's study the Irish Sea, the Celtic Sea, English Channel and the Bristol Channel are all included. Table 2.1 from Chapter 2 also indicate that when the Celtic Sea is included in the model the resonant period is likely to be larger compared to that only includes the Bristol Channel. Additionally, the present model applies a coarser mesh than the one of Serhadlıoğlu's. These may both contribute to the peak shift of the resonant response.

Fig 4.4 illustrates the amplification of the response along the Bristol Channel by normalising the response of the Channel by the elevation at the Channel mouth (blue curve). The figure also shows the amplification within the inner Channel (red curve) and in the outer Channel (green curve). The inner section of the Bristol Channel shows an
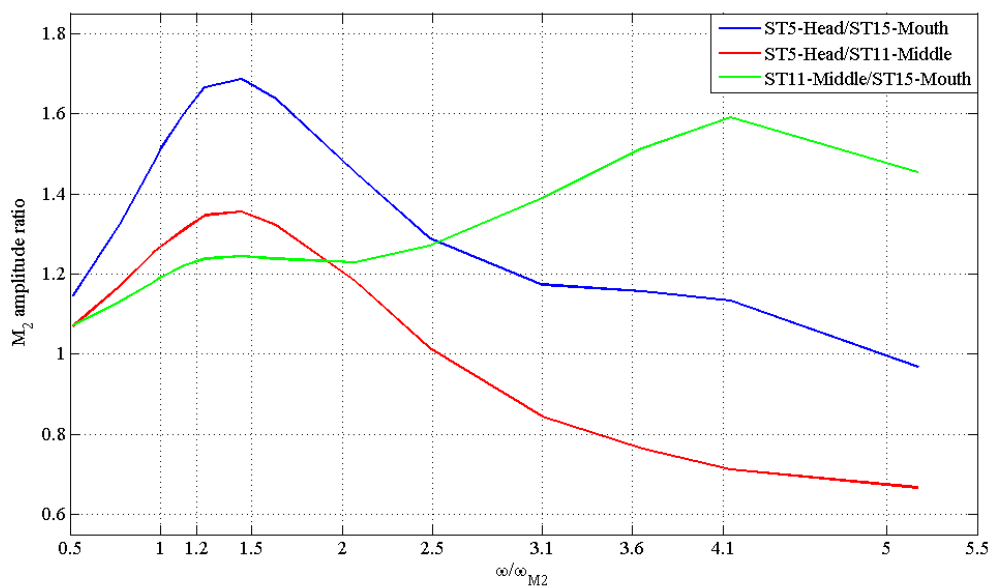
Fig 4.4 Amplification of the response observed in the Bristol Channel.

58

amplified response over the frequency range ω/ω_{M_2} ratio of 1.2-1.5 while the outer Channel exhibits an apparent resonance around the ratio of 4.1.

The result indicates a coupled resonant system of the Bristol Channel: the main peak might be the dominant resonant mode (ω/ω_{M_2} =1.3) of the Bristol Channel, while the second peak (ω/ω_{M_2}=4.1) might be due to the response of the Channel to the forcing at its mouth. This complicated resonance pattern was also found by Liang *et al*. (2014). They suggested that some regions in the outer Bristol Channel also experience significant, if not greater, resonances when the ω/ω_{M_2} ratio lies in the range of 3-6.

Fig 4.6 presents the comparison of M_2 response curves obtained from the original model and the results from three different boundary positions (shown in Fig 4.5). The model with boundary 2 (blue line) is the original one adopted in this study. Each ocean boundary is driven by same oscillation tidal frequency, but the M_2 amplitudes are different for each boundary and are interpolated from Serhadlıoğlu's model (2014) relevant to their position. It is seen that the peak at around ω/ω_{M_2}=1.2-1.4 is not shifted with changing
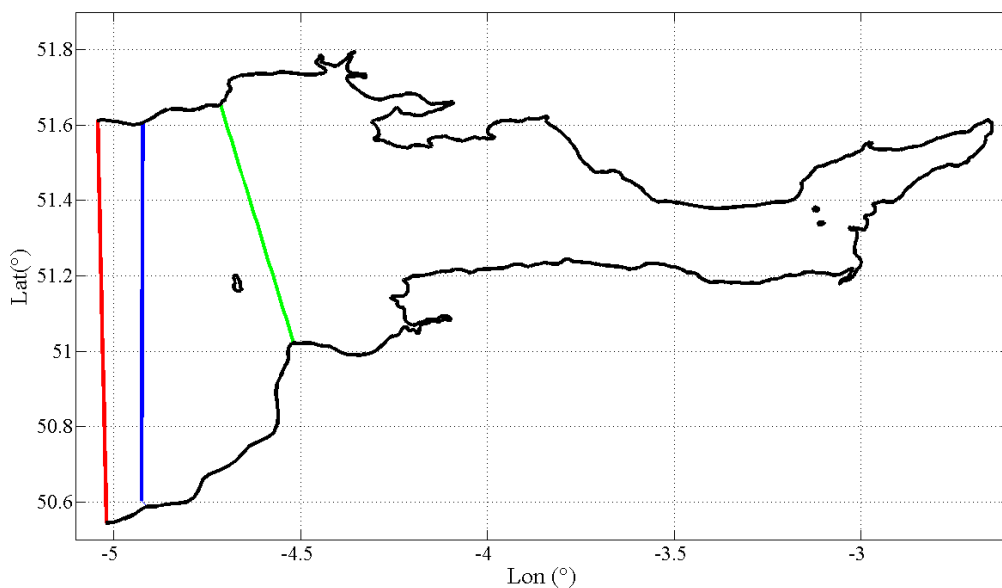
Fig 4.5 Model with boundary 1 (red), 2 (blue) and 3(green).

boundary position, while the second peak is apparently boundary-dependent because it is shifted from around a ratio of 3.1 to around 4.1 with the boundary moving up to the Channel head. This again indicates that the second peak should be the tidal response with the open boundary at the outer Channel. It is also worth noticing that the response amplitudes decrease with the boundary position moving from the ocean to the Channel head. Therefore, in the present study, the dominant resonant mode of the M_2 response in the Bristol Channel is hardly affected by the slight changing of boundary position.
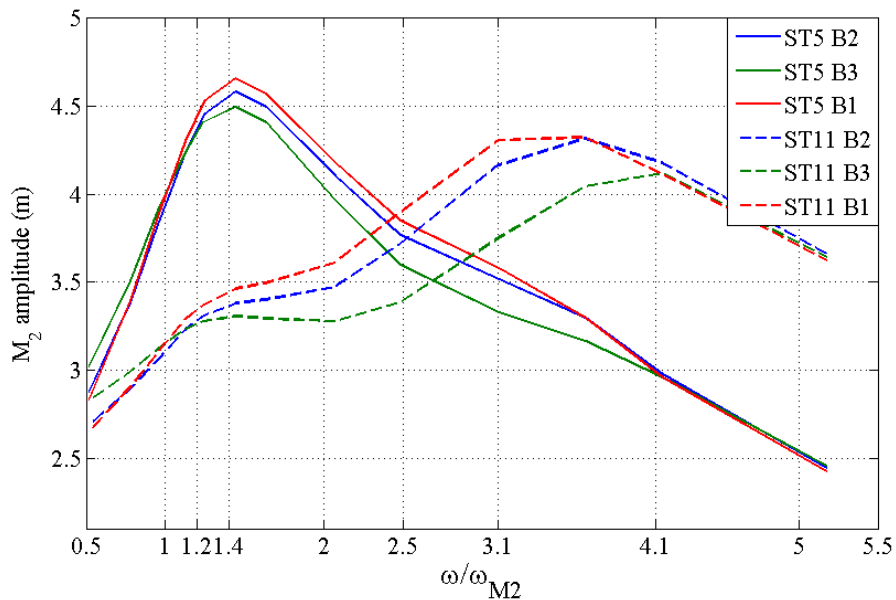
Fig 4.6 Response curves of ST5 and ST11 with different boundary positions.

The Bristol Channel is a complex hydrodynamic system and sensitive to small changes. Factors such as bed friction can have influences on the resonant period. As seen in Fig 4.7, it is obvious that the amplitudes of M_2 response curves drop with increasing bed friction coefficient. However, we also find that the bed friction can affect the resonant period since a shift of the peak can be seen from a ratio of $\omega/\omega_{M_2} = 1.3$ to $\omega/\omega_{M_2} = 1.5$ in the inner Channel (ST6). Even for simple mass-spring-damper systems changing only the damping

can significantly shift the frequency of the resonant peak response.

There is obviously a great deal of interest in extracting energy from the Bristol Channel, and adding bottom friction would be a simplistic representation of modelling this in the model. This implies that the impact of resonances on the Channel should be taken into account by tidal energy development.
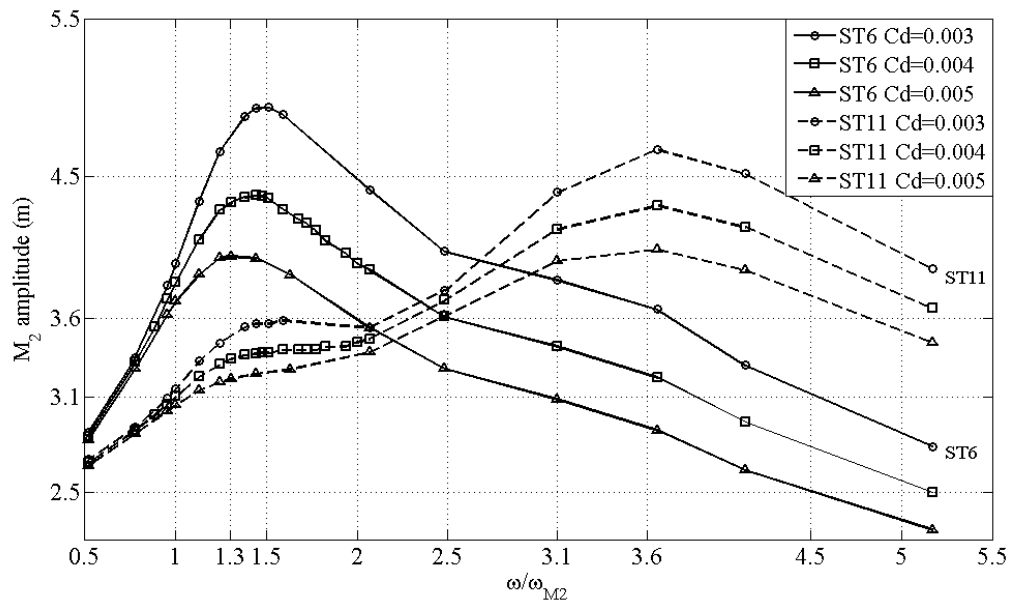
Fig 4.7 Response curves of ST5 and ST11 with different bed frictions.

4.4 Sensitivity tests

The results of the sensitivity tests on water level, 18.6-year nodal cycle and bed friction in both inner (ST5) and outer (ST11) parts of the Channel are shown in Fig 4.8. The response tides are driven by tidal forcing of M_2 constituent.

Sea level rise (SLR) is the dominant influence on any far-field impacts and has influenced the tidal regimes in the past. In the present study, however, with water level varying from 4m lower to 4m higher than the real situation, the tidal heights do not present visible change in the Bristol Channel. Pickering *et al.* (2012) and Ward *et al.* (2012) have
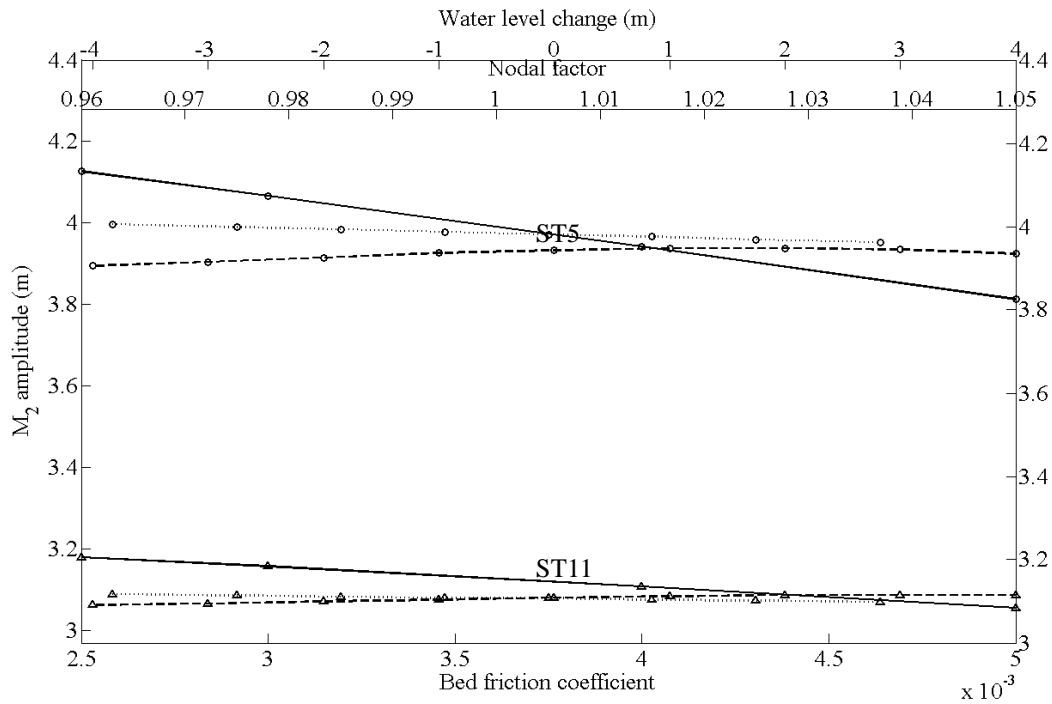
Fig 4.8 Sensitivity test results on water level (dashed lines), 18.6-year nodal cycle (dotted lines) and bed friction (solid lines) at ST5 (lines with circle markers) and ST11 (lines with triangle markers).

investigated the effects how large levels of future SLR may impact on the tides on the European Shelf and both studies found significant but contrasting results. Pickering *et al.* (2012) found that varying the water level may alter the oscillation period and moves it away from resonance causing the decreases in tidal range. However, Ward *et al.* (2012) showed even moderate SLR may have significant impact on the tides on the European shelf. Pelling *et al.* (2013) found that the way sea level rise was implemented-whether land was allowed to flood (or not)-significantly affected the response of the tides to SLR, as the newly flooded areas change the distribution of tidal energy dissipation. Later in 2014, Pelling and Green (2014) investigated the response of the tides on the European Shelf to realistic levels of SLR, implemented with three levels of present day coastal defences. Surprisingly, they found the largest response was simulated when flood defences were implemented allowing only part of the coastline to flood. They explained the results by a

combination of a change in the magnitude and spatial distribution of tidal energy dissipation and resonance effects in the Irish Sea. All these studies show how sensitive regional tidal systems can be to SLR which is same with what our sensitivity test indicates, and our results agree with Pickering *et al.*'s findings (2012). In this study, the sea level rise/fall effect is done by increasing/decreasing the bathymetry of the model mesh. This means many intertidal areas in the original model may now be always wet after increasing the bathymetry. Variation in bathymetry will cause significant influence in reality but may not be indicated by the present model results. Therefore, this may also indicate one of the limitations of the model.

The angle between the plane of the Moon's orbit around the earth and the plane through the equator of the Earth varies with a period of 18.6 years, and the nodal tidal cycle is usually represented as a linear modulating factor in the calculation of the tidal amplitudes (Adcock *et al*., 2014). Thus for the M$_2$ constituent:

$$\eta_{M2} = f_{M2} \times a_{M2} \cos(\omega_{M2} t + \alpha), \tag{4.2}$$

where η_{M2} is the water level variation at the frequency of M$_2$, f_{M2} is the nodal factor, a_{M2} is the amplitude of the M$_2$ constituent, ω_{M2} is the frequency of the M$_2$ tide and α its phase. M$_2$ was the only tidal constituent used in this model, therefore f_{M2} dominates the annual water level variation. Over a period of 9.3 years, the M$_2$ nodal factor changes from its minimum value 0.96, to its maximum 1.04; however, during this time period the relative response of M$_2$ tidal heights almost remain unchanged. This suggests the response is essentially linear over the range of interest.

The bed friction is seen to be the dominant effect on the tidal response, since the M$_2$

amplitude at ST11 decreases by around 0.2m with the quadratic friction coefficient increasing from 0.0025 to 0.005. The bed friction has even greater influence on the shallower areas: at ST5 the amplitude change reaches more than 0.3m. In nature the forced resonant oscillations cannot grow indefinitely because the leakage of energy due to friction increases more rapidly than the amplitudes of the oscillations themselves. Tidal amplitude is strongly affected by frictional resistance especially in shallow channels. When friction is incorporated, the progressive waves are damped so that the elevation decreases with distance in the wave propagation direction, and the reflected waves may also travel along with lower amplitudes (Allen, 2009).

4.5 Response to disturbances

An alternative approach to investigating the resonant frequency is to examine the response to disturbances. In this case we apply a shear stress, which can be thought of as surface forcing due to wind, and examine the subsequent oscillations once the wind is removed. Simulations were run with winds blowing over the whole model domain from five different directions: South, Southwest, West, Northwest and North. The wind applied here is created using MATLAB code and varies linearly with time. In this section the modelling area includes not only the Bristol Channel, but also the Celtic Sea, the Irish Sea and the English Channel, which is the same model used in the next chapter (see also Chapter 3 for more model details).

Five locations in the upper Channel: Avonmouth, Hinkley Point, Newport, Ilfracombe and Mumbles were selected as the model sites (Fig 4.9). Simulations were set to increase the winds from 0 to 30ms^{-1} on Day 7 from 00:00 to 12:00, keep constant from Day 7 12:00
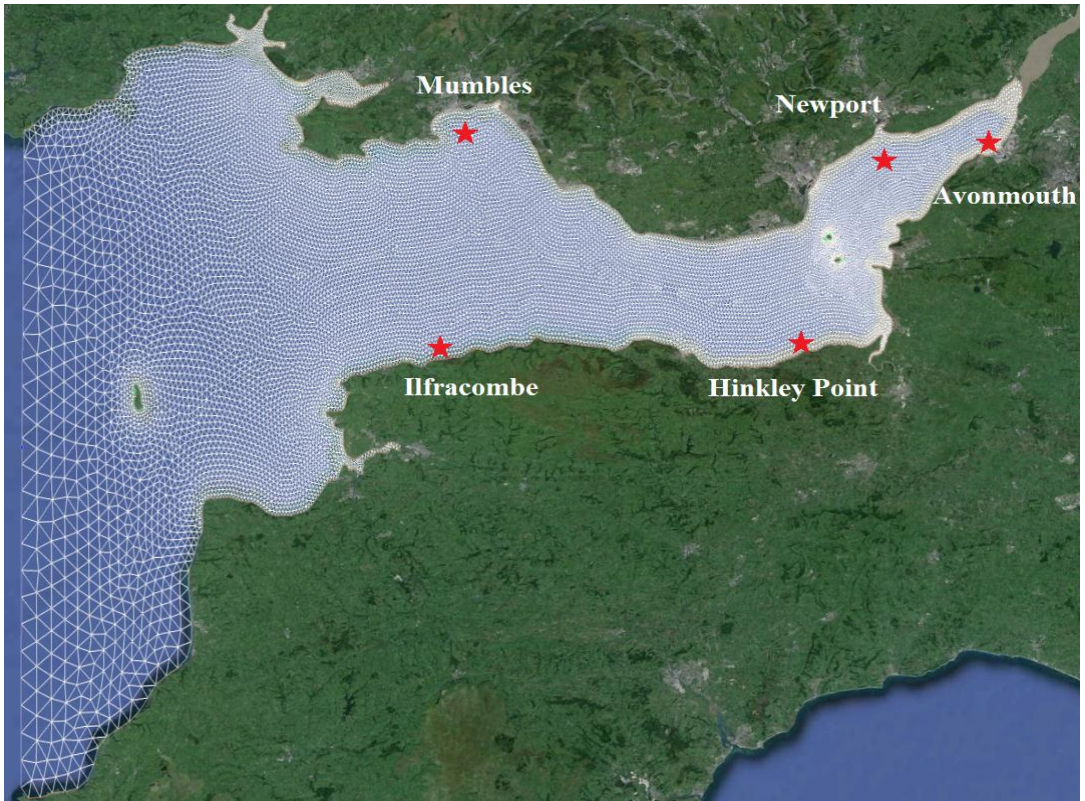
Fig 4.9 Model mesh shown in Google Earth with five observation stations (Avonmouth, Newport, Hinkley Point, Mumbles and Ilfracombe).
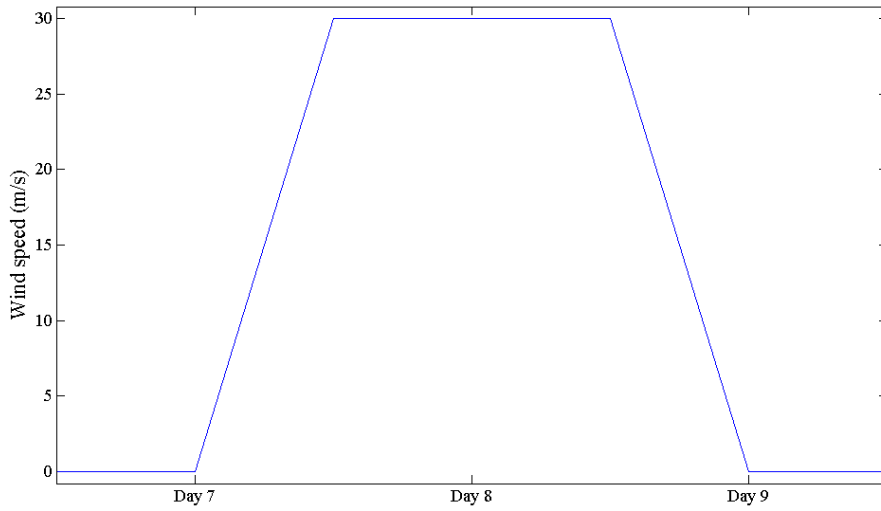
Fig 4.10 Variation of input wind forcing with time.

to Day 8 12:00, then decrease to 0 from Day 8 12:00 to Day 9 00:00 (Fig 4.10).

On Day 9 the Southerly winds stops but it is seen in Fig 4.11 that the surge overshoots and becomes negative. Higher frequency oscillations can be seen between Day 9 and Day 10. The cause for this is unclear and might worth further investigation in future studies. From Day 10 the residuals display the development of oscillations with similar period and heights ranging from around -0.2m to 0.2m in all the five sites. It takes around four days for the oscillations to decay. An explanation for the development of such oscillations would be that the system is freely resonating.
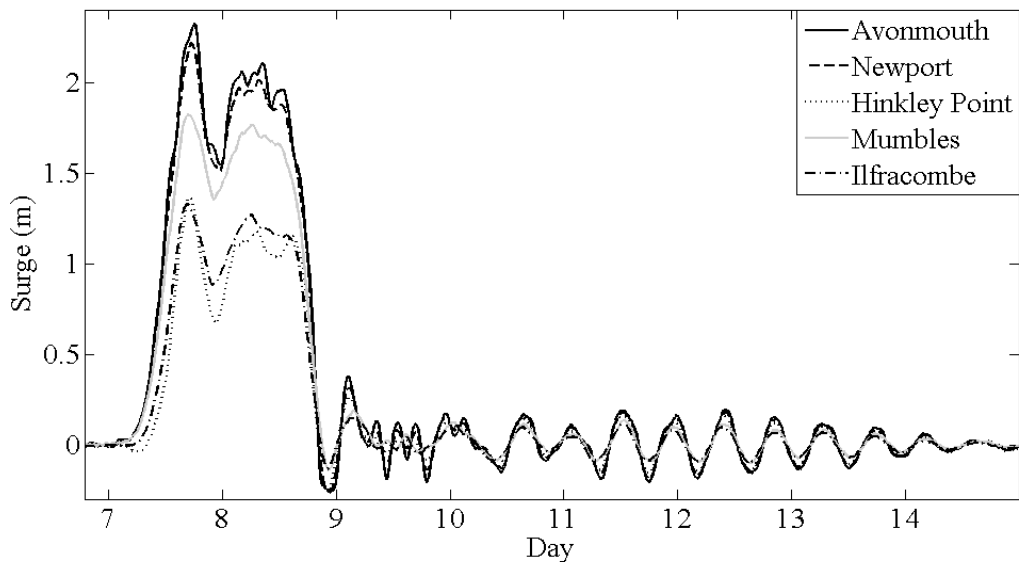
Fig 4.11 Wind-driven surge at Avonmouth, Newport, Hinkley Point, Mumbles and Ilfracombe. Repetitive oscillations can be seen at all five stations after Southerly winds stop running.

The Fast Fourier Transform (FFT) was used as the source of information from which the period of resonance can be determined. Surge data from Day 11 to Day 14 (Fig 4.11) was taken for FFT analysis. Fig 4.12 shows the normalised amplitude spectrum by the peak response over a period of surges that resulted from South-Westerly winds at all the

five locations in the Channel. A dominant peak can be seen which indicates the dominant

oscillation period of around 10.3 hours. Similar results occurred when wind from different

directions were used. This matches the resonance period of the Bristol Channel found in

this study (8-10 hours).
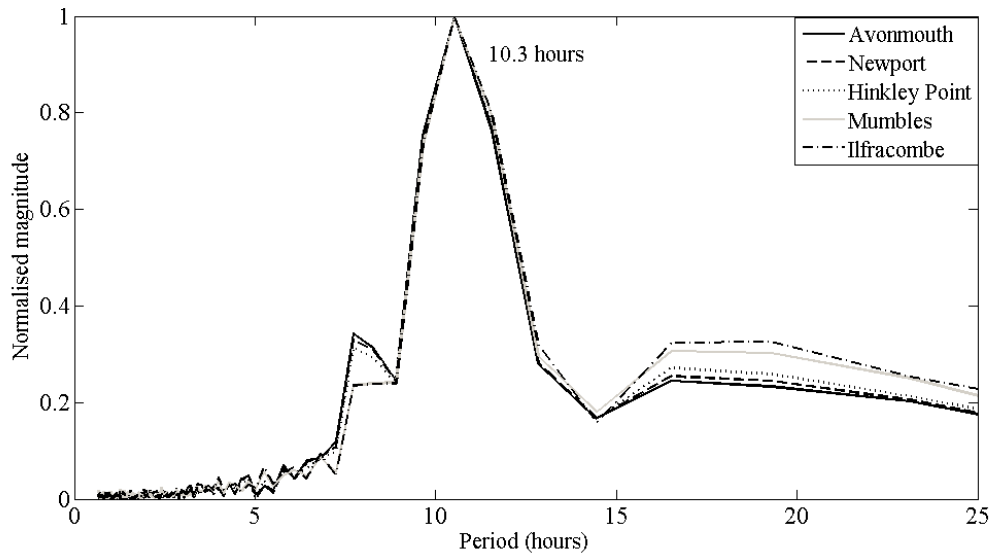
Fig 4.12 Normalised magnitude spectrum over period of surge with South-Westerly winds imposed at Avonmouth, Newport, Hinkley Point, Mumbles, and Ilfracombe.

Webb (2013) investigated the resonances of the English Channel and Irish Sea by

running a rewritten Arakawa C-grid model code (Arakawa, 1966), based on the

energy-conserving form of the shallow-water equations, at angular frequencies between 0

and 30 radians per day. On the open boundary the model was forced with Atlantic

semi-diurnal and diurnal tides. The modelling results showed the key resonances have real

angular velocity between 13 and 14 radians per day, which means the resonant period is

between 10.8 and 11.6 hours. He also found the amplitude responses peaked between 20

and 30 radians per day, suggesting the resonant periods of 5 and 8 hours; however these

modes have a more complicated structure and it was more difficult to relate the modes to

specific physical features of the system. The results in Fig 4.11 indicate that the Bristol Channel is a coupled resonance system with a dominant resonant period of 10.3 hours but with other less significant resonance. The key resonant periods of 7.8 hours and 17 hours resonance are also found but the cause is unclear. This is in close agreement with Webb's study and also Liang *et al.* (2014) and Serhadlıoğlu (2014)'s, which suggested a coupled resonance system in the Bristol Channel.

If zooming in Fig 4.11, oscillation with higher frequencies can be found from Day 9 to Day 10. Therefore, we use the FFT analysis to investigate the magnitude spectrum of wind-driven surge between Day 9 and Day 10. Fig 4.13 shows that at the Channel head (Avonmouth, Newport and Hinkely Point) the surge oscillation frequencies are higher and more complicated; while at the mid-Channel (Mumbles and Ilfracombe) the surge oscillation frequencies are lower.
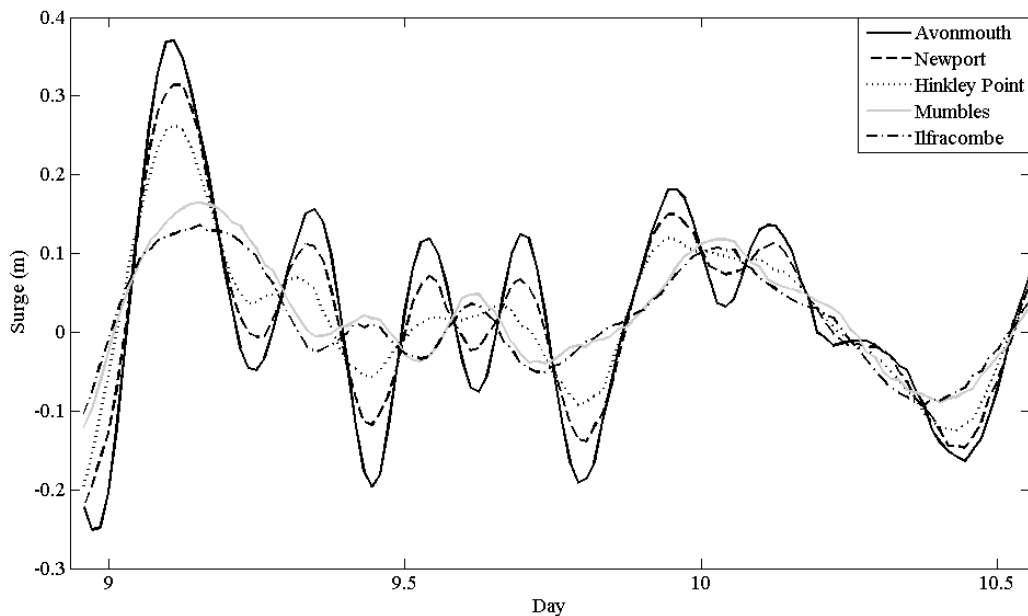
Fig 4.13 Wind-driven surge at Avonmouth, Newport, Hinkley Point, Mumbles and Ilfracombe between Day 9 and Day 10.

The FFT analysis was used taken the surge data from Day 9 to Day 10. Fig 4.14 shows the amplitude spectrum over a period of surges that resulted from Southerly winds at all the five locations in the Channel. We use Avonmouth and Mumbles to represent the Channel head and the mid-Channel respectively. The dominant resonant mode (10.3 hours) and the 17-hour resonance can still be found in the analysis results. At Avonmouth, resonant periods of 4 hours, 5 hours and 7 hours can also be found; whereas at Mumbles, only a 5-hour resonant period can be found. The reason for these higher frequencies oscillations is not clear but this again suggests that the Bristol Channel is a complex system with coupled resonances going on.
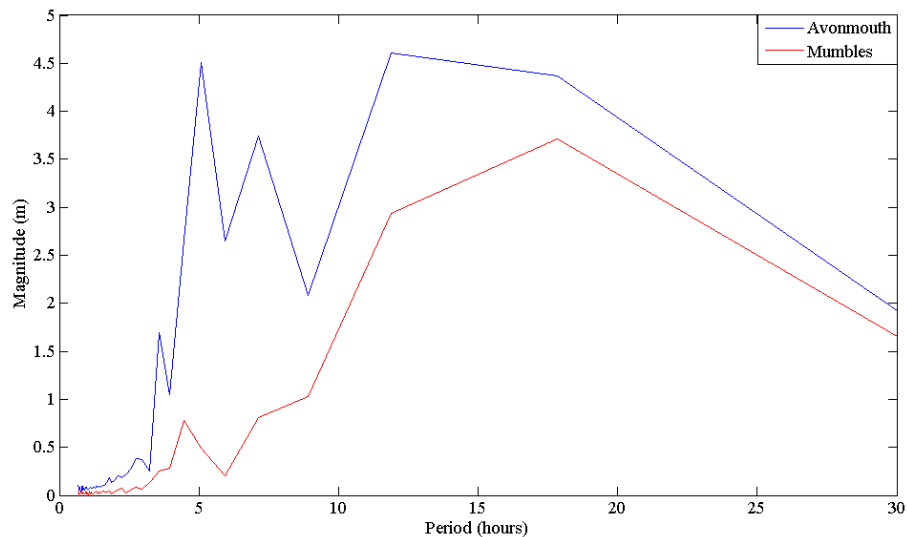
Fig 4.14 Magnitude spectrum over period of surge with Southerly winds imposed at Avonmouth and Mumbles.

Rather than applying a wind disturbance over the whole model domain and exciting the model with various tidal forcing frequencies at the ocean boundary, here we suggest another way of investigating the dynamics, which would be to raise the water level in the Bristol Channel, and drive the model with surge offset between the outer levels with inner levels in the Bristol Channel. This will likely to get an equivalent sloshing effect with the results in this chapter.

Chapter 5

Storm surge

5.1 Introduction

Storm surge caused by atmospheric forcing can be devastating, with long-lasting and diverse consequences. Historically, the UK has suffered major storm surge events. In this study our focuses are on the Bristol Channel. In this chapter, the statistical analyses are first applied to understand the surge and wind in the Bristol Channel, then dynamic model studies are applied to investigate the potential conditions under which a large surge might occur. When analysing the results, we use the term "residual" when implying the difference between overall water levels and predicted tidal levels governed by the wind stress and local atmospheric pressure; otherwise, we refer to "surge" which is a genuine meteorological without tidal contribution to sea level (see Fig 5.1 and Fig 5.10). We also discuss the skew surge, which is the difference between the maximum observed sea level and the maximum predicted tide regardless of their timing during the tidal cycle.

5.2 Return levels

The term 'storm surge' means a rise/fall of sea level generated by a meteorological event, and is usually defined as the difference between the observed and predicted tidal levels in statistical analysis. The characteristics of the storm surge events in the Bristol Channel are first examined using statistics derived from the measured data from the British Oceanographic Data Centre (BODC: www.bodc.ac.uk) where the residual is the difference between the harmonic prediction of the tide and the measured water level. The sample

intervals are one hour from 1961 to 1992 and fifteen minutes from 1993 to 2015. Fig 5.1

presents the measured water levels and the residuals in January 2012 at Avonmouth. It is

noticed that the magnitude of residual during neap tide is slightly higher than that during

spring tide. Further investigation will be conducted in the numerical modelling analysis.
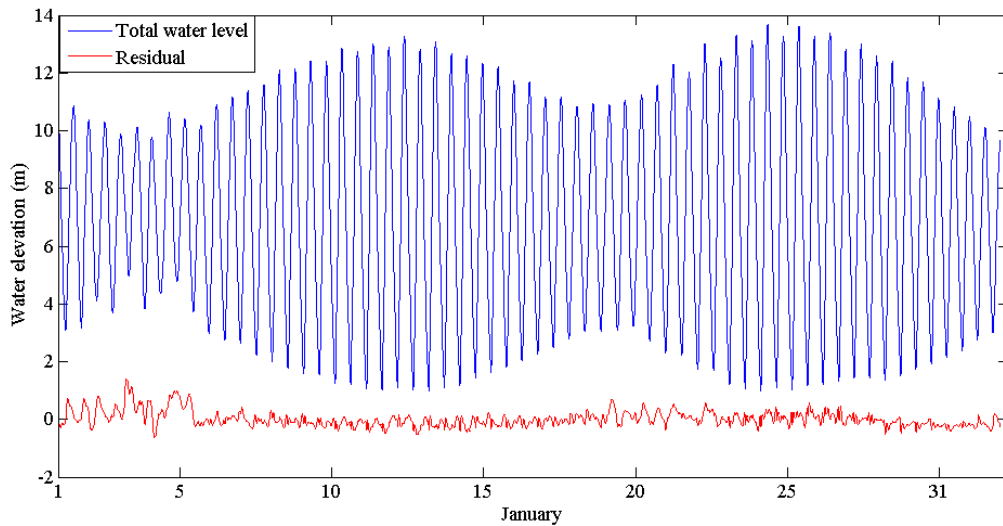
Fig 5.1 An example time-series of total water levels and residuals data at Avonmouth, 2012
(data accessed from BODC).

Our study is restricted to the five sites (Avonmouth, Newport, Hinkley Point, Mumbles

and Ilfracombe) for which sea level records are available for 20 or more of the years in the

period 1961-2015 and the observed data periods used in this study are different for each

station (Fig 5.2). The total raw data has around 10% of the data missing. Some missing

data are the whole data from a single month in a year, some are the data of few days during

which the water levels may be so extreme that the recorders broke down. The Hinkley

Point and Newport stations show missing data fractions less than 5% of complete data, the

Ilfracombe and Mumbles stations show missing data fractions less than 15%, while the

Avonmouth station shows missing data fractions less than 20%. When we are doing the

statistical analysis we only analyse the available data (i.e. ignoring the missing data),

therefore the data is slightly biased. We define annual data starting from July to June of the next year so that winter storms are not split between different years; and the winter, autumn and spring data from December to February, from September to November and from March to May respectively.
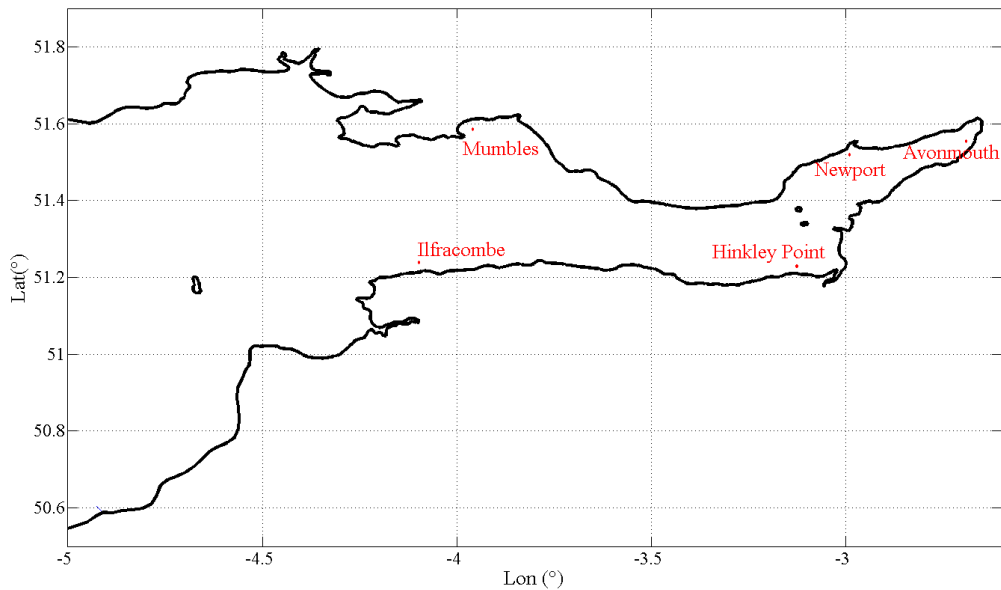
Fig 5.2 Map of measuring stations in the Bristol Channel.

All the measured residual data (difference between observed water levels and predicted tidal levels) are fitted to a GEV distribution (see Chapter 2, Equation 2.12) to estimate the 1 in 10 and 1 in 50 year return levels of storm surge (Table 5.1). A simple parametric bootstrap approach has been used for estimating the efficiency of the three parameters derived from GEV distribution. 200 re-samples have been used for 1000 times of bootstrapping at each of the five locations in the Bristol Channel, and the means of the bootstrapping estimates are shown in Table 5.1. In general, storm surges are higher at locations closer to the Channel head than that near the Channel mouth: the 1 in 50 year level annual maximum at Avonmouth (2.97m) is nearly double of that at Ilfracombe (1.7m). This could correspond with the resonance of the Channel and the funneling effect.

The winter maxima estimates are relatively close to the annual maxima but slightly smaller, indicating the storm surges are most likely to occur in winter months when winds are strong with low atmospheric pressure. The autumn maximum estimates at most of the locations are around 20% lower than the annual maxima, while the spring maximum estimates are around 30% lower, except for Ilfracombe where the autumn maxima are about 30% lower than the annual maxima and the spring maxima are about 15% lower. Despite the fact that limited data points and gaps in data lead to some uncertainty in bootstrapped data, the results from bootstrapping seem to be consistent with the estimates from original data giving confidence that the general trend has been identified (Table 5.1).

	Location		Return period (years)	Annual return level (m)	Mean of bootstrapped estimate of annual return level (m)	Winter return level (m)	Autumn return level (m)	Spring Return level (m)
	Lat (N)	Lon (W)						
Avonmouth	51°30' 39.2''	02°42' 53.9''	10	2.47	2.45	2.33	1.92	1.72
			50	2.97	2.96	2.96	2.33	2.19
Newport	51°33' 00.0''	02°59' 14.8''	10	2.26	2.30	2.20	1.77	1.56
			50	2.67	2.71	2.64	2.10	1.96
Hinkley Point	51°12' 54.9''	03°08' 03.6''	10	1.88	1.87	1.87	1.35	1.22
			50	2.26	2.27	2.27	1.59	1.68
Mumbles	51°34' 12.0''	03°58' 31.6''	10	1.51	1.52	1.46	1.14	0.95
			50	2.18	2.40	2.03	1.35	1.24
Ilfracombe	51°12' 39.5''	04°06' 39.4''	10	1.38	1.38	1.27	0.99	1.10
			50	1.70	1.69	1.66	1.22	1.56

Table 5.1 Annual and seasonal estimates of 10-year and 50-year return levels and annual bootstrapped estimates.

Table 5.2 summarises the interpolated estimates of 1 in 10 years return levels of the residual data (difference between measured water levels and predicted tidal levels) by taking the fourth annual maximum from the 44-year annual surge maxima. By comparing Table 5.1 and Table 5.2, it is found that the interpolated results generally agree well with the GEV estimates of the 1 in 10 years return levels. However it should be noticed that, the GEV fit for Mumbles overestimates the return levels by around 15%. This may be due to lack of extreme surge data at this location.

	Location		Return period (years)	Annual return level (m)	Winter return level (m)	Autumn return level (m)	Spring return level (m)
	Lat (N)	Lon (W)					
Avonmouth	51°30' 39.2''	02°42' 53.9''	10	2.47	2.36	1.81	1.70
Newport	51°33' 00.0''	02°59' 14.8''	10	2.15	2.15	1.69	1.46
Hinkley Point	51°12' 54.9''	03°08' 03.6''	10	1.86	1.79	1.22	1.08
Mumbles	51°34' 12.0''	03°58' 31.6''	10	1.32	1.30	0.91	0.76
Ilfracombe	51°12' 39.5''	04°06' 39.4''	10	1.47	1.38	0.91	1.09

Table 5.2 Interpolated annual and seasonal estimates of 10-year return levels.

Recently, some studies demonstrated that in a tidal regime the best measure of a storm surge is the skew surge, which is the difference between the observed and predicted high water within a tidal cycle (Fig 5.3). Table 5.3 summarises the GEV and interpolated estimates (taking the fourth annual maximum value from 44-year of annual maxima) of the return levels of the annual skew surge maxima. It is found that the return levels of skew surges are always lower than that of the residuals. This is because meteorological effects can have a notable effect on sea level and can alter the timing of tide. Williams *et al.*
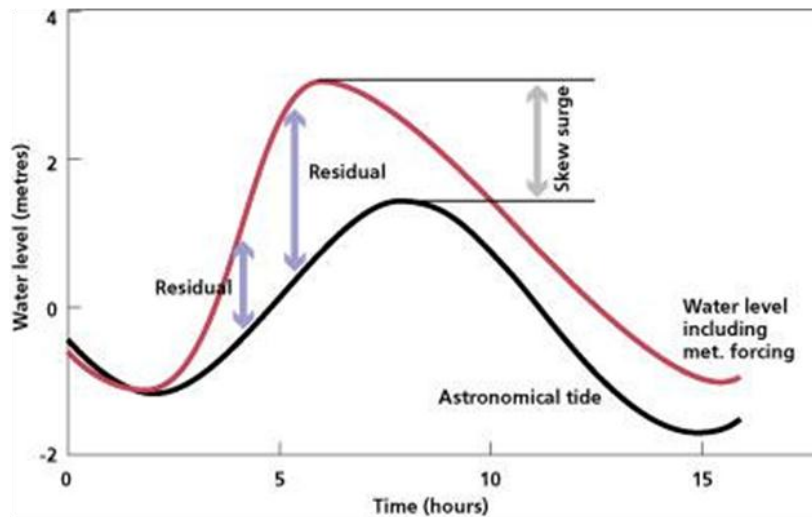
Fig 5.3 Schematic of a skew surge (www.ntslf.org).

(2016) found that the magnitude of high water exerts no influence on the size of the most
extreme skew surges. This is essential for understanding worst-case scenarios, because the
lack of skew surge generation dependency on water depth emphasizes the dominant
natural variability of weather system in an observation-based analysis. Understanding the
relationship between skew surge and tide will avoid misleading conclusions for future
impacts being drawn from nontidal residual properties.

	Location		Return period (years)	GEV annual return level (m)	Interpolated return level (m)
	Lat (N)	Lon (W)			
Avonmouth	51°30' 39.2''	02°42' 53.9''	10	1.69	1.68
			50	2.64	
Newport	51°33' 00.0''	02°59' 14.8''	10	1.36	1.22
			50	1.79	
Hinkley Point	51°12' 54.9''	03°08' 03.6''	10	1.12	1.04
			50	1.57	
Mumbles	51°34' 12.0''	03°58' 31.6''	10	0.89	0.79
			50	1.34	
Ilfracombe	51°12' 39.5''	04°06' 39.4''	10	0.823	0.94
			50	1.064	

Table 5.3 Interpolated annual and seasonal estimates of return levels of the annual skew surge maxima.

Fig 5.4 illustrates the relationship between storm surge and return period ranging from 5 years to 1000 years in the Bristol Channel. The return period is estimated using the GEV distribution and is plotted on a logarithmic scale with base 10. Given the nature of the data it is clear that caution must be used in interpreting the higher return periods on this figure. It is seen from Table 5.1 and Fig 5.4 that the Channel head should be paid greater attention for dynamic modelling due to its high storm surges at various return levels. The curve of Mumbles is the steepest with the highest predicted long-term storm surges. Fig 5.5 shows the 95% and 5% confidence intervals for the estimates of all the five locations using bootstrap. It is seen that the data from Avonmouth and Ilfracombe show best guess of the return levels among the five stations, while Hinkely Point and Newport have wider 95% confidence intervals. The width of 95% confidence interval is the widest at Mumbles which indicates the lowest accuracy of the estimate at this location. There are only 22 annual maximum values available for analysis for Mumbles, while for other locations the
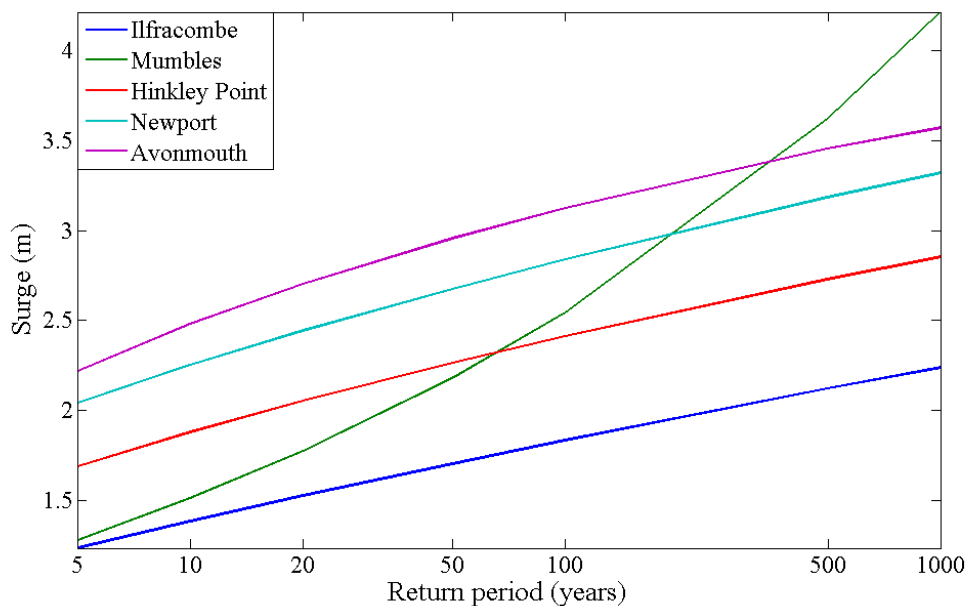
Fig 5.4 Annual estimates of 5-, 10-, 20-, 50-, 100-, 500- and 1000-year return levels
of residual at Ilfracombe, Mumbles, Hinkley Point, Newport and Avonmouth.

annual maximum values are more than 30. This may have compromised the analysis of this station and lead to lower quality of the fitting curve for Mumbles.
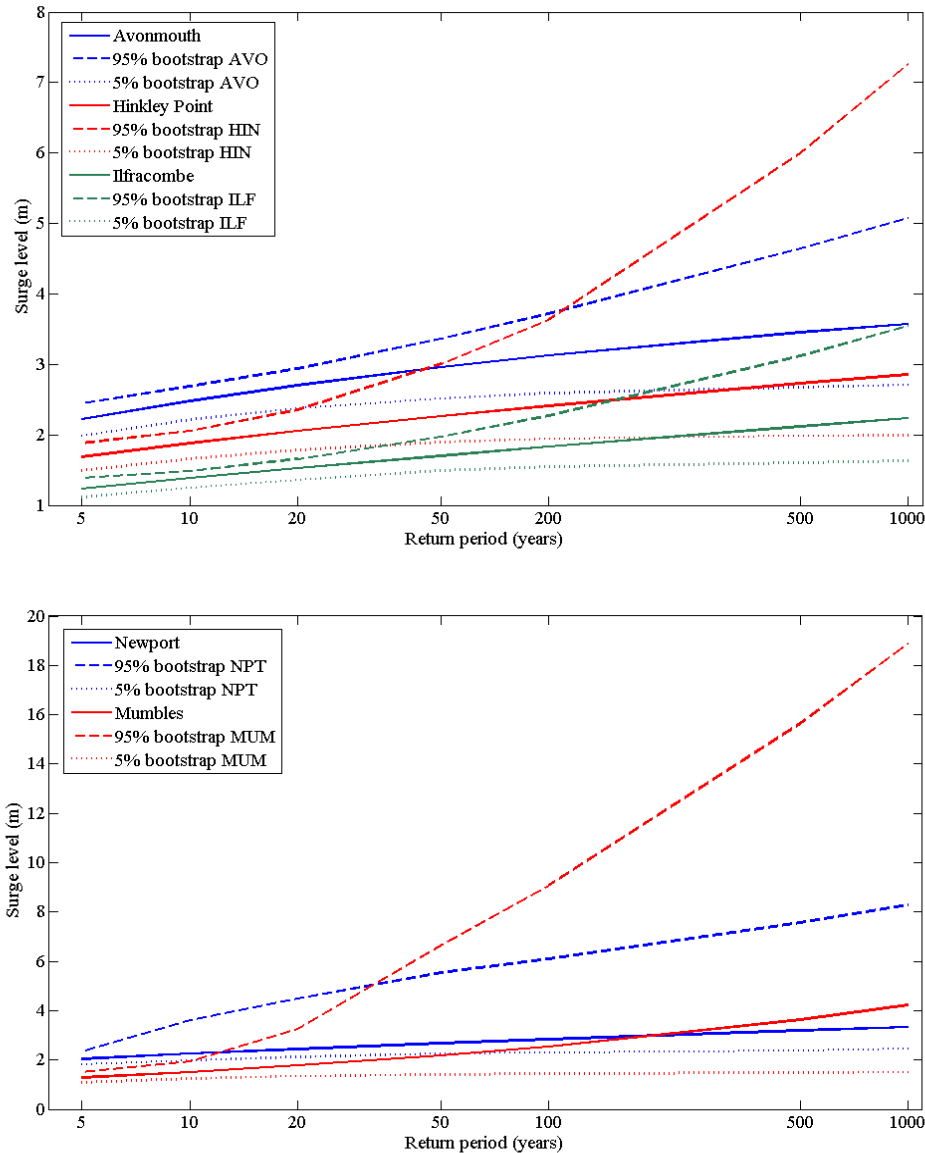
Fig 5.5 Annual estimates of 5-, 10-, 20-, 50-, 100-, 500- and 1000-year return levels of residual at: Avonmouth, Hinkley Point, Ilfracombe (top figure), Newport and Mumbles (bottom figure) with confidence intervals.

It is seen from the statistics that the Channel head should be paid more attention for dynamic modelling due to its high storm surges at 10- and 50-year return levels, thus Avonmouth is chosen to be a main observational site. The seasonal variation of the storm surge heights are strongly influenced by the seasonably varied wind speed and direction,

and their relation is investigated in the following study.

5.3 Atmospheric data 1979-2014

The atmospheric data used here was the ERA-Interim reanalysis data produced by the European Centre for Medium-Range Weather Forecasts (ECMWF) (Dee *et al.*, 2011). The ERA-Interim contains 6 hourly *u-* and *v*-components of the 10m wind and the surface pressure at longitude -4.830, latitude 51.300 from 01/01/1979 00:00 to 31/12/2014 18:00 (Fig 5.6).

Fig 5.6 Map of the Bristol Channel that shows the position of the ERA-Interim station (yellow pin).

Fig 5.7 shows the wind rosette diagrams of wind pattern in the Bristol Channel from 1979 to 2014. The top left diagram is the wind pattern for the entire time period; the top right, bottom left and bottom right diagrams are the wind patterns in winter (December to February), autumn (September to November) and spring (March to May) respectively. The length of each spoke shows the frequency of wind blowing to a particular direction.

It is seen from the top left diagram that the overall mean wind speed in the Channel is 7.1m/s and maximum is over 20ms^{-1}; the dominant wind speed is 5-10ms^{-1} and the dominant wind directions are Westerly and South-westerly winds. In winter months, the average wind speed is 1.4ms^{-1} higher than the overall average value and the peak wind is the fastest; in autumn months, the average wind speed is also higher than the overall average speed while the peak speed is slightly lower. In autumn and winter, the dominant wind speed is 10-15ms^{-1} and the dominant wind directions are Westerly and South-westerly; while in spring, the average wind speed and peak wind speed are both lower than the overall averages, winds from the South-westerly quadrant are more
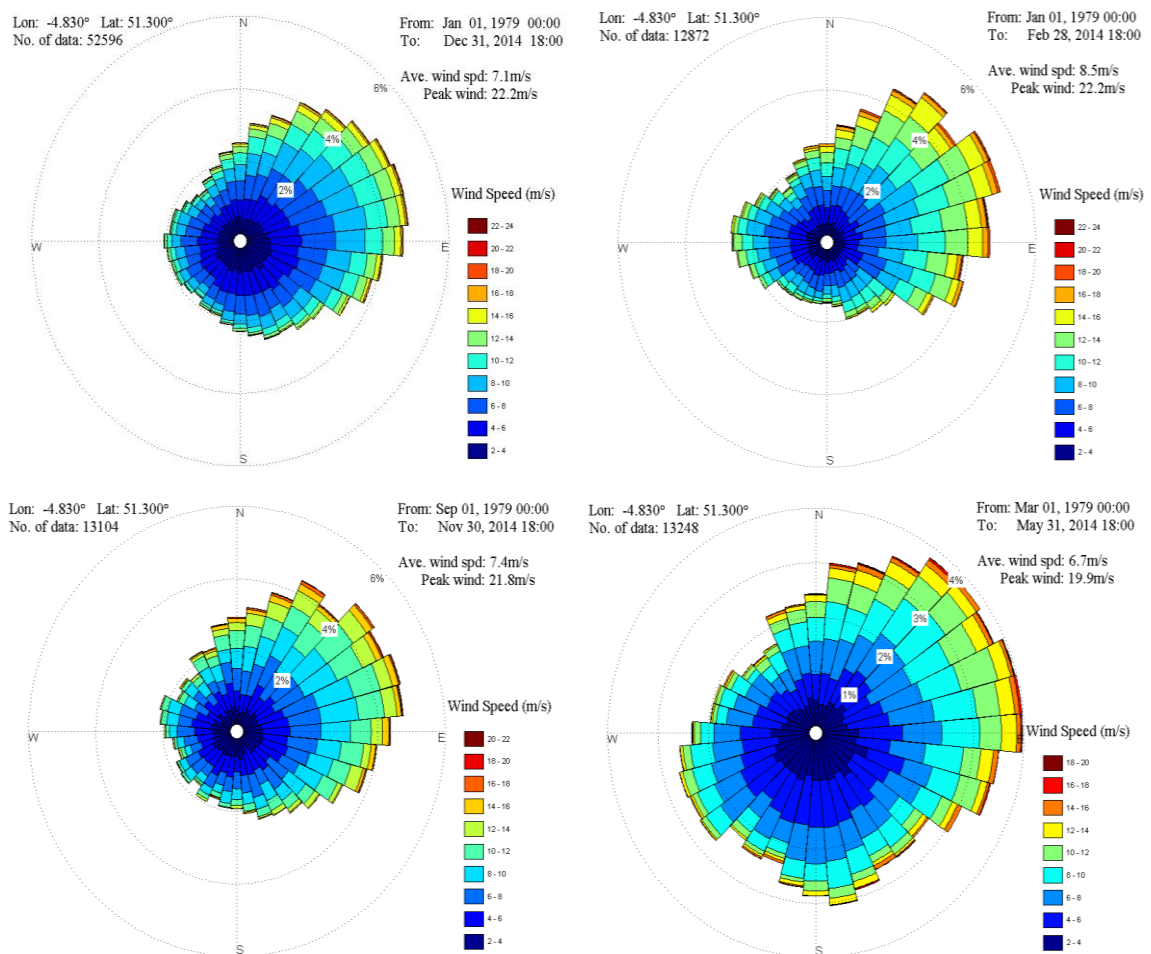
Fig 5.7 Wind rosettes of wind data from 1979 to 2014. Top left: wind rosette of the whole time period; top right: wind rosette of winter wind data (December to February); bottom left: wind rosette of autumn wind data (September to November); bottom right: wind rosette of spring wind data (March to May).

frequently than winds from other directions. This suggests that the winds are stronger in autumn and winter than spring or summer in the Bristol Channel with extreme winds reaching over 20ms^{-1}; winds from the South-westerly quadrant are stronger and more frequent than from other directions.

5.4 Most extreme surge and wind cases

Storm surge data derived from BODC have been further investigated to look at the most extreme positive and negative surges. The atmospheric data referred in the tables (Table 5.2-5.5) was from ERA-Interim with a standard surface pressure of 101325Pa. Five most extreme positive storm surge events have been summarised in Table 5.2. The duration of storm surge events refers to the time period when surge heights were larger than 1m. As seen in Table 5.2, the storm surges in the Bristol Channel lasted around 4 to 8 hours; their heights were site-dependent and ranged from 1.5m to 3m. The Channel head has experienced worse surges than the mid-Channel, for example, during the 25th January 1990 storm surge event, the surge at Avonmouth was close to 3m while at Ilfracombe it was only 1.5m. Looking at the atmospheric data, it is found that the maximum wind speeds for 4 out of 5 storm surge events coincided with either the annual maximum wind speed or seasonally maximum wind speed during that year (numbers highlighted in red); and the winds were always blowing from the West and Southwest. It is also worth noticing that each of the positive surge events was correlated with low atmospheric pressure compared to the mean sea level pressure (101325Pa). During the 19th January 1995 event, the wind was weaker compared to other four storm surge events (10-15 ms^{-1}); however, the atmospheric pressures were relatively low during the whole process, which might be the

Date and duration (surge>1m)	Location(s) affected	Max surge (m)	Atmospheric variation				Annual max wind (m/s)	Seasonally max wind (m/s)
			Time	Wind speed (m/s)	Wind direction	Surface pressure (Pa)		
25/01/90 0900-1600 7hrs	Avonmouth	2.909	06:00	17.82	SW	98028	**21.58**	21.58
	Ilfracombe	1.508	12:00	**21.58**	W	96898		
			18:00	14.98	W	98836		
04/01/98 1000-1815 8hrs15mins	Avonmouth	2.907	06:00	14.40	S	98921	22.17	**20.98**
	Newport	2.452	12:00	**20.99**	WSW	97547		
	Hinkley Point	2.206	18:00	16.55	W	99026		
	Mumbles	1.969						
19/01/95 1315-1745 4hrs30mins	Avonmouth	2.575	06:00	9.81	SSW	99600	20.69	20.69
	Newport	2.541	12:00	15.62	W	97897		
	Hinkley Point	1.83	18:00	9.79	WSW	98722		
	Ilfracombe	1.128						
13/12/00 0000-0345 3hrs45mins	Avonmouth	2.527	12/12 18:00	15.79	SSW	99207	**22.17**	22.17
	Newport	2.307	13/12 00:00	**22.17**	WSW	99464		
	Hinkley Point	1.987	06:00	14.34	WSW	100294		
			12:00	16.60	WSW	100353		
	Mumbles	1.586	18:00	12.38	W	100783		
12/02/14 1115-1715 6hrs	Newport	2.287	06:00	12.56	SSW	99428	**21.06**	21.06
	Hinkley Point	1.895	12:00	**21.06**	SW	97875		
	Ilfracombe	1.462	18:00	16.57	WSW	98417		

Table 5.2 Five worst positive storm surge events in the Bristol Channel (derived from BODC) and their atmospheric data (gained form ECMWF).

cause for more than 2m in surge heights at Avonmouth and Newport.

Negative storm surges are rare in the Bristol Channel but can be as large as 1.9m around the Channel head. Five largest negative storm surges for each of the five observation stations have been summarised in Table 5.3. It can be seen that only Avonmouth and Newport have experienced negative storm surges larger than 1m.

Time	Location(s) affected	Min surge (-m)
20/02/1996 05:30	Avonmouth	1.622
27/02/1993 07:00		1.211
23/03/2011 17:15		1.2
04/05/2010 17:30		1.196
19/11/2004 03:45		1.19
20/02/1996 16:14	Newport	1.9510
03/04/2000 13:44		1.4300
14/12/1995 19:59		1.3420
07/03/1996 15:44		1.1900
30/01/2003 12:30		1.1830
04/03/2008 12:15	Hinkley Point	0.9400
29/01/2003 12:15		0.8650
19/11/2004 02:14		0.8330
19/02/1996 04:59		0.808
24/11/2008 12:45		0.8030
13/02/2005 19:00	Mumbles	0.9040
30/01/2003 15:15		0.8560
22/12/2006 11:15		0.7400
24/11/2008 12:30		0.7340
24/11/2005 21:00		0.7320
12/10/1997 02:00	Ilfracombe	0.758
16/12/1997 15:45		0.762
29/01/2003 12:45		0.7
23/12/1991 18:00		0.682
25/01/1998 20:45		0.648

Table 5.3 Five worst negative surges at each of the five locations in the Bristol Channel (data derived from BODC).

Table 5.4 is a summary of five largest negative storm surge events in the Bristol Channel. The duration of events were calculated when negative surge heights larger than 0.5m. As shown in Table 5.4, the negative surges in the Channel lasted around 3 hours to 8 hours. The Channel head experienced worse negative surges than the mid-Channel, which was the same situation as positive storm surges in this area. The atmospheric forcing during negative surges were totally different from that in the positive ones: wind speed

during negative surges was no more than 16ms^{-1} and tended to blow from north and northeast; atmospheric pressure was always higher than the standard pressure value (101325Pa) during negative surges except for the 3rd April 2000 event.

Date and duration (surge< -0.5m)	Location(s) affected	Min surge (-m)	Time	Atmospheric variation		
				Wind speed (m/s)	Wind direction	Pressure (Pa)
20/02/96	Avonmouth	1.622	00:00	14.82	NNE	102339
			06:00	14.34	NNE	102697
0315-0800		1.9510	12:00	14.60	NE	103128
4hrs45mins	Newport		18:00	12.96	NE	103268
30/01/03	Newport	1.1830	06:00	13.98	NW	101492
1045-1830			12:00	13.96	N	101584
7hrs45mins	Mumbles	0.8560	18:00	14.19	N	102097
	Avonmouth	0.838	06:00	12.49	NNE	99075
			12:00	15.41	NNE	99300
03/04/00	Newport	1.4300	18:00	15.53	NNE	99469
1315:1615 3hrs	Hinkley Point	0.399	04/04/00 00:00	15.44	NNE	99757
	Mumbles	0.387	06:00	13.62	NNE	100016
	Avonmouth	1.133	12:00	10.71	ENE	103238
			18:00	10.92	ENE	103067
14/12/95	Newport	1.3420				
			15/12/95 00:00	11.12	ENE	102963
1715-2315 6hrs	Ilfracombe	0.441	06:00	12.09	ENE	102628
			12:00	13.05	ENE	102354
24/11/08	Hinkley Point	0.8030	06:00	11.00	NNW	99256
			12:00	12.05	NNE	100419
1030-1600			18:00	11.04	NNE	101388
5hrs30mins	Mumbles	0.7340	00:00	10.92	N	101964

Table 5.4 Five largest negative storm surge events in the Bristol Channel (derived from BODC) and their atmospheric data (gained form ECMWF).

Five most extreme wind cases have also been summarised in Table 5.5. Winds faster than 20ms^{-1} all blew from west and southwest with relatively low surface pressure. Surges

at shallower Channel regions were around 2-3m, while in the mid-Channel areas were around 1m. It is worth noting that the two extreme wind cases on 13th December 2000 and 25th January 1990 can also be found in the table of five largest positive surges (Table 5.2). This indicates the significant impact winds have on the positive storm surges in a shallow area like the Bristol Channel.

Time	Wind speed (m/s)	Direction	Surface pressure (Pa)	Surge			Duration (surge >1m)
				Location	Height (m)	Time	
13/12/00 00:00	22.17	WSW	99464	Avonmouth	2.57m	02:44	0000-0345 3hrs45mins
				Newport	2.307m	02:29	
				Hinkley Point	2.124m	01:30	
				Mumbles	1.586m	00:00	
28/10/96 18:00	21.77	WSW	98329	Avonmouth	1.303m	19:00	1500-2030 5hrs30mins
				Newport	1.692m	15:44	
				Hinkley Point	1,047m	17:59	
				Ilfracombe	0.759m	16:30	
25/01/90 12:00	21.57	W	96898	Avonmouth	2.909m	15:00	0900-1600 7hrs
				Ilfracombe	1.508m	13:00	
03/12/06 00:00	21.29	SSW	99261	Avonmouth	1.615m	05:15	0045-0630 5hrs45mins
				Newport	1.545m	05:15	
				Hinkley Point	1.315m	04:45	
				Mumbles	1.004m	03:30	
				Ilfracombe	0.994m	03:30	
08/12/93 18:00	21.20	W	98886	Avonmouth	2.092m	19:29	1645-2200 5hrs15mins
				Newport	1.7m	19:29	
				Hinkley Point	1.593m	17:59	
				Ilfracombe	1.003m	16:15	

Table 5.5 Five most extreme wind cases in the Bristol Channel (data gained form ECMWF) and their surge data (derived from BODC).

Therefore it can be concluded from the tables above that in the Bristol Channel, positive surges are likely to coincide with Westerly and South-westerly winds and low atmospheric pressure, while negative surges with Northerly and North-easterly winds and high atmospheric pressure. Positive surges occur more frequently in the Channel than negative surges with higher amplitudes. In general, large positive surges are more frequent

than large negative ones. This is partly because depressions (which cause positive surges) tend to be more intense and associated with more severe winds than anticyclones (negative surges) (Thomas and Hall, 2015). Negative surges are less dangerous than positive storm surges as they do not bring the risk of flooding, although they can damage ships in port and leave them stranded until the water level rises again. Therefore, in this study we concentrate on the analysis of positive surges in the Channel.

5.5 Introducing different winds

In order to model the impact of wind has on sea surface levels, simulations were run with constant winds with speed of 30 ms^{-1} from five different directions: South, Southwest, West, Northwest and North. Five locations in the upper Channel: Avonmouth, Hinkley Point, Newport, Ilfracombe and Mumbles (as shown in Fig 5.2) are selected to investigate the effects of wind conditions on the water surface levels. The simulations were set to increase the wind from 0 to 30 ms^{-1} linearly in time on Day 3 00:00-12:00, keep constant from Day 3 12:00 to Day 4 12:00, and decrease to 0 from Day 4 12:00 to Day 5 00:00 (Fig
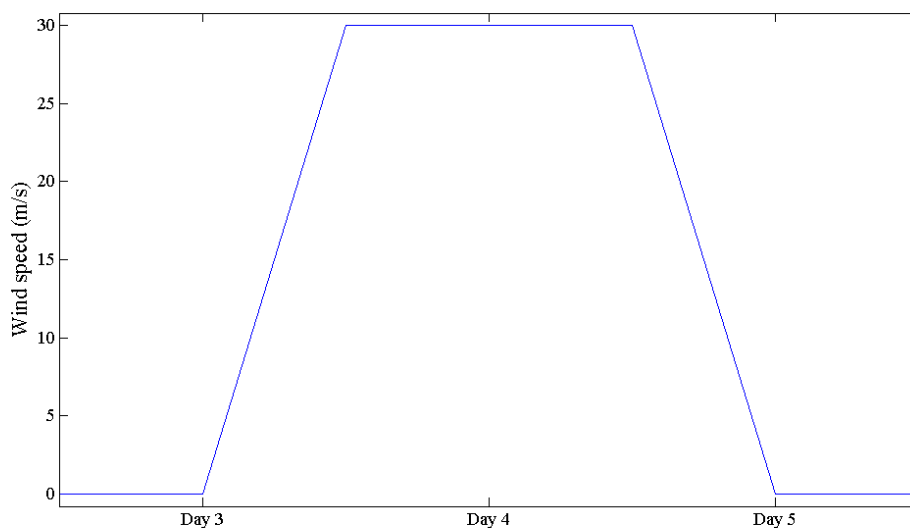
Fig 5.8 Variation of input wind forcing with time.

5.8). When analysing the results, we use the term "residual" when implying the result affected by both winds and tides; otherwise, we refer to "surge" which is a genuine meteorological without tidal contribution to sea level (see Fig 5.12).

It is seen in Fig 5.9 that when introducing Northerly winds, negative storm surges appear; when introducing North-Westerly winds, both positive and negative storm surges appear at Avounmouth, Newport and Hinkley Point, but only negative storm surges appear at Mumbles and Ilfracombe; when applying Southerly, South-Westerly and Westerly winds, significant positive storm surges appear at all the five sites. When the winds become zero on Day 5 00:00, it takes around one day for the winds to stop affecting the overall water levels. Among the five observation stations, Avonmouth experiences the highest water surface elevations with the largest residual being observed, the residual peak reaches 4m before the South-Westerly wind begins to decrease on Day 4. Ilfracombe has the lowest water surface elevations with smallest residual with a residual peak of around 1.5m when introducing Southerly wind.

A transition of dominant wind appears to occur from mid-Channel to the Channel head. In the higher reaches of the Channel (Avonmouth), the South-Westerly and Westerly winds provoke highest water levels. However, in the mid-Channel (Mumbles and Ilfracombe) Southerly wind has the largest effect on the water heights. As the storm surge propagates upstream, the water is subjected to two effects: the funnelling effect and the shoaling effect of the Channel. These two effects contribute to the building up of waters travelling up to the Channel head. The transition of dominant wind directions could be the result of Ekman flow. Ekman transport is a result of the combination of the Coriolis Effect from the Earth's
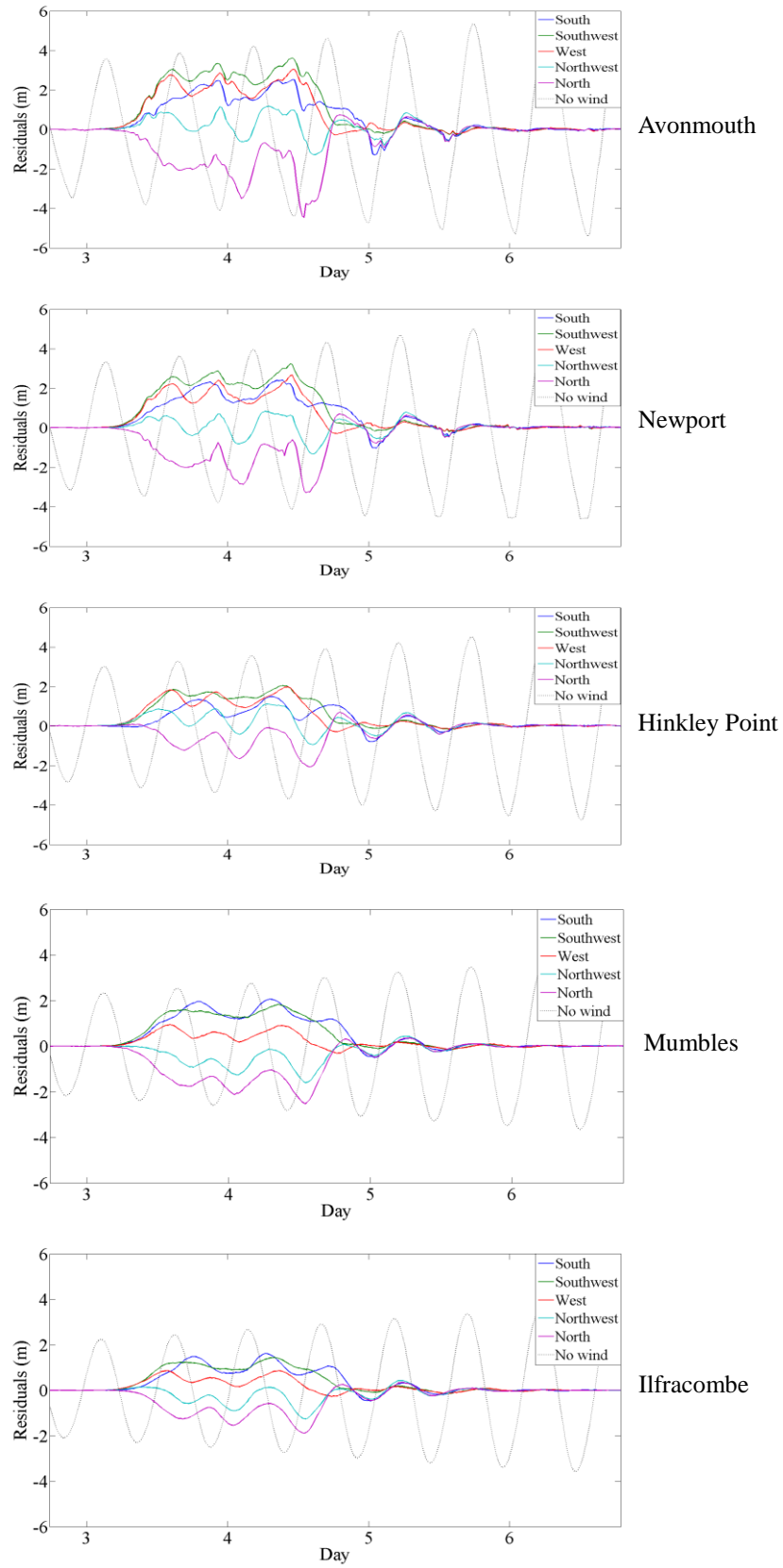
Fig 5.9 Residuals calculated at Avonmouth, Newport, Hinkley Point, Mumbles and Ilfracombe (top down). Dotted curves refer to the water elevations when only tides are included in the model.

rotation and the drag related to the winds blowing over the water surface (Pugh, 1996).

Therefore the Southerly wind results in water from the Irish Sea being pushed into the

Channel. Due to the too shallow topography of the upper reaches of the Channel, it is more

difficult to develop a full Ekman spiral. Hence, the South-Westerly and Westerly winds

may have more significant effects further up inland, forcing water in a direction more

parallel to the wind and more parallel to the length of the Channel itself.

5.6 Tide-surge interaction

Due to the non-linear effect of wind speed on water elevations (wind stress is
proportional to square of wind speed seen from Equation 2.8), the 30ms^{-1} winds have
much more significant impact than 10ms^{-1} winds (Fig 5.10). At Avonmouth, the 30ms^{-1}
winds generate residuals as high as 2.5m while the 10ms^{-1} winds only generate some
fluctuations no higher than 0.1m. The non-linear terms are important in shallow water,
where they generate an interaction between components of the motion. In particular, where
the tides are large and the water shallow, interaction occurs between the tide and surge
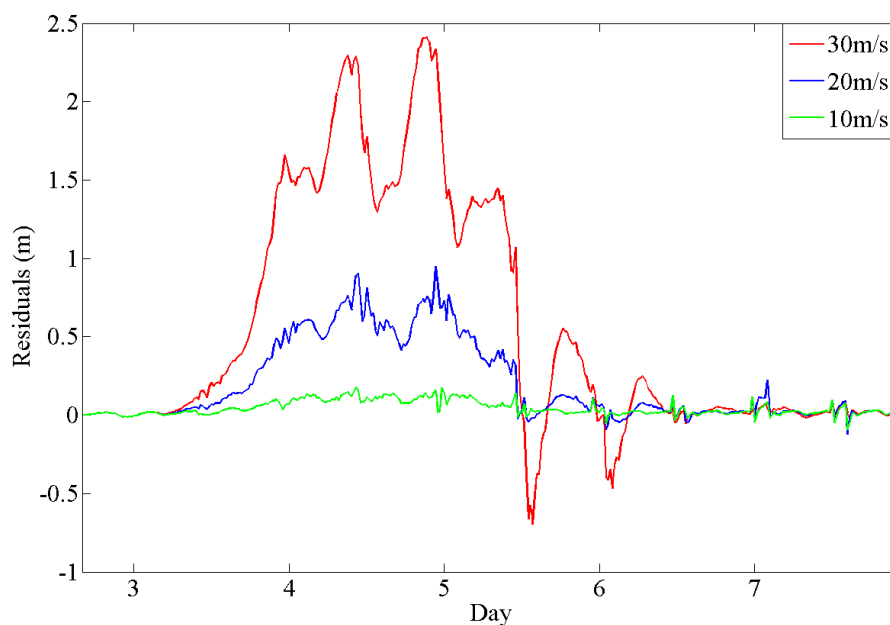
Fig 5.10 Residuals with Southerly winds at different speeds at Avonmouth.

making the two components interdependent (Pugh, 1996; Capel, 2001). Therefore the residuals produced by given meteorological forces at a certain state of the tide may differ significantly from the surge resulting from identical forcing when there is no tide.

An example of the water surface elevations at Avonmouth with 30ms^{-1} Southerly wind applied can be seen in Table 5.6, Fig 5.11 and Fig 5.12. The wind is constant from Day 3 12:00 to Day 4 12:00 in this example. The sum of water surface levels resulted from tidal and wind effects are indeed slightly different than that forced by the combined effect of tides and winds: for the results of the sum of A+B, the high tides are higher–and low tides are lower–than that of C when the winds are blowing in the model (Fig 5.10). After the

A	Model results with tidal forcing running only
B	Model results with 30m/s Southerly wind running only
C	Model results with tides and 30m/s Southerly wind running

Table 5.6 Simulations with different input.
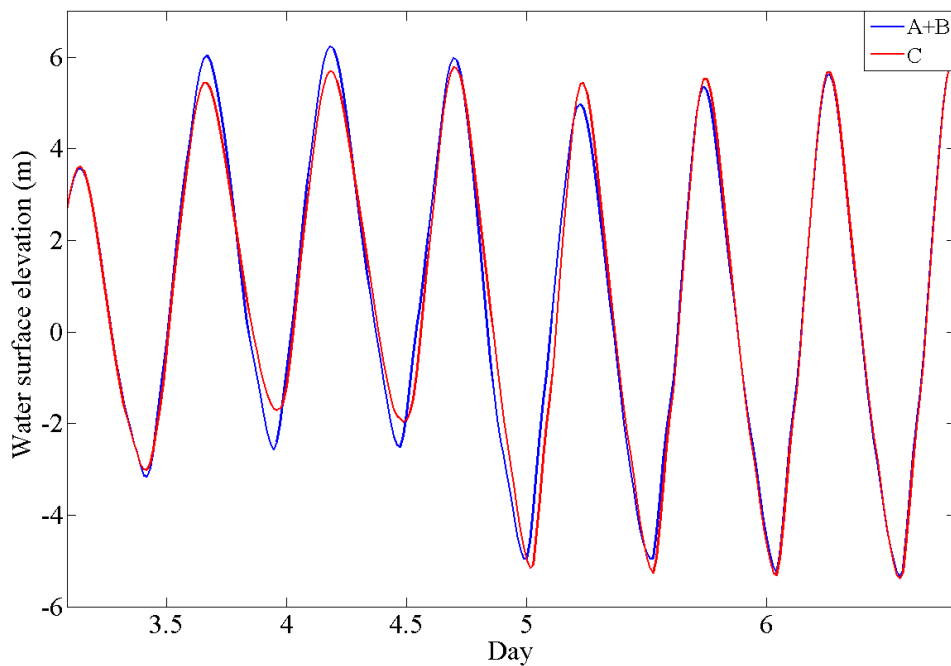
Fig 5.11 Water surface elevations with different combinations of inputs at Avonmouth.

wind stops on Day 5 00:00 it takes around one day for the two curves to overlap again with each other. It is also worth noticing that, the high water is slightly delayed for simulation C when both tides and wind are applied to the model. This is probably due to the dynamic balance between forcing, friction, and also different water depths (therefore different tidal propagation speed) for different simulations.

When comparing the residuals with the surges, it is interesting to note that there are significant oscillations of the residuals and several peak residuals can be seen (Fig 5.12). The oscillations of the residuals might be due to the tide-surge interactions and their oscillation period may be related to the resonant period of the Channel. Moreover, the maximum difference between the peak residuals and surges is nearly 1m with either Southerly or Westerly wind applied. When the Northerly wind is included, the maximum difference is more than 2m. This implies that the response of the Bristol Channel to the large scale development of meteorological forcing is affected by local tidal response. More
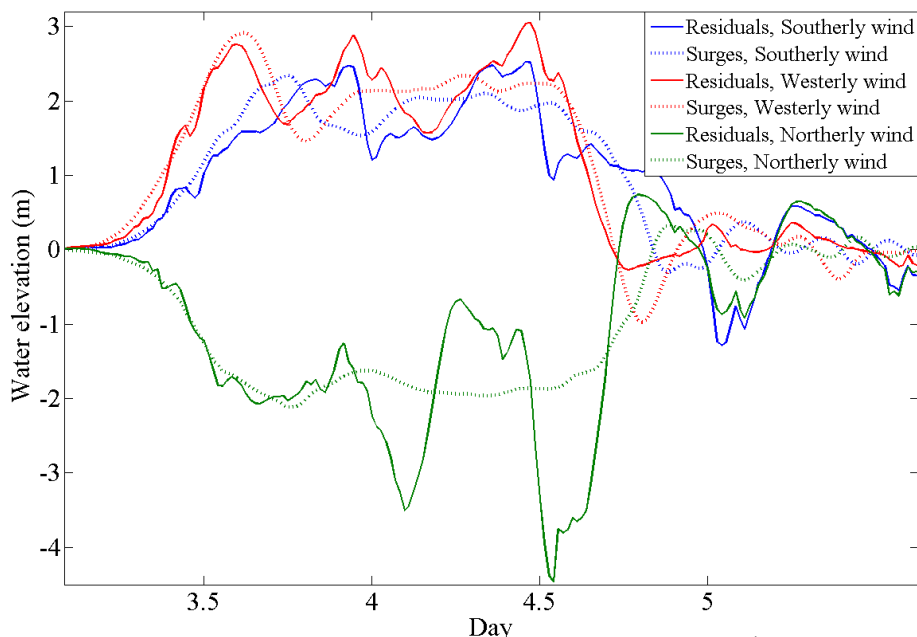
Fig 5.12 Residuals (solid curves) and surges (dotted curves) with 30ms^{-1} Southerly, Westerly and Northerly winds applied at Avonmouth.

importantly, this suggests that the approach to the data analysis used at the start of this chapter, where we assumed the response to meteorological forcing could be linearly added to the tidal response, may be over-simplistic.

5.7 Spring-neap cycles

A spring-neap tidal cycle could potentially have significant effects on the water level variations and has been taken into consideration for many shallow water modelling studies (Fig 5.13). The spring-neap cycle in semidiurnal tidal amplitudes is due to the various combinations of lunar and solar semidiurnal tides. When the Moon is full or new, the gravitational pull of the Moon and Sun are combined, thus larger than average tides can be seen—known as spring tides. During the Moon's quarter phases the Sun and Moon work at right angles, causing the bulges to cancel each other, therefore we get smaller tides known as neap tides. Two periods of spring and neap tides can be seen during one lunar cycle (28 days). Here in this study, M_2 and S_2 tidal constituents were input as fundamental semidiurnal lunar and solar tides respectively.
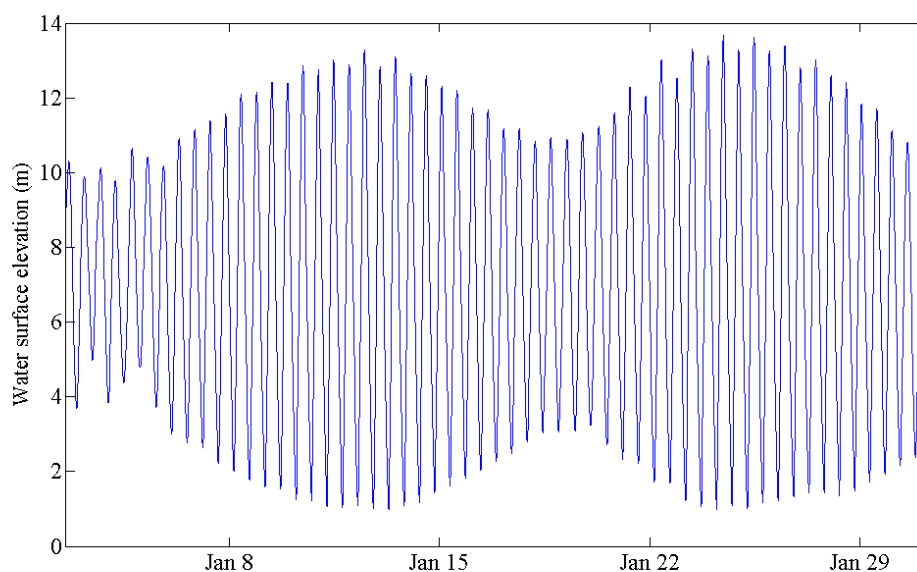
Fig 5.13 Spring and neap cycle in Avonmouth, Bristol Channel, January 2012 (measured data accessed from British Oceanographic Data Centre (BODC).

The spring and neap cycle simulations were run on 13th January 1950 and 06th January 1950 respectively, separated by 7 days and thus at as similar time of year as possible. Simulations were set to increase the winds from 0 to 30ms^{-1} Day 7 from 00:00 to 12:00, keep constant from Day 7 12:00 to Day 8 12:00, then decrease to 0 from Day 8 12:00 to Day 9 00:00. The results depicted in Fig 5.14 indicate that, the overall water levels in the spring simulations are higher than those in the neap simulations.
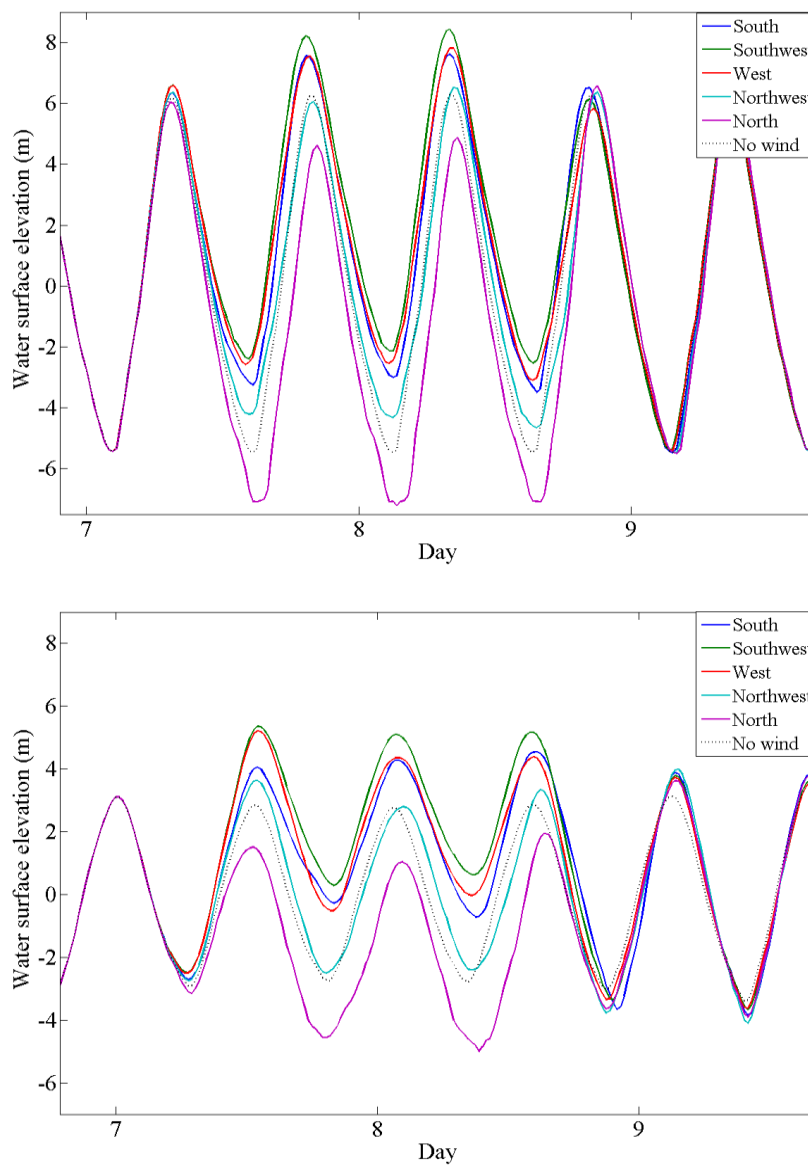
Fig 5.14 Water surface elevations with influences of 30ms^{-1} winds from various directions during spring (top) and neap (bottom) tides at Avonmouth.

However, it is seen in Fig 5.15 that the magnitudes of residuals observed with each wind is very similar for both the neap and spring tides with regard to their respective directions, although the residuals in spring tide are slightly higher than those during neap tide when wind is blowing from Southwest direction. Interestingly, if we look at the results from Day 7 12:00 to Day 8 12:00 when the winds are constant, the occurrence of residual peaks always coincides with low tide during both spring and neap tide. Therefore, the
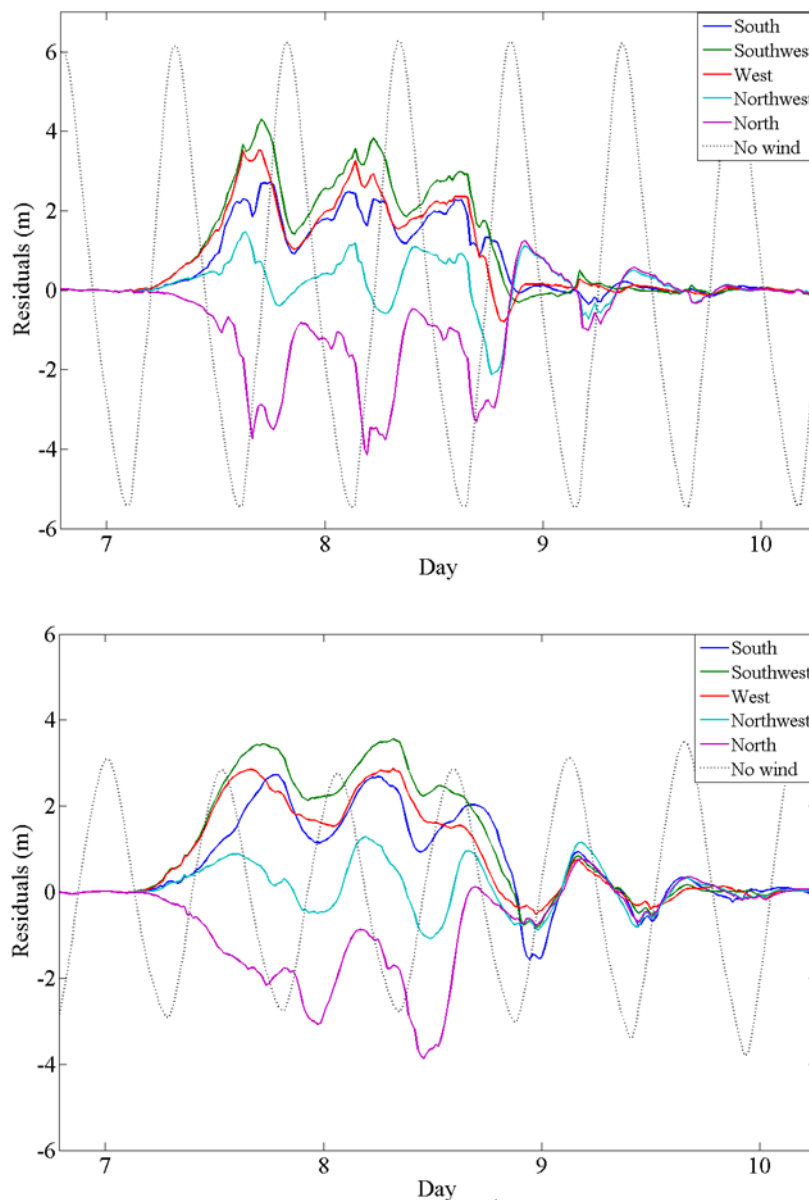
Fig 5.15 Residuals with influences of 30ms^{-1} winds form various directions during spring (top) and neap (bottom) tides at Avonmouth.

residual is likely to be more extreme at low tide during spring tide. Similar results were obtained by previous studies (Prandle and Wolf, 1978; Woodworth and Blackman, 2002; Horsburgh and Wilson, 2007) for different UK tide gauges. They showed that residual peaks seldom, if ever, occurred at high tide; they tend to occur before high and during rising tide. This phenomenon probably results from non-linear interaction between tide and surge; in reality interaction may be more complex. It also indicates the dominant effect of shallow-water and bottom friction (Weisse, 2010). We also notice that the structures of residuals during spring and neap tides are different. The residual curve in spring tide is more asymmetric, non-linear and noisy than that during neap tide; interestingly, the residual peaks coincide with rising tide during spring tide while with falling tide during neap tide.

To dig further into the influence of wind starting time on surge levels, simulations of 30ms^{-1} wind were started on low tide and high tide during spring tide in the Channel. Fig 5.16 shows the results of Avonmouth with 30ms^{-1} Westerly wind starting at different times. This shows that the total water level is highest when wind starts at high tide during spring
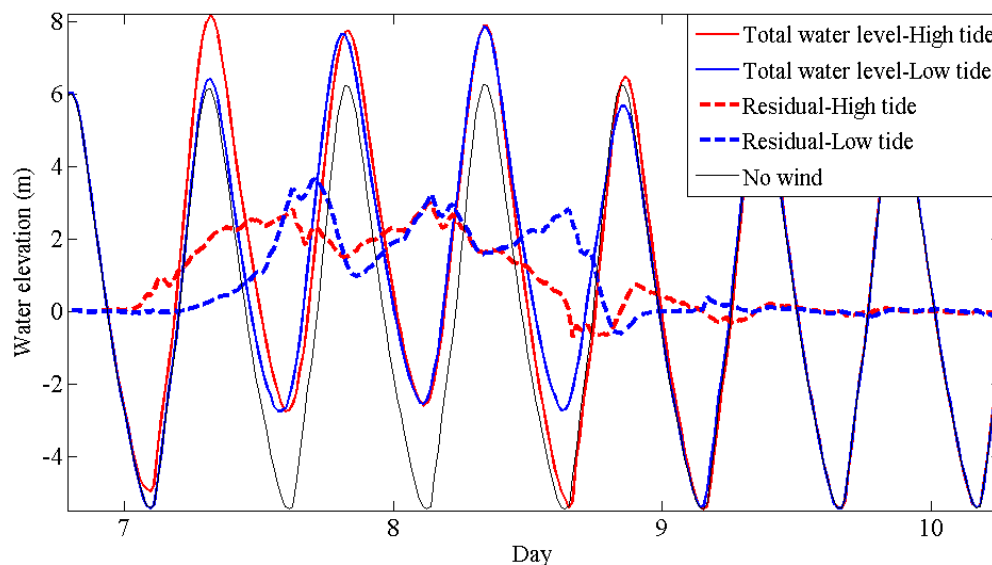
Fig 5.16 Total water levels and residuals with 30ms^{-1} Westerly winds starting at spring high tide and low tide in Avonmouth.

tide; and the skew surges are almost the same with wind starting at high tide and low tide. However the residual is slightly higher when wind starts at low tide. When the Westerly wind starts at low tide, this means the wind will blow with flood during which the wind is going in the same direction with tide; when the Westerly wind starts at high tide, the wind will blow with ebb during which the wind is going in the opposite direction with tide. Since the bed friction is always opposing the direction of tidal movement, we would expect larger bed friction during ebb than flood. Therefore, a slightly higher residual level when wind starts at low tide than that with wind starting at high tide.

This finding indicates that the exact timing of storm does matter, however, it is not as bad as we would expect since the residual peak hardly coincides with high water (Fig 5.14). The tide-surge interactions and bed friction are non-linear, and their effects are complicated, but this analysis helps us better understand the size of the storm surge.

Chapter 6

Case study—1607 storm surge event

6.1 Introduction

At approximately 0900 on 30th January 1607, the lowlands surrounding the Bristol Channel suffered possibly the worst coastal flooding on record (Horsburgh and Horritt, 2006). Here we assess the wind and tidal conditions required to produce the water levels reported in the historical writings. We use the same computational model for storm surge study in Chapter 5 to reproduce a typical storm surge in the Bristol Channel. Fig 6.1 shows the affected regions, there is reliable evidence of flooding on the east coast of England on the same day (Stow, 1631), however we only study the Bristol Channel region.

Fig 6.1 Locations affected by the 30th January 1607 flooding (RMS, 2007).

6.2 Reconstruction of the 1607 storm surge event

6.2.1 New style and old style dates

By the seventeenth century the Julian calendar was 11 days out of step with the passage of the seasons since 365.25 days is a slight over-estimate of the true length of a year (Horsburgh and Horritt, 2006). To correct this, Great Britain switched from the Julian Calendar to the Gregorian Calendar as a result of an Act of Parliament in 1752. The official start of year was also changed to 1 January. Prior to 1752 in England, the year began on 25th March (Lady Day), referred to as 'old style' by historians. Lady Day is one of the Quarter Days, which are still used in legal circles. In this study we used the new style date of 30 January 1607 to describe the event, which refers to 20 January 1606 for the old style date.

6.2.2 Tide and weather on 30 January 1607

A prediction of the tide in the Bristol Channel for January 1607 is possible since we know the periodicities of the astronomical forces. Therefore, the phase of M_2 tide was calculated and set for that on 24th January 1607, and the simulation time was 14 days; the nodal factors of M_2 and S_2 tides were set as 1 since nodal factors do not contribute significantly to the tidal level variation (see Chapter 4 Fig 4.8).

The weather preceding and during the flooding provides the key to the possibility of a storm surge. The most authoritative account is that of the annalist John Stow (1631) who noted that a westerly wind blew for 16 hours; Stow was also aware that it was a spring tide. Camden (1789) recorded that a strong South-westerly wind blew for three days without intermission, and the Barnstaple church register noted that the storm persisted from 0300

until noon. More contemporary references to weather conditions are collected in Horsburgh and Horritt (2006)'s studies. Taking all material into consideration, we introduced 30ms^{-1} Westerly, South-westerly and Southerly winds which blew from 1200 29th Jan to 1200 31st Jan. Pressure is set as a constant value of 101325Pa throughout the simulations.

6.2.3 Simulation of the 1607 storm surge

The model is forced with M$_2$ and S$_2$ tidal forcing at the ocean boundary with no current specified. The coastline is interpolated with 6m above the mean sea level. The simulation time period is from 24th January 1607 to 06th February 1607 with a spin-up period of 2 days, and the 30ms^{-1} wind is applied from 1200 29th January to 1200 31st January. Fig 6.2 shows the tidal response without wind forcing in the upper Channel (Avonmouth) for the period. The figure indicates that during the week of 1607 event there was spring tide in the Bristol Channel. On 30th January 1607 the spring tidal height reaches its peak value, which is more than 6m.
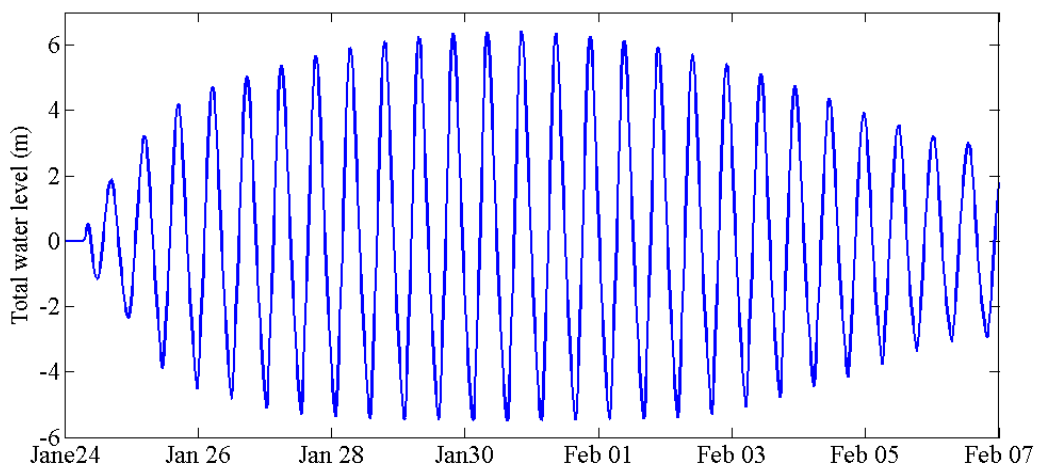
Fig 6.2 Total water level at Avonmouth during 30th January 1607 event.

It is shown that the simulation results for 30th January 1607 event provides sufficient water level to inundate the towns and villages indicated in Fig 6.1. Avonmouth, Newport and Hinkley Point show maximum residual height of 3.5m, 3m, 2m respectively (Fig 6.3).
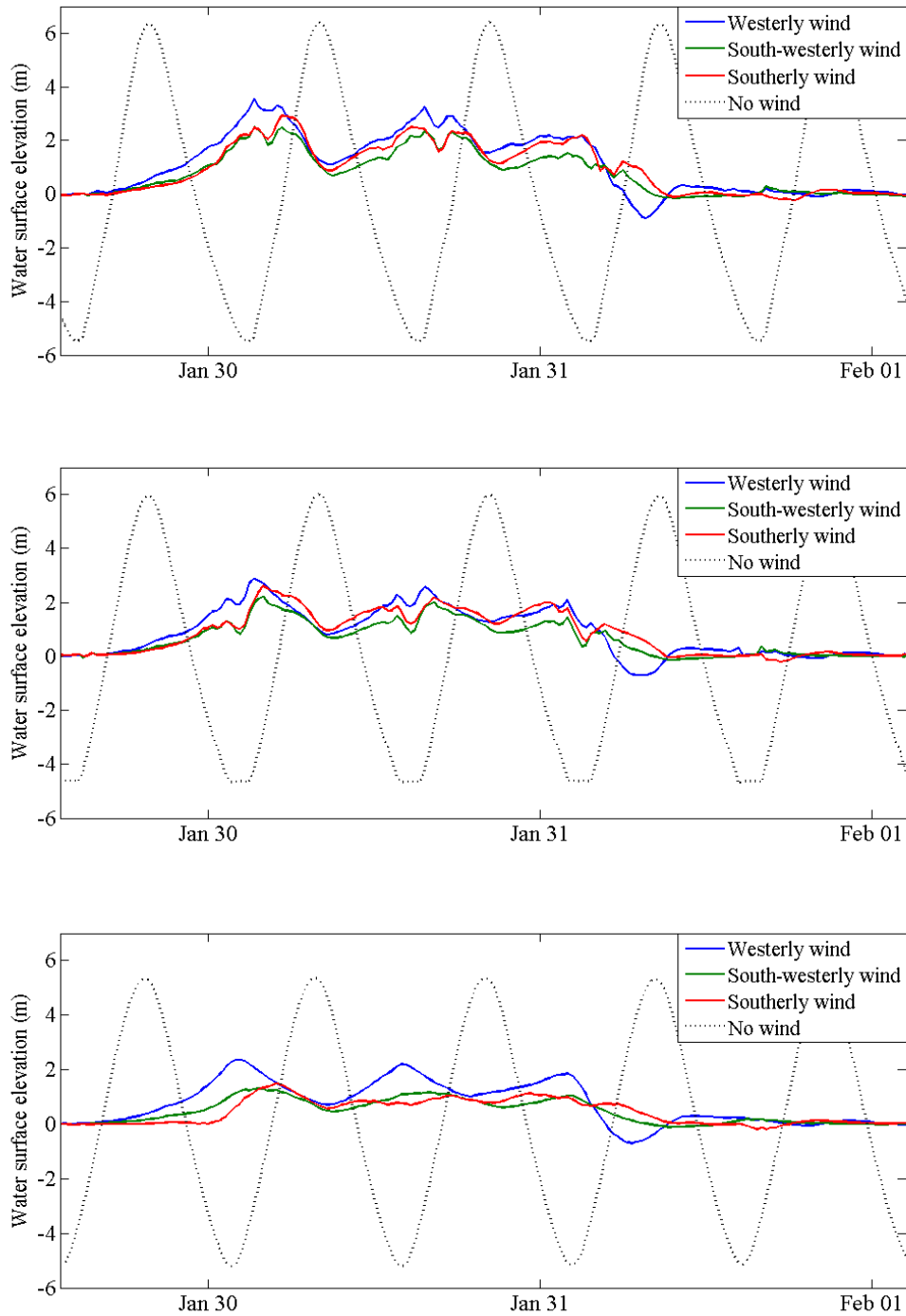
Fig 6.3 Residuals at Avonmouth (top), Newport (middle) and Hinkley Point (bottom) with winds blowing from different directions from 30th January to 01st February 1607.

Around 1800 on 30th January the total water level reaches the highest value (Fig 6.4); in

Avonmouth it reaches 8m (with a datum of 6m mean sea level). The two high waters on

30th January show a difference of no more than 20cm. According to Chapter 5, the start
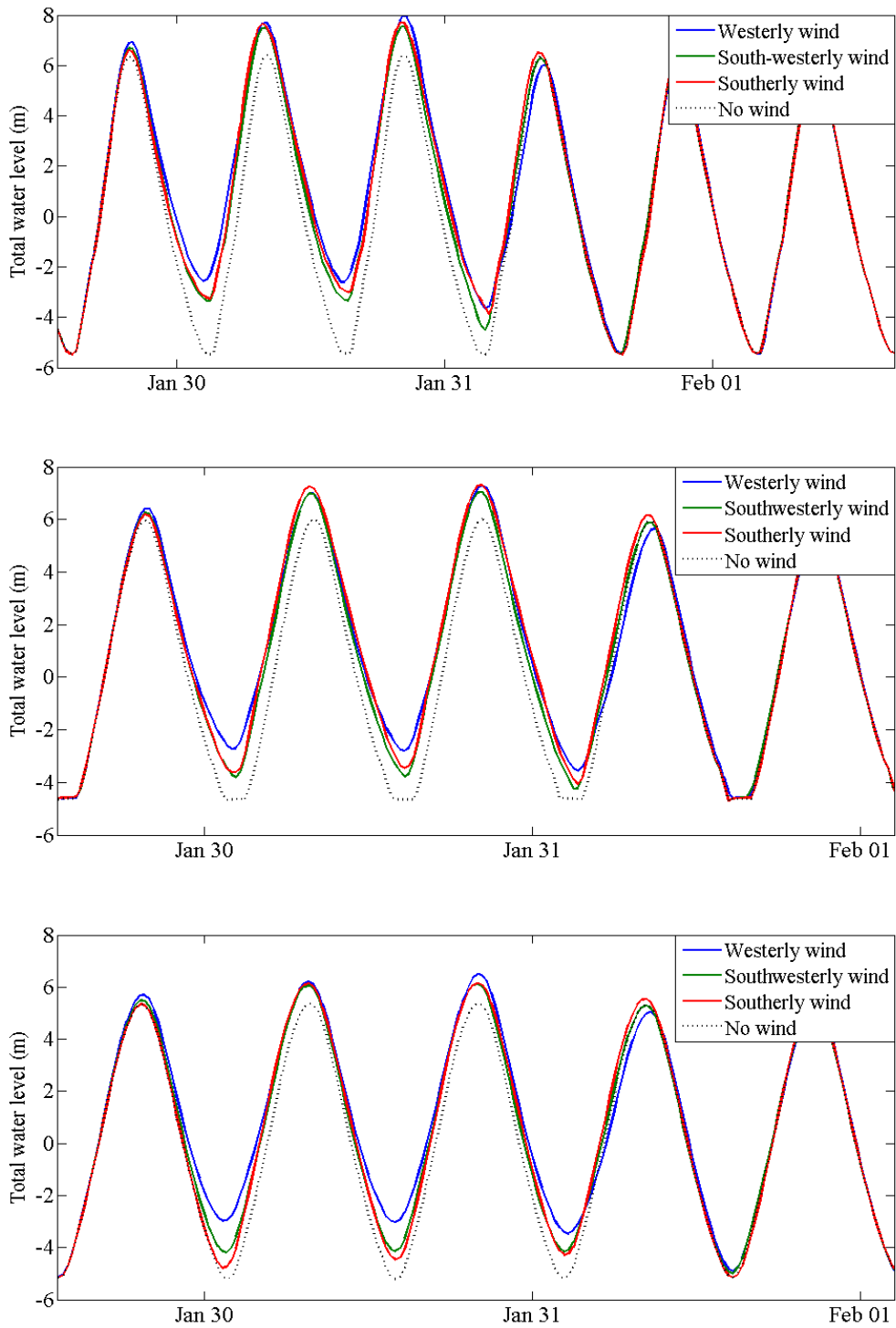
Fig 6.4 Total water levels at Avonmouth (top), Newport (middle) and Hinkley Point (bottom)
with winds blowing from different directions from 30th January to 01st February 1607.

time of wind simulation has some influence on the peak surge height and the overall water level, however the difference is not very significant (no more than 30cm) between wind starting at high tide and wind starting at low tide. Therefore similar results would be obtained even if the storm started few hours earlier or later than the storm start time set in the present study.

Westerly wind seems to cause highest residual level in the upper Channel compared to Southerly and South-westerly winds. This agrees with historical writings (e.g. John Stow, 1631). Results from Chapter 5 suggests that the most extreme case of the residual peak coinciding with high water will not very likely to happen, and this is still the case for the simulations of 1607 storm surge in the Channel.

Fig 6.5 and Fig 6.6 are the contours of highest total water levels and residuals in the Bristol Channel on 30th January interpolated in Google Earth. The highest water levels occurred at 0800 on and the highest residuals occurred at 0440 on 30th January. The total water level and residual of the locations affected at the upper Channel reach over 6m and 2m respectively.

According to historical documents, the Somerset Levels as far inland as Glastonbury Tor, 14 miles (23km) from the coast were affected. The sea wall at Burnham-on-Sea gave way, and the water flowed over the low lying levels and moors (RMS, 2007). In the River Parrett the residual is more than 3m (where the yellow lines lie near Burnham-on-Sea shown in bottom figure of Fig 6.6). Coupled with the nature of low lying land in Somerset, this could bring devastating flooding to this area.

Fig 6.5 Contours of total water levels in the Bristol Channel at 0800 on 30th January 1607 (Google Earth, 2016).

There is likely to have been significant morphological change since 1607, both from natural causes and improvement works on the levels. A uniform value of the bed friction coefficient c_d=0.003 was used which is same with that used in Chapter 5. We did not take into account variations in roughness due to variation of vegetation types with time, however the results should still be representative of the magnitude of total water levels and surge levels of the Bristol Channel back in 1607.
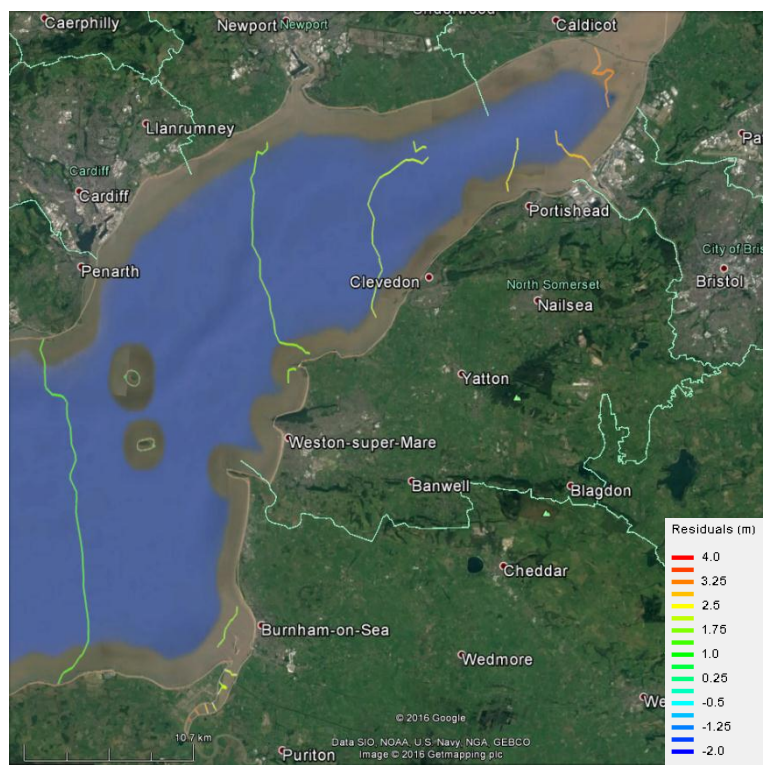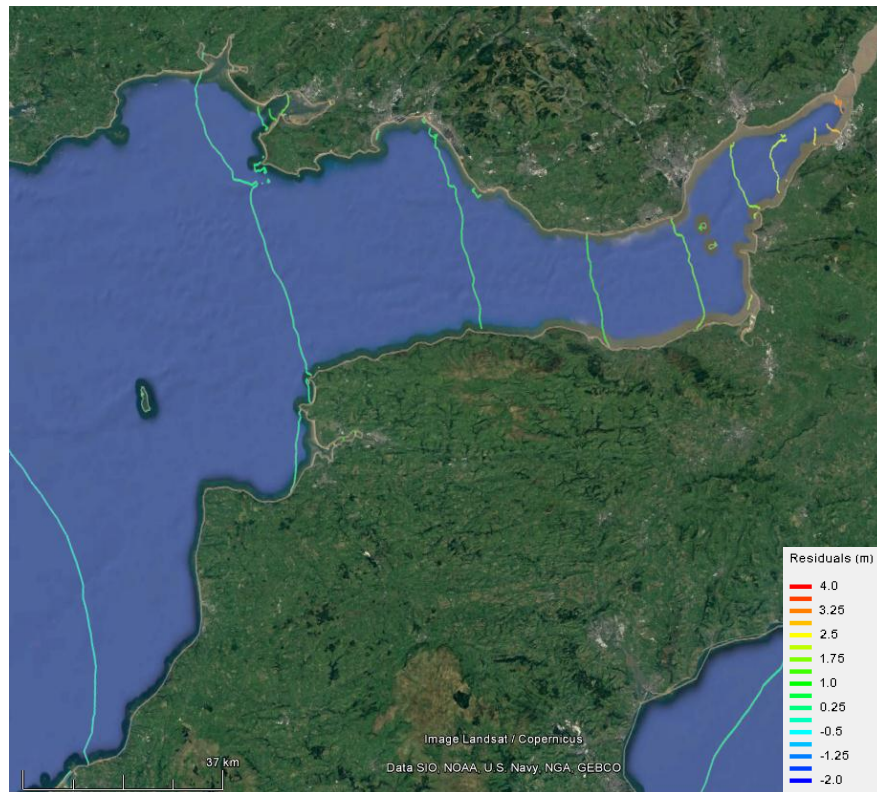
Fig 6.6 Contours of residuals in the Bristol Channel (top) and in the upper Channel (bottom) at 0540 on 30th January 1607 (Google Earth, 2016).

Chapter 7

Conclusions

Two two-dimensional shallow hydrodynamic models based on an unstructured triangular mesh have been used to study the tidal resonance and storm surge phenomena in the Bristol Channel. For the tidal resonance study, the domain incorporates the Bristol Channel and the Severn Estuary; for the storm surge study, the domain includes the Bristol Channel, the English Channel, the Celtic Sea and the Irish Sea. These models used discontinuous and continuous Galerkin finite element methods respectively to solve the 2D shallow water equations. Details were given of the model calibration and verification processes (see Chapter 3), which indicate that the numerical model predictions generally agreed closely with the observed data.

In Chapter 4, the model was first refined to cover the Bristol Channel and Severn Estuary to study the long-wave-induced hydrodynamic processes in the Bristol Channel. The frequency response characteristics of the water body were assessed by both forcing sinusoidal tidal wave excitation and wind disturbance at the open ocean boundary. The simulation results with tide alone and wind alone show that the quarter-wavelength resonant period of the Bristol Channel has a coupled resonance system with dominant resonant period of 8-10 hours. This is close to but shorter than the semi-diurnal tidal band (12 hours), suggesting that the basin length of the Bristol Channel is shorter than the resonant quarter wavelength. Generally speaking, the main resonance of the channel seems consistent with previous studies, and the second peak at about $\omega/\omega_{M2}=3.1$ might be the

resonant response of the outer Channel itself. The cause for the resonant periods of 7.8 hours and 17 hours found during wind disturbance simulations are unclear and future investigation is needed. The maximum tidal range was confirmed to occur in the upper part of the Severn Estuary, where the input wave (2m) was amplified by up to three times (6m).

The main resonance is slightly sensitive to increased bed friction which may have implications for tidal energy extraction. Neither the amplitude on the boundary nor the mean water level has a significant impact on the resonant response, suggesting that the nodal factor of the tide, or any possible sea-level rise, will not dramatically influence the tidal response in the Channel. The sensitivity of resonance to bed friction should be taken into account when extracting tidal energy from the Channel.

The present method has been proved to be a valid method to examine the fundamental mode of resonance in harbours and bays in response to the attack of long waves. It should be noted that this is a preliminary research. Although maximum tidal range has been found to occur at ST1 (the most easterly point in the Channel head), more monitoring points will be required to determine the maximum tidal amplitude in the upper Channel and River Severn which have not completed by this study.

In Chapter 5, the characteristics of the storm surges in the Bristol Channel were examined using extreme value analysis and numerical modelling. The *in situ* tidal data used for extreme value analysis is from 1961 to 2015, and both 10- and 50-year return levels indicated that the Channel head is expected to experience the largest storm surges. After examining the observed ECMWF atmospheric data, it is found that positive surges are likely to coincide with Westerly and Southerly winds and low atmospheric pressure,

while negative surges with Northerly and North-easterly winds and high atmospheric pressure; positive surges have more devastating results than negative surges in the Channel. The observed ECMWF atmospheric data also suggest that South-westerly and Westerly winds are prevailing in the Bristol Channel, and the wind is stronger in winter and autumns.

After introducing different wind conditions to the 2-D shallow water model, the largest storm surge event again occurred at the Channel head. It was also found that the surge levels vary by location, and have a complicated dependency on wind speed, wind direction, tide-surge interactions, the spring-neap cycle and with respect to the state of the tide. Most observation sites in the Channel experience larger storm surges with Southerly wind; however, when going further inland, the largest storm surges would occur with South-westerly and Westerly wind. The transition of dominant wind directions could be the result of Ekman flow. Results from simulations with tide and wind and with wind only suggested that storm surge in the Bristol Channel is affected by local tidal response, and there are strong tide-surge interactions. This suggests that the response to meteorological forcing could not be linearly added to the tidal response, and using the difference between observed and predicted tidal levels as 'storm surge' in statistical analysis may be over-simplistic.

The storm surges are likely to have more impact during spring tide than neap tide, causing relatively high overall water levels; however the difference in residuals is minimal between spring and neap tide. During a spring-neap cycle, the significant storm surges are likely to occur when high winds coincide with low tide during spring. This probably

results from non-linear interaction between tide and surge and also indicates the dominant effect of shallow-water and bottom friction. The start time of wind does matter; when wind starts to blow at low tide the peak height is larger than that with wind starting at high tide. However the impact is not significant, only causing a difference in peak surge height of no more than 30cm.

Although wind stress is the predominant atmospheric factor forcing surge, air pressure also contributes to the surge heights. A reduction in normal atmospheric pressure by 1 millibar will raise the sea level by about 1 cm (inverse barometer effect), therefore low air pressure clearly contributes to positive storm surge, but its overall impact is modest. Moreover, this study focused on explaining the key physics of storm surge in the Bristol Channel, pressure variations are important when modelling real events. Therefore, without inputting air pressure the simulated storm surge results are sufficient for our study. However, for future study it would be better to include air pressure in the model to gain more accurate results.

The reconstruction of 30th January 1607 storm surge event has shown that the tide and probable wind conditions at that time were capable of generating a surge that is consistent with the observed inundation. The event of January 1607 provides a reminder of the destructive capability of storm surges. It would have been more realistic to incorporate other factors, such as the mesh of low lying lands around the Channel, the air pressure variation and the river input. It also would have been better to adjust the mesh boundary and bed roughness to match the geographical conditions in the 16th Century. However, given the limited data, only a finite amount can be achieved in reconstruction of the event.

Chapter 6 is a preliminary study of the January 1607 event and demonstrates the capability of ADCIRC model to produce reasonable results for a particular storm surge event. We suggest further studies of the 1607 event incorporate more details to the model based on the historical writings.

References

Ackers, P., and Ruxton, T. (1974) Extreme levels arising from meteorological surges. *Coastal Engineering Proceedings*, 1(14).

ADCIRC user's manual v51 (2015) Single file meteorological input file (fort.22) [online]. Available from:http://adcirc.org/home/documentation/users-manualv51/input-file-descriptions/single-file-meteorological-forcinginput-fort-22/.

Adcock, T.A.A and Draper, S. (2014) On the tidal stream resource of two headland sites in the English Channel: Portland Bill and Isle of Wight. In *ASME 2014 33rd International Conference on Ocean, Offshore and Arctic Engineering*: V09AT09A003-V09AT09A003. American Society of Mechanical Engineers.

Adcock, T.A.A, Draper, S., Houlsby, G.T., Borthwick, A.G.L and Serhadlıoğlu, S. (2014) Tidal stream power in the Pentland Firth–long-term variability, multiple constituents and capacity factor. *Proceedings of the Institution of Mechanical Engineers*, Part A: Journal of Power and Energy, p.0957650914544347.

Allen, P.A. (2009) Earth surface processes. John Wiley & Sons.

Godin, G., 1993. On tidal resonance. *Continental Shelf Research*, 13(1):89-107.

Baker, C. (1991) Tidal power, *Energy Policy*, 19(8):792-797.

Blackman, D. L. and Graff, J. (1978) The analysis of annual extreme sea levels at certain ports in southern England. *Proceedings of the Institution of Civil Engineers*, Part 2. 65: 339-357.

Bokhove, O. and van der Vegt, J.J. (2005) Introduction to (dis) continuous Galerkin finite element methods. *Department of Applied Mathematics, University of Twente*.

Bondi, H. (1981) Tidal Power from the Severn Estuary, vol. 1. *Severn Barrage Committee Report to the Secretary of State of Energy*.

Bresch, D. and Noble, P. (2007) Mathematical Justification of a Shallow Water Model. *Methods and Applications of Analysis,* 14(2): 87-118.

Brewer, A.J. (1962) Model investigation of storm surges in a shallow sea. DPhil. University of Oxford.

Brown, J.M. and Wolf, J. (2009) Coupled wave and surge modelling for the eastern Irish Sea and implications for model wind-stress. *Continental Shelf Research*, 29(10):1329-1342.

Bryant, K.M. and Akbar, M. (2016) An Exploration of Wind Stress Calculation Techniques in Hurricane Storm Surge Modeling. *Journal of Marine Science and Engineering*, 4(3): 58.

Camden, W. (1789) *Britannia*-translated by Philemon Holland in three volumes, T. Payne and Son, London.

Capel, A. (2001) *Tropical cyclone-induced storm surges* (Doctoral dissertation, TU Delft, Delft University of Technology).

Charnock, H. (1955) Wind stress on a water surface. *Quarterly Journal of the Royal Meteorological Society*, 81(350): 639-640.

Christie, E., Li, M. and Moulinec, C. (2012) Comparison of 2d and 3d large scale morphological modeling of offshore wind farms using HPC. *Coastal Engineering Proceedings, 1*(33): 42.

CIRIA, CUR and CEFMEF, (2007) Physical site condition and data collect. In the Rock Manual, C683.

Coles, S., Bawa, J., Trenner, L., and Dorazio, P. (2001) *An introduction to statistical modeling of extreme values*, volume 208. Springer.

Coles, S.G. and Tawn, J.A. (2005) Bayesian modelling of extreme surges on the UK east coast. *Philosophical Transactions of Royal Society A*, 363:1387–1406.

Davies, J. R. and Webber, N. B. (1976) An investigation of the frequency of occurrence of extreme high water levels at Portsmouth. Department of Civil Engineering. University of Southampton. Internal Report.

Davies, A.M. and Jones, J.E. (1992) A three-dimensional wind driven circulation model of the Celtic and Irish Seas. *Continental Shelf Research*, 12(1):159-188.

Davies, A. (2014) Storm surges in the Bristol Channel. 4th Year Project, University of Oxford.

Dee, D.P., Uppala, S.M., Simmons, A.J., Berrisford, P., Poli, P., Kobayashi, S., Andrae, U., Balmaseda, M.A., Balsamo, G., Bauer, P. and Bechtold, P. (2011) The ERA-Interim reanalysis: Configuration and performance of the data assimilation system. *Quarterly Journal of the Royal Meteorological Society*, 137(656):553-597.

Dietrich, J.C., Bunya, S., Westerink, J.J., Ebersole, B.A., Smith, J.M., Atkinson, J.H., Jensen, R., Resio, D.T., Luettich, R.A., Dawson, C. and Cardone, V.J. (2010) A high-resolution coupled riverine flow, tide, wind, wind wave, and storm surge model for southern Louisiana and Mississippi. Part II: Synoptic description and analysis of Hurricanes Katrina and Rita. *Monthly Weather Review*, 138(2): 378-404.

Diaconis, P. and Efron, B. (1983) Computer intensive methods in statistics. *Scientific American*, 248 (5): 116.

Falconer, R. A. (1993) An introduction to nearly horizontal flows. *In Coastal, Estuarial and Harbour Engineers' Reference Book* (Abbott, M. B. and Price, W. A., eds). E and FNSpon Ltd., London, pp.736.

Flather, R.A. (1976) Results from a storm surge prediction model of the north-west European continental shelf for April, November and December 1973. Report No.24. Institute of Oceanographic Sciences.

Flather, R.A., Draper, L. and Proctor, R. (1982) Coastal Flooding in the Bristol Channel and Severn Estuary on 13th December 1981.

Flather, R.A. (1979) Recent results from a storm surge prediction scheme for the North Sea. *Elsevier Oceanography Series*, 25:385-409.

Flather, R.A. (1981) Practical surge prediction using numerical models. In *Floods due to high winds and tides* (pp. 21-43). Academic Press London.

Flather, R.A., Smith, J.A., Richards, J.D., Bell, C., and Blackman, D.L. (1998) Direct estimates of extreme storm surge elevations from a 40-year numerical model simulation and from observations. *The Global Atmosphere and Ocean System*. 6: 165–176.

Fong, S. W and Heaps, N. S (1978). *Note on Quarter Wave Tidal Resonance in the Bristol Channel*. Bidston Observatory, Birkenhead, Institute of Oceanographic Sciences, 11pp. (I.O.S. Report No. 63) (Unpublished).

Garratt, J.R. (1977) Review of drag coefficients over oceans and continents. *Monthly weather review*, 105(7): 915-929.

Graff, J. and Blackman, D. L. (1979) Analysis of maximum sea levels in southern England. *Proceedings 16th Coastal Engineering Conference, Hamburg, 1978, Vol. 1*. American Society of Civil Engineers, New York. 931-947.

Godin, G. (1993) On the tidal resonance. *Continental Shelf Research*, 13(1):89-107.

Google Earth 7.1.7.2606 (2016). http://www.earth.google.com. *51°03'02.37"N, 3°50'40.98"W, Eye alt 199.53km*. Landsat/Corpernicus, viewed October 6 2016.

Haigh, I. D., Wadey, M. P., Gallop, S. L., Loehr, H., Nicholls, R. J., Horsburgh, K., Brown, J. M. and Bradshaw, E. (2015) A user-friendly database of coastal flooding in the United Kingdom from 1915-2014, *Scientific data*, 2.

Hashemi, M.R., Abedini, M.J., Neill, S.P. and Malekzadeh, P. (2008) Tidal and surge modelling using differential quadrature: A case study in the Bristol Channel. *Coastal Engineering*, 55(10): 811-819.

Heath, R. (1981) Resonant period and Q of the Celtic Sea and Bristol Channel. Estuarine, *Coastal and Shelf Science*, 12(3):291–301.

Horsburgh, K. and Horritt, M. (2006) The Bristol Channel floods of 1607—reconstruction and analysis. *Weather*, 61(10):272-277.

Horsburgh, K.J. and Wilson, C. (2007) Tide‑surge interaction and its role in the distribution of surge residuals in the North Sea. *Journal of Geophysical Research: Oceans*, 112(C8).

Hubbert, G.D. and Mclnnes, K.L. (1999) A storm surge inundation model for coastal planning and impact studies. *Journal of Coastal Research*, pp.168-185.

Jenkinson, A. F. (1955) The frequency distribution of the annual maximum (or minimum) values of meteorological elements. *Quarterly Journal of the Royal Meteorological Society*. 81: 158-172.

Johnson, B.H., Kim, K.W., Heath, R.E., Butler, H.L. and Hsieh, B.B. (1991) *User's guide for a three-dimensional numerical hydrodynamic, salinity, and temperature model of Chesapeake Bay* (No. WES/TR/HL-91-20). ARMY ENGINEER WATERWAYS EXPERIMENT STATION VICKSBURG MS HYDRAULICS LAB.

Joseph, S.S., Francoise, R.R., Mark, E.F. and Robert, J.Y. (2000) A user's guide for the CALMET

meteorological model. *Earth Tech, Inc*.

Karniadakis, G. and Sherwin, S. (2013) *Spectral/hp element methods for computational fluid dynamics*. Oxford University Press.

Kubatko, E .J., Westerink, J.J., andDawson, C. (2006) hp Discontinuous Galerkin methods for advection dominated problems in shallow water flow. *Computer Methods in Applied Mechanics and Engineering*, 196: 437-451.

Kubatko, E.J., Bunya, S., Dawson, C., Westerink, J.J. and Mirabito, C. (2009) A performance comparison of continuous and discontinuous finite element shallow water models, *Journal of Scientific Computing*, 40(1-3): 315-339.

Lee, H. (2014) Modelling extreme sea levels due to sea level rise and storm surge in the Seto Inland Sea, Japan. *Coastal Engineering Proceedings.* 1 (34). Management. 1.

Lennon, G.W., (1963b) A frequency investigation of abnormally high tide levels at certain west coast ports. *Proc. Institution of Civil Engineers*. 25: 451–483.

Li, B.Q. (2006*) Discontinous Finite Elements in Fluid Dynamics and Heat Transfer.* Springer-Verlag London. 1st edition.

Liang, D., Xia, J., Falconer, R. A., and Zhang, J. (2014) Study on tidal resonance in Severn Estuary and Bristol Channel. *Coastal Engineering Journal*, 56(01):1450002.

Lowe, J. A., Gregory, J. M., Flather, R. A. (2001) Changes in the occurrence of storm surges around the United Kingdom under a future climate scenario using a dynamic storm surge model driven by the Hadley Centre climate models, *Climate Dynamics*, 18: 179-188.

Needham, H., Keim, B.D., (2011) *Storm surge: physical processes and an impact scale.* INTECH Open Access Publisher.

Neill, S.P. and Couch, S.J. (2011) September. Impact of Tidal Energy Converter (TEC) Array Operation on Sediment Dynamics. *In Proceedings of the 9th European Wave and Tidal Energy Conference.*

O'Neill, C., Saulter, A., Williams, J. and Horsburgh, K. (2016) NEMO-surge: Application of atmospheric forcing and surge evaluation Technical report 619.

Pelling, H.E., Green, J.M. and Ward, S.L. (2013) Modelling tides and sea-level rise: To flood or not to flood. *Ocean Modelling*, 63:21-29.

Pelling, H.E. and Green, J.M. (2014) Impact of flood defences and sea-level rise on the European Shelf tidal regime. *Continental Shelf Research*, 85:96-105.

Pickands, J. (1971) The two-dimensional Poisson process and extremal processes. J. *Applied Probability,* 8: 745–756.

Pickands, J. (1975) Statistical inference using extreme order statistics. *Annals of Statistics,* 3: 119–131.

Pickering, M.D., Wells, N.C., Horsburgh, K.J. and Green, J.A.M. (2012) The impact of future

sea-level rise on the European Shelf tides. *Continental Shelf Research*, 35:1-15.

Prandle, D. and Wolf, J. (1978) The interaction of surge and tide in the North Sea and River Thames. *Geophysical Journal International*, 55(1), pp.203-216.

Proctor, R. and Flather, R.A. (1989) Storm surge prediction in the Bristol Channel —the floods of 13 December 1981. *Continental Shelf Research*. 9(10): 889-918.

Pugh, D. T. and Vassie, J. M. (1979) Extreme sea levels from tide and surge probability. *Proceedings of the 16th Coastal Engineering Conference, 1978, Hamburg, 1:* 911–930. New York: American Society of Civil Engineers.

Pugh, D. T. (1996) *Tides, surges and mean sea-level (reprinted with corrections)*, Johan Wiley & Sons Ltd.

Pugh, D. and Woodworth, P. (2014) *Sea-Level Science: Understanding Tides, Surges, Tsunamis and Mean Sea-Level Changes*, Cambridge University Press.

RMS. (2007) 1607 Bristol Channel Floods: 400-year retrospective. Risk management Solutions Report. RMS SPECIAL REPORT. p.12.

Roll, H.U. (1965) *Physics of the Marine Atmosphere*. Academic Press, p.426.

Serhadlıoğlu, S., Adcock, T. A. A., Houlsby, G.T., Draper, S. and Borthwick, A. G. L. (2013) Tidal stream energy resource assessment of the Anlesey Skerries, *International Journal of Marine Energy*, 3:e98-e111.

Serhadlıoğlu, S. (2014) Tidal stream resource assessment of the Anglesey Skerries and the Bristol Channel. DPhil. University of Oxford.

Sheng, Y.P., Davis, J.R., Figueiredo, R., Liu, B., Liu, H., Luettich, R., Paramygin, V.A., Weaver, R., Weisberg, R., Xie, L. and Zheng, L. (2012) A Regional Testbed for Storm Surge and Coastal Inundation Models–An Overview. *In Proceedings of the 12th international conference on estuarine and coastal modeling. St. Augustine, Fl, ASCE*, 476-495.

Shim, J.S., Kim, J., Kim, D.C., Heo, K., Do, K. and Park, S.J. (2013) Storm surge inundation simulations comparing three-dimensional with two-dimensional models based on Typhoon Maemi over Masan Bay of South Korea. *Journal of Coastal Research,* 65(sp1):392-397.

Smith, S. and Banke, E. (1975) Variation of the sea surface drag coefficient with wind speed. *Quarterly Journal of the Royal Meteorological Society*, 101(429):665–673.

Soulsby, R. (1997). *Dynamics of Marine Sands*. Thomas Telford Services Limited.

Stow, J, Buck, G. and Howes, E (1631). *Annales, Or, a Generall Chronicle of England. Begun by Iohn Stow: Continued and Augmented with Matters Forraigne and Domestique, Ancient and Moderne, Vnto the End of This Present Yeere. By Edmund Howes, Gent.* Early English Books Online. Londini: [Printed by John Beale, Bernard Alsop, Thomas Fawcett, and Augustine Mathewes] Impensis Richardi Meighen, 1632. Available in Bodelian Library, University of Oxford.

Sutcliffe, R.C. and Lennon, G.W. (1963) The identification of weather conditions associated with

the generation of major storm surges along the west coast of the British Isles. *Quarterly Journal of the Royal Meteorological Society,* 89(381):381-394.

Suthons, C.T. Cdr, (1963) Frequency of abnormally high sea levels on the east and south coasts of England. *Proceedings of the Institution of Civil Engineers.* 25: 433–450.

Tawn, J. A. (1988a) An extreme value theory model for dependent observations. *Journal of Hydrology.* 101: 227–250.

Tawn, J. A. (1988b) Bivariate extreme value theory: models and estimation. *Biometrika* 75: 397–415.

Tawn, J. A. and Vassie, J. M. (1989) Extreme sea levels: the joint probabilities method revisited and revised. *Proceedings of the Institution of Civil Engineers*. Part 2 87: 429–442.

Tawn, J. A. and Vassie, J. M. (1990) Spatial transfer of extreme sea level data for use in the revised joint probability method. *Proceedings of the Institution of Civil Engineers, Part 2* 89: 433–438.

Tawn, J. A. (1992) Estimating probabilities of extreme sea-levels. *Applied Statistics,* 41: 77–93.

Thomas, R.S. and Hall, B. (2015) Seawall design. Butterworth-Heinemann.

Ward, B. (2014) The costs of the UK storms and floods in context. LSE Grantham Institute.

Ward, S.L., Green, J.M. and Pelling, H.E. (2012) Tides, sea-level rise and tidal power extraction on the European shelf. *Ocean Dynamics*, 62(8):1153-1167.

Walton Jr, T.L. (2000) Distributions for storm surge extremes. *Ocean Engineering*. 27: 1279-1293.

Webb, D.J. (2013) On the shelf resonances of the English Channel and Irish Sea. *Ocean Science*, 9(4):731-744.

Weisse, R. (2010) *Marine climate and climate change: storms, wind waves and storm surges.* Springer Science & Business Media.

Willis, M, Masters, I, Thomas, S, Gallie, R, Loman, J, Cook, A, Ahmadian, R, Falconer, R.A., Lin, B, Gao, G and Cross, M (2010). Tidal turbine deployment in the Bristol Channel: a case study, *Proceedings of the Institution of Civil Engineers-Energy*, 163(3): 93-105.

Williams, J.A. and Horsburgh, K.J. (2013) Evaluation and comparison of the operational Bristol Channel Model storm surge suite. Southampton, UK: National Oceanography Centre, 37pp. *National Oceanography Centre Research and Consultancy Report,* No. 38

Williams, J., Horsburgh, K.J., Williams, J.A. and Proctor, R.N. (2016) Tide and skew surge independence: New insights for flood risk. *Geophysical Research Letters*, 43(12): 6410-6417.

Williams, J., Wilson, C., and Horsburgh, K. (2012) Re-analysis of the December 1981 storm surge event in the Bristol Channel using the current operational tide-surge model suite, *Ocean Science*, 5(3): 369-378.

Woodworth, P.L. and Blackman, D.L. (2002) Changes in extreme high waters at Liverpool since 1768. *International Journal of Climatology*, 22(6)):697-714.

Woodworth, P.L., Flather, R.A., Williams, J.A., Wakelin, S.L., and Jevrejeva, S. (2007) *Continental Shelf Research*. 27: 935-946.

Wolf, J. and Flather, R.A. (2005) Modelling waves and surges during the 1953 storm. Phil. Trans. R. Soc. A. 363:1359-1375.

Wu, J. (1980) Wind-stress coefficients over sea surface near neutral conditions—A revisit. *Journal of Physical Oceanography*, 10(5): 727-740.

Zheng, L., Weisberg, R.H., Huang, Y., Luettich, R.A., Westerink, J.J., Kerr, P.C., Donahue, A.S., Crane, G. and Akli, L. (2013) Implications from the comparisons between two‐ and three‐dimensional model simulations of the Hurricane Ike storm surge. *Journal of Geophysical Research: Oceans,* 118(7)*:*3350-3369.